ETH Zurich
Department of Physics

Master's Thesis

Effect of a positive cosmological constant on quasinormal modes of rotating black holes

Stefania Mombelli

Supervisors:
Dr. Shubhanshu Tiwari[1]
Prof. Dr. Philippe Jetzer[1]

Co-Supervisor:
Prof. Dr. Gian Michele Graf[2]

8th September 2020

Abstract

We review the theory of black holes in de Sitter spacetime and discuss a way to classify them based on the relative position of their event horizons. Following some papers, we implement numerical methods to compute the quasinormal mode frequency spectra of Kerr-de Sitter black holes. By means of these methods, we investigate the fundamental modes of some astrophysical black hole types, focusing on gravitational perturbations. We study the qualitative and quantitative differences between these spectra and the known spectrum of Kerr-Minkowski black holes, in the attempt to quantify the effects of a positive cosmological constant on quasinormal mode frequencies. We find that these differences are extremely tiny and thus not detectable.

Universität Zürich[UZH]

[1]University of Zurich, Department of Physics
[2]ETH Zurich, Institute for Theoretical Physics

Contents

1 Introduction **4**

2 Theoretical background **6**
2.1 De Sitter universe 6
2.2 Black holes in de Sitter universe 9
2.2.1 Schwarzschild-de Sitter black holes 9
2.2.2 Kerr-de Sitter black holes 10
2.3 Scales and units 14
2.3.1 Astrophysical black holes 16

3 Quasinormal modes of black holes in de Sitter spacetime **17**
3.1 Introduction on quasinormal modes 17
3.2 Motivation and goal 21
3.3 Schwarzschild-de Sitter spacetime 23
3.3.1 Quasinormal mode frequencies via the Pöschl-Teller potential approximation 25
3.3.2 Implementation 27
3.3.3 Results 27
3.4 Kerr-de Sitter spacetime 29
3.4.1 Quasinormal mode frequencies via the Heun's function method 31
3.4.2 Implementation 37
3.4.3 Results 39
3.4.4 Quasinormal mode frequencies via the continued fractions method 43
3.4.5 Implementation 48
3.4.6 Results 49
3.5 Detectability of quasinormal modes 50
3.5.1 Theory 50
3.5.2 Results 51
3.6 Results 51

4 Summary and outlook **54**

A Spin-weighted spheroidal harmonics **56**

B Heun's differential equation **58**
B.1 Wronskian method 59

C The 'qnm' package for python **62**
C.1 Modified Lentz's algorithm 62

D The numerical codes **66**
D.1 Schwarzschild-de Sitter 66
D.2 Kerr-de Sitter 66
D.2.1 Quasinormal mode frequencies via the continued fractions method 66
D.2.2 Quasinormal mode frequencies via the Heun's function method 73

E Tunneling formalism in the study of particle emission rates from black holes due to Hawking radiation **77**
E.1 Theory 77
E.1.1 Emission rates 77
E.1.2 Hawking radiation as tunneling 78
E.1.3 Choice of the coordinates 79
E.1.4 WKB approximation 79
E.1.5 Detailed balance condition 81
E.1.6 Results 82
E.2 Problems 82
E.3 Summary 83

1 Introduction

The no-hair theorem states that *the external gravitational and electromagnetic fields of a stationary black hole are determined uniquely by the hole's mass M, charge Q and intrinsic angular momentum J* (cf. [1]). Observation of electromagnetic and gravitational radiation emitted by the black hole allows therefore to infer the value of its parameters. Of particular interest are the so-called *quasinormal modes*, damped single-frequency oscillations that dominate the black hole's response to external perturbations at late times.
The recovery of the black hole parameters is done by measuring the quasinormal mode frequencies and damping times, and by comparing the values with the quasinormal mode spectra determined by means of black hole perturbation theory. The study of these spectra is therefore of fundamental importance for observational tests of the no-hair theorem. Typically, one focuses on gravitational radiation, which interacts extremely weekly with matter and thus reaches the gravitational wave detectors while remaining unchanged.

The quasinormal modes of the Schwarzschild black hole in asymptotically Minkowski spacetime were first studied by Vishveshwara [2], based on the pioneering work of Regge and Wheeler [3], and further investigated by Chandrasekhar and Detweiler ([4], [5]). Thanks to the work of Teukolsky and Press ([6], [7], [8]), who derived the master equations for perturbations of rotating black holes, the quasinormal modes of Kerr-Minkowski black holes began to be studied (see Chandrasekhar and Detweiler [9], Detweiler [10]). Ferrari and Mashhoon [11] developed an analytic method to compute quasinormal mode frequencies by rewriting the master equation in a Schrödinger-like form and by approximating the potential with a *Pöschl-Teller potential*. An alternative method, which is not based on an approximation, was developed by Leaver [12] and is called the *continued fractions technique*.
Later, the computation of quasinormal mode spectra was extended to black holes in an asymptotically de Sitter spacetime, characterized by the presence of a positive cosmological constant. Otsuki and Futamase ([13]) first computed the quasinormal mode frequencies of a Schwarzschild-de Sitter black hole based on the *WKB approximation*. The Pöschl-Teller approximation devised by Ferrari and Mashhoon and the continued fractions method developed by Leaver were also extended and applied to Schwarzschild-de Sitter black holes by Moss and Norman [14], Cardoso and Lemos [15] and Yoshida and Futamase [16]. Based on Leaver's method and on the work of Suzuki, Takasugi and Umetsu ([17], [18]), who showed that the Teukolsky equation for Kerr-de Sitter black holes can be mapped to the so-called Heun's equation, Yoshida, Uchikata and Futamase [19] first computed the quasinormal mode frequencies of Kerr-de Sitter black holes numerically. Their work was recently improved by Hatsuda

[20], who made use of the 'HeunG' function implemented in *Mathematica 12.1* to compute the quasinormal mode solutions.
Quasinormal modes of Anti-de Sitter black holes, i.e. black holes in a spacetime with a negative cosmological constant, were also studied (cf. [14], [21]).

So far, the recovery of black hole parameters has been achieved by making use of a Kerr-Minkowski spectrum. However, observations (cf. [22]) suggest that the cosmological constant has a positive value, although very small. For this reason, one should use a Kerr-de Sitter model instead.

The goal of this thesis is to establish whether the use of a Kerr-de Sitter quasinormal mode spectrum rather than a Kerr-Minkowski one causes some differences in the parameter estimation of astrophysical black holes. To do this, we examine both qualitative and quantitative differences between the two frequency spectra and determine whether these differences are detectable or not with current gravitational wave detectors. We restrict ourselves to gravitational perturbations.
In writing this thesis, we noticed a lack of clarity in defining the scale of the problem and in determining the most convenient units to use. For this reason, we decided to elaborate a clear explanation for this, which also allowed us to find a way to classify Kerr-de Sitter black holes.

This thesis is organised as follows. In Section 2 we provide the necessary theoretical background to study black holes in a de Sitter universe. In Section 3 we first introduce quasinormal modes and then discuss possible methods to compute the frequency spectra of Schwarzschild-de Sitter and Kerr-de Sitter black holes numerically. Finally, we discuss the differences between Kerr-Minkowski and Kerr-de Sitter spectra, focusing on their detectability.

2 Theoretical background

2.1 De Sitter universe

It is known from observations that the universe is expanding in an accelerated way. A model that describes this universe rather well is the de Sitter model, which attributes the expansion entirely to the presence of a positive cosmological constant. In this chapter, we first motivate the choice of this model, referring to [23] and [24], and then give a more mathematical description of the de Sitter spacetime, following [25] and [26]. We use the signature $(-,+,+,+)$ and work in geometrized units ($G = c = 1$).

We start by briefly recapitulating some important concepts of cosmology. As it is well known, the Einstein field equations (EFE) read:

$$R_{\mu\nu} - \frac{1}{2}Rg_{\mu\nu} + \Lambda g_{\mu\nu} = 8\pi T_{\mu\nu}, \tag{2.1}$$

where Λ is the cosmological constant. Assuming spatial homogeneity and isotropy, one can make the following ansatz:

$$ds^2 = -dt^2 + a^2(t)d\vec{x}^2, \tag{2.2}$$

$$T_{\mu\nu} = (\rho + p)u_\mu u_\nu + pg_{\mu\nu}, \tag{2.3}$$

where ρ and p indicate the fluid density and pressure, respectively. $a(t)$ is the scale factor which parametrizes the expansion of the universe. By inserting this ansatz into equation (2.1) and by considering the following transformation,

$$\tilde{\rho} = \rho + \frac{1}{8\pi}\Lambda, \tag{2.4}$$

$$\tilde{p} = p - \frac{1}{8\pi}\Lambda, \tag{2.5}$$

the EFE can be rewritten as

$$R_{\mu\nu} - \frac{1}{2}Rg_{\mu\nu} = 8\pi\tilde{T}_{\mu\nu}, \tag{2.6}$$

where

$$\tilde{T}_{\mu\nu} = (\tilde{\rho} + \tilde{p})u_\mu u_\nu + \tilde{p}g_{\mu\nu}. \tag{2.7}$$

The cosmological constant is therefore absorbed by the stress-energy tensor, and one can define

$$\rho_\Lambda := \frac{1}{8\pi}\Lambda, \tag{2.8}$$

$$p_\Lambda := -\frac{1}{8\pi}\Lambda, \tag{2.9}$$

with $p_\Lambda = -\rho_\Lambda$. By solving the EFE with this ansatz, one obtains the *Friedmann equations* (cf. [24]), which lead to

$$H^2 = H_0^2 \left(\Omega_{r0} a(t)^{-4} + \Omega_{m0} a(t)^{-3} + \Omega_K a(t)^{-2} + \Omega_\Lambda\right), \tag{2.10}$$

where $H(t) := \frac{\dot{a}(t)}{a(t)}$ is the Hubble constant and $\Omega_{i0} := \frac{8\pi}{3H_0^2}\rho_{i0}$ is called density parameter, with $1 = \Omega_{r0} + \Omega_{m0} + \Omega_K + \Omega_\Lambda$. The subscript 0 indicates the quantities at the present epoch, r stands for "radiation", m for "matter" and K for "curvature". As can be seen from equation (2.10), the different energy densities scale differently with the expansion of the universe. The energy densities of the components other than the cosmological constant decrease as the universe expands. At some point in the past, the cosmological constant Λ became the dominant term in the total energy density, and the other components' densities became smaller than Ω_Λ. As time moves forward, the universe approaches a universe described by

$$\rho = -p, \qquad T_{\mu\nu} = -\Lambda g_{\mu\nu}, \qquad \Omega_\Lambda = 1, \qquad H^2 = H_0^2 = \frac{\Lambda}{3}. \tag{2.11}$$

From the definition of the Hubble constant, one easily derives the scale factor $a(t)$ for this universe:

$$a(t) = a_0 e^{Ht} = e^{Ht} = e^{\sqrt{\frac{\Lambda}{3}}t}, \tag{2.12}$$

where we have set $a_0 = 1$.

Observations suggest that the value of Λ is positive. This value can be obtained from the observational values (cf. [22])

$$H_0 = (67.36 \pm 0.54)\,\mathrm{km\,s^{-1}Mpc^{-1}}, \tag{2.13}$$

$$\Omega_\Lambda = 0.6847 \pm 0.0073, \tag{2.14}$$

using relation (2.11), which in SI units is given by:

$$\Lambda = 3\left(\frac{H_0}{c}\right)^2 \Omega_\Lambda. \tag{2.15}$$

The result, in geometrized units, is

$$\Lambda = (1.089 \pm 0.029) \cdot 10^{-52}\mathrm{m}^{-2}. \tag{2.16}$$

For $\Lambda > 0$, the model described by (2.11) and (2.12) represents an empty universe expanding forever due to the presence of the cosmological constant, and is indeed the *de Sitter* (henceforth dS) *universe*.

One peculiarity of the dS universe is that it expands so rapidly that, for each observer, there are regions from which not even light can ever reach him.

The boundary of this region is called the *cosmological event horizon* (CEH) of the observer and its radius, r_C, can be determined using the Hubble law,

$$v = H_0 D, \tag{2.17}$$

where v is the recessional velocity of galaxies and D is the proper distance between the galaxy and the observer (cf. e.g. [27]). By setting $v = c = 1$ and $D = r_C$, one can determine the position of the CEH in the reference system of (2.2):

$$r_C = \frac{1}{H_0} = \sqrt{\frac{3}{\Lambda}}. \tag{2.18}$$

Note that, because of the assumptions of homogeneity and isotropy, the position of the CEH is observer-dependent, and the observer lies at $r = 0$.

We now move to a more formal description of the dS spacetime. One can write the dS metric by combining (2.2) and (2.12):

$$ds^2 = -dt^2 + a(t)^2 d\vec{x^2} = -dt^2 + e^{2\sqrt{\frac{\Lambda}{3}}t} d\vec{x^2} \tag{2.19}$$

$$= -dt^2 + e^{2t/r_C} d\vec{x^2} = -dt^2 + e^{2t/r_C}(dx^2 + dy^2 + dz^2). \tag{2.20}$$

The following coordinate transformations will clarify the mathematical structure of dS spacetime. First, one can consider the transformation

$$X_0 = r_C \sinh(t/r_C) + r^2 e^{t/r_C}/2r_C, \tag{2.21}$$

$$X_1 = r_C \cosh(t/r_C) - r^2 e^{t/r_C}/2r_C, \tag{2.22}$$

$$X_2 = e^{t/r_C} x, \tag{2.23}$$

$$X_3 = e^{t/r_C} y, \tag{2.24}$$

$$X_4 = e^{t/r_C} z, \tag{2.25}$$

where $r^2 = x^2 + y^2 + z^2$. One notices that the relation

$$-X_0^2 + X_1^2 + X_2^2 + X_3^2 + X_4^2 = r_C^2 \tag{2.26}$$

is fulfilled. The dS spacetime can therefore be represented as a 4-dimensional hyperboloid embedded in a 5-dimensional flat Minkowski spacetime $ds^2 = -dX_0^2 + dX_1^2 + dX_2^2 + dX_3^2 + dX_4^2$. However, these coordinates only cover half of the hyperboloid ($X_0 + X_1 > 0$).

One can also choose another set of coordinates, (t', r', θ, ϕ), and consider the transformation $(t', r', \theta, \phi) \to (X_0, X_1, X_2, X_3, X_4)$ given by:

$$X_0 = \sqrt{r_C^2 - r'^2} \cosh(t'/r_C), \tag{2.27}$$

$$X_1 = \sqrt{r_C^2 - r'^2} \sinh(t'/r_C) \tag{2.28}$$

$$X_2 = r' \sin\theta \cos\phi, \tag{2.29}$$

$$X_3 = r' \sin\theta \sin\phi, \tag{2.30}$$

$$X_4 = r' \cos\theta. \tag{2.31}$$

The coordinates (t', r', θ, ϕ) are called static coordinates and the metric in these coordinates is given by:

$$ds^2 = -f(r')dt'^2 + f(r')^{-1}dr'^2 + r'^2(d\theta^2 + \sin^2\theta d\phi^2), \tag{2.32}$$

where $f(r') = \left(1 - \frac{\Lambda}{3}r'^2\right)$. Static coordinates are relevant for two reasons. First, one sees that the static slicing has a null boundary where $1 - \frac{\Lambda}{3}r'^2 = 0$, i.e. at $r' = r_C = \sqrt{\frac{3}{\Lambda}}$, which corresponds to the position of the cosmological horizon. Second, when a black hole (BH) is present in dS spacetime, their metric is usually presented in terms of them, and the horizon strucuture is more transparent in these coordinates, as we will see later.

Static coordinates are valid only for $r < r_C$, but the singularity at $r = r_C$ in the metric (2.32) is not physical. Coordinate systems in which the metric can be extended analytically to the whole spacetime are, e.g., the "Kruskal coordinates" (U, V, θ', ϕ'). The coordinate transformation $(U, V, \theta', \phi') \to (t', r', \theta, \phi)$ is given by

$$r' = 3^{1/2}\Lambda^{-1/2}(UV + 1)(1 - UV), \tag{2.33}$$

$$e^{2\Lambda^{1/2}3^{-1/2}t'} = -VU^{-1} \tag{2.34}$$

$$\theta = \theta' \tag{2.35}$$

$$\phi = \phi' \tag{2.36}$$

The metric in these coordinates is

$$ds^2 = 3\Lambda^{-1}(UV - 1)^{-2} \cdot \left[-4dUdV + (UV + 1)^2(d\theta^2 + \sin^2\theta d\phi^2)\right]. \tag{2.37}$$

In this work, we are interested in considering BHs in dS spacetime. Therefore, we will not make use of Kruskal coordinates, but we will use the static coordinates for the reasons stated above.

2.2 Black holes in de Sitter universe

In this section, we discuss the BH solutions of the EFE in a non-flat dS background, following [25], [26] and [19]. We start with the simple case of an uncharged non-rotating solution (the Schwarzschild-de Sitter BH) and then move to the more complicated case of an uncharged rotating solution (the Kerr-de Sitter BH), which represents the most astrophysically relevant BH.

2.2.1 Schwarzschild-de Sitter black holes

Schwarzschild-de Sitter (SdS) spacetime is a spherically symmetric uncharged BH solution of the EFE which is described by two parameters: the mass $M \geq 0$ of the BH and the cosmological constant $\Lambda \geq 0$.

In static coordinates, the metric is given by the expression:

$$ds^2 = -f(r)dt^2 + f(r)^{-1}dr^2 + r^2(d\theta^2 + \sin^2\theta d\phi^2), \tag{2.38}$$

where $f(r) = 1 - \frac{2M}{r} - \frac{\Lambda r^2}{3}$. As for dS spacetime, the positions of the event horizons correspond to the coordinate singularities of the metric (2.38), which are given by the solutions of the equation:

$$f(r) = 1 - \frac{2M}{r} - \frac{\Lambda r^2}{3} = 0. \tag{2.39}$$

Equation (2.39) is a truncated cubic equation and generally yields three complex roots. In order for the solutions of (2.39) to represent physical positions, they must be real. The condition for this to happen is $0 \leq \Lambda \leq 1/(9M^2)$, which means that, for a fixed value of M, the value $\Lambda_{\max}(M) = 1/(9M^2)$ gives an upper bound for the value of the cosmological constant[3]. However, even if this condition is satisfied, only two of these three solutions are positive. The smaller positive solution, r_+, represents the black hole event horizon (BEH), while the larger one, r'_+, corresponds to the CEH. The negative solution has no physical meaning. For $\Lambda < \Lambda_{\max}(M)$, then the two positive solutions are distinct and $r_+ < r'_+$, i.e. the size of the BEH is smaller than the size of the CEH. If $\Lambda = \Lambda_{\max}(M)$, the two horizons coincide, i.e. $r_+ = r'_+$, and the BH is said to be extremal.

2.2.2 Kerr-de Sitter black holes

The axially symmetric uncharged solution of the EFE representing a rotating BH in dS spacetime is called Kerr-de Sitter (KdS) BH. It is described by three parameters: the mass $M \geq 0$, the spin parameter $a = J/M \geq 0$ (J is the angular momentum, which we choose to be positive) and the cosmological constant $\Lambda \geq 0$.

In Boyer-Lindquist coordinates, the metric takes the form

$$\begin{aligned} ds^2 = &-\frac{\Delta_r}{(1+\alpha)^2\rho^2}(dt - a\sin^2\theta d\phi)^2 \\ &+ \frac{\Delta_\theta \sin^2\theta}{(1+\alpha)^2\rho^2}\cdot\left[adt - (r^2+a^2)d\phi\right]^2 + \rho^2\left(\frac{dr^2}{\Delta_r} + \frac{d\theta^2}{\Delta_\theta}\right), \end{aligned} \tag{2.40}$$

[3]Or, equivalently, for a fixed value of Λ, the value $M_{\max}(\Lambda) = 1/(3\sqrt{\Lambda})$ gives an upper bound for the BH mass. Note that, if $\Lambda = 0$, the black hole's mass M has no upper limit. Since M determines the size of the black hole's horizon, a positive cosmological constant has the effect to restrict the size of the universe.

Throughout the report, we will often fix a value of M and allow the value of Λ to vary, even if we know that, to study astrophysical BHs, we should do the opposite. However, as we will also discuss in section 2.3, fixing M and varying Λ is equivalent to fixing Λ and varying M. We choose the first possibility because it will allow us to compare BHs in dS background with BHs in Minkowski background ($\Lambda = 0$) in a more convenient way.

where

$$\Delta_r = (r^2 + a^2)\left(1 - \frac{\alpha}{a^2}r^2\right) - 2Mr, \tag{2.41}$$

$$\Delta_\theta = 1 + \alpha\cos^2\theta, \tag{2.42}$$

$$\rho^2 = r^2 + a^2\cos^2\theta, \tag{2.43}$$

$$\alpha = \frac{\Lambda a^2}{3}. \tag{2.44}$$

We now study the limits of the metric (2.41) for $a \to 0$, $M \to 0$ and $\Lambda \to 0$. In the limit $a \to 0$, one sees that the metric (2.41) becomes the SdS metric (2.38). In the limit $\Lambda \to 0$, the KdS metric reduces to the KM metric (cf. [28]):

$$\begin{aligned} ds^2 = &-\left(1 - \frac{2Mr}{\Sigma}\right)dt^2 + \frac{\Sigma}{\Delta}dr^2 + \Sigma d\theta^2 \\ &+ \left(r^2 + a^2 + \frac{2Mra^2}{\Sigma}\sin^2\theta\right)\sin^2\theta d\phi^2 - \frac{2Mra\sin^2\theta}{\Sigma}dtd\phi, \end{aligned} \tag{2.45}$$

where

$$\Sigma = r^2 + a^2\cos^2\theta, \tag{2.46}$$

$$\Delta = r^2 - 2Mr + a^2. \tag{2.47}$$

This metric has coordinate singularities where $\Delta = 0$, i.e. for $r_\pm = M \pm \sqrt{M^2 - a^2}$, which are the positions of the inner and outer BEH. Finally, in the limit $M \to 0$, the KdS metric (2.41) reduces to the metric

$$\begin{aligned} ds^2 = &(r^2 + a^2\cos^2\theta)\left[\frac{dr^2}{(r^2 + a^2)(1 - \frac{\Lambda r^2}{3})} + \frac{d\theta^2}{1 + \frac{\Lambda}{3}a^2\cos^2\theta}\right] \\ &+ \sin^2\theta\frac{1 + \frac{\Lambda}{3}a^2\cos^2\theta}{r^2 + a^2\cos^2\theta}\left[\frac{adt - (r^2 + a^2)d\phi}{1 + \frac{\Lambda}{3}a^2}\right]^2 \\ &- \frac{(r^2 + a^2)(1 - \frac{\Lambda r^2}{3})}{r^2 + a^2\cos^2\theta}\left[\frac{dt - a\sin^2\theta d\phi}{1 + \frac{\Lambda}{3}a^2}\right]^2. \end{aligned} \tag{2.48}$$

This metric is the dS metric in Boyer-Lindquist coordinates. These coordinates can be "untwisted" by the following coordinate transformation

$$\begin{gathered} T = \frac{t}{1 + \frac{\Lambda}{3}a^2}, \quad \bar{\phi} = \phi - \frac{a\Lambda t}{3(1 + \frac{\Lambda}{3}a^2)}, \quad y\cos\Theta = r\cos\theta \\ y^2 = \frac{1}{1 + \frac{\Lambda}{3}a^2}\left[r^2\Delta_\theta + a^2\sin^2\theta\right] \end{gathered}, \tag{2.49}$$

and one obtains the dS metric in the known form (static coordinates):

$$ds^2 = -\left(1 - \frac{\Lambda y^2}{3}\right)dT^2 + \frac{1}{1 - \frac{\Lambda y^2}{3}}dy^2 + y^2(d\Theta^2 + \sin^2\Theta d\bar{\phi}^2). \tag{2.50}$$

To understand the horizon structure of the KdS spacetime, one can look for the locations of the apparent radial singularities of the metric (2.41), in the same way as it was done for the SdS case. The position of the event horizons is then given by the equation:

$$\Delta_r = (r^2 + a^2)\left(1 - \frac{\alpha}{a^2}r^2\right) - 2Mr = 0. \tag{2.51}$$

This equation is a quartic equation and generally yields four complex solutions. As before, the solutions are required to be all real in order to represent positions. Even in the case of four real solutions, equation (2.51) gives only three positive roots. Real roots can be written in ascending order

$$r'_- < r_- < r_+ < r'_+, \tag{2.52}$$

where r'_- is the negative root and has no physical meaning, r_- represents the position of the inner BEH, r_+ is the position of the outer BEH and r'_+ is the position of the CEH.

If we fix a value of M and a, for example, the condition for the solutions to be real translates into two relations, which determine an upper bound and a lower bound for the value of Λ.
The upper bound for the value of Λ, which we call $\Lambda_{\max} = \Lambda_{\max}(a, M)$, must satisfy the following relation:

$$\begin{aligned} 0 = &\left[\frac{1}{\Lambda_{\max}}(1 - \alpha_{\max}) - 4a^2\right]^3 \\ &- \frac{1}{\Lambda_{\max}}\left[(1 - \alpha_{\max})\left[\frac{1}{\Lambda_{\max}}(1 - \alpha_{\max})^2 + 12a^2\right] - 18M^2\right]^2, \end{aligned} \tag{2.53}$$

where $\alpha_{\max} = \Lambda_{\max}a^2/3$. For $\Lambda = \Lambda_{\max}$, the outer BEH and the CEH coincide ($r_+ = r'_+$) and the BH is extremal.
The second condition, which determines a lower bound for Λ, reflects another extremal case where the inner and the outer BEHs coincide, i.e. when $r_- = r_+$. Since $r_\pm$ are roots of the fourth order polynomial $\Delta_r(r)$, the only possibility to have $r_+ = r_-$ is when the two roots merge at a local extremum of $\Delta_r(r)$ (cf. [25]). The lower bound $\Lambda_{\min} = \Lambda_{\min}(a, M)$ must then satisfy the equation

$$\partial_r \Delta_r(r = r_\pm) = 0. \tag{2.54}$$

This equations gives positive solutions for $\Lambda_{\min}$ only for $a > 1$. We therefore consider $\max\{0, \Lambda_{\min}(a, M)\}$ as a lower bound for Λ at fixed a and M.

These results are summarized in Figure 1. Here, we choose units[4] of $M = 1$ and plot $\Lambda_{\max}$ (in blue) and $\Lambda_{\min}$ (in red) as functions of the spin parameter

[4]See section 2.3 for a more detailed discussion about the units and scale system.

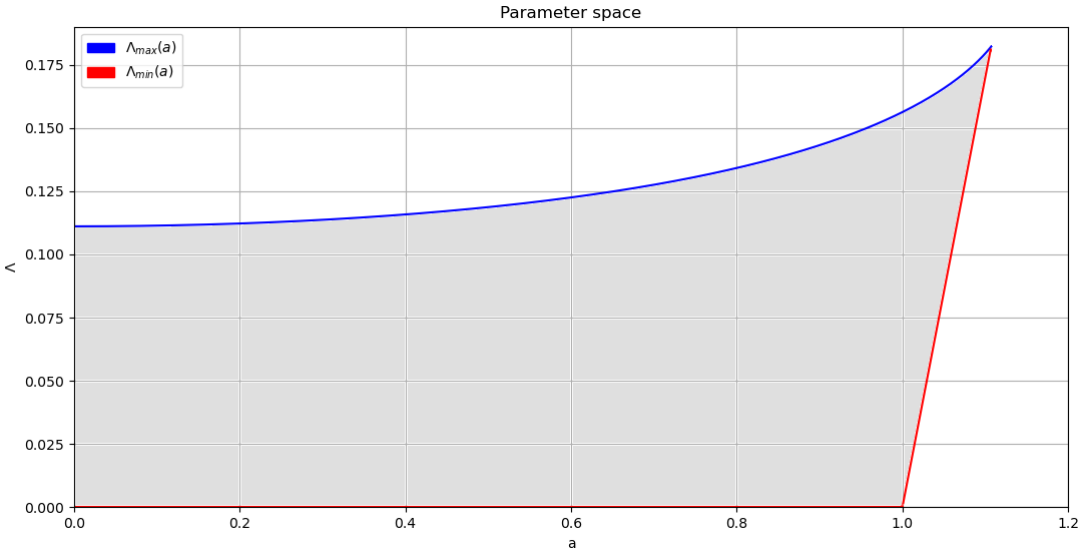

Figure 1: Here, we plot $\Lambda_{\rm max}$ and $\Lambda_{\rm min}$ versus the spin parameter a in units of $M = 1$. The grey region represents the parameter space for BH solutions.

a. The grey region contains all pairs (Λ, a) for which $\Lambda > 0$ and for which equation (2.51) has four distinct real solutions. Hence, it represents the space of parameters for which a BH solution exists. The blue line represents the extremal case $r_+ = r'_+$. For $a > 1$, the red line represents the extremal case $r_- = r_+$, while for $a \leq 1$ it represents the $\Lambda = 0$ (KM) case. The point where the blue line meets the red line is the triply degenerate limit of KdS, where the three horizons coincide ($r_- = r_+ = r'_+$).

We check that in the limit $a \to 0$, equation (2.53) yields $\Lambda_{\rm max} = 1/(9M^2)$ (which is equal to $0,\bar{1}$ in units of $M = 1$) that corresponds to the upper bound of the SdS case. In the limit $\Lambda \to 0$, one obtains $a_{\rm max}(\Lambda) = M$ (equal to 1 in units of $M = 1$), which is the upper bound for the spin parameter in the KM case. We note that a BH solution with a spin $a > M$ is only possible in presence of a non-zero cosmological constant, and that if the cosmological constant exceeds $1/(9M^2)$, a BH solution is only possible if the BH is spinning.

We conclude the discussion about the horizons structure with a remark on the comparative horizon size of the empty dS, the SdS and the KdS BHs. We report here a list of results derived in Appendix A of [26]:

- The increase of M (holding a and Λ fix) increases the size of the BEHs but decreases the size of the CEH.
- The increase of Λ (holding a and M fix) increases the size of the BEHs but decreases the size of the CEH.
- The increase of a (holding M and Λ fix) decreases the size of the BEHs but increases the size of the CEH.

Therefore, the CEH of empty dS spacetime is not at $r_C = \sqrt{3/\Lambda}$ anymore when a BH is present. In the same way, the event horizons of a Kerr BH are not in the same position ($r_\pm = M \pm \sqrt{M^2 + a^2}$) anymore in presence of a non-zero cosmological constant.

From the considerations reported in this section, we see that the horizon structure of the KdS spacetime only depends on the parameters M, Λ and a. In the next section, we analyze how these parameters set the scale of the problem and we discuss a choice of units suitable for our purposes.

2.3 Scales and units

When dealing with the spacetimes which we have discussed above, the relevant quantities are the mass M of the BH, the cosmological constant Λ and the BH's spin parameter a (which determine the position of the horizons). Another important quantity for this work, which we include in our discussion on units, is the frequency ω of the so-called quasinormal modes, which will be defined in the next section.

Throughout this report, we make use of geometrized units ($G = c = 1$). In this unit system, the mass and the spin parameter have the geometric dimension of a length (L), the frequency has dimension L^{-1} and the cosmological constant has dimension L^{-2}. We denote by a, ω, M and Λ (without any subscript) the quantities expressed in these units. Depending on the spacetime considered, other quantities besides G and c can be set to unity in order to simplify the notation and to make the problem scale-invariant. In the following, we fix a value of the spin parameter a and discuss the possible length scales of the various spacetimes.

In the KM spacetime, for fixed a, the only length scale is given by the mass M, which determines the position of the event horizons. Therefore, setting $M = 1$ is equivalent to rescaling all the quantities by the mass in geometrized units. If we denote by a_M and ω_M the quantities in these units, this means that $a_M = a/M$ and $\omega_M = \omega M$. All the quantities become therefore adimensional and scale-invariant. Note that all KM BHs can be scaled into each other.

In dS spacetime, the length scale is given by the position of the CEH $r_C = \sqrt{3/\Lambda}$ (cf. above and [25]). For this reason, it makes sense to set $r_C = 1$, i.e. $\Lambda = 3$ (as in [19]). This is equivalent to rescaling all the quantities by r_C. If we denote with ω_Λ the frequency in these units, we have $\omega_\Lambda = \omega r_C$.

If one considers KdS spacetime, the situation becomes slightly more complicated, because the spacetime is characterized by the relative position of the BEH and of the CEH, and it is not possible to define a single length scale. For this reason, either the BH mass or the position of the CEH can be chosen as a scale for the problem. Setting $r_C = 1$ (choosing r_C as a length scale) is equiv-

alent to writing $a_\Lambda = a/r_C$, $M_\Lambda = M/r_C$ and $\omega_\Lambda = \omega r_C$, while setting $M = 1$ (choosing M as a length scale) is equivalent to writing $a_M = a/M$, $\omega_M = \omega M$ and $\Lambda_M = \Lambda M^2$ (the subscripts Λ and M denote the quantities expressed in units of $r_C = 1$ and $M = 1$, respectively, as we have defined above).

Depending on the situation, either one or the other unit system is more convenient. If we are interested in studying BHs with fixed mass for $\Lambda \to 0$, we choose the $M = 1$ system. In fact, $r_C = 1$ units are not suitable in this case, because some quantities such as the frequency would tend to infinity as $\Lambda \to 0$ in this unit system[5]. Conversely, if we want to study a spacetime characterized by a fixed value of Λ containing BHs with very small masses, we choose $r_C = 1$ units, because some quantities such as the spin parameter tend to infinity[6] as $M \to 0$. In cases where we do not intend to study these limits, both systems are good.

In KdS spacetime, for fixed a, the quantity ΛM^2 (or M/r_C, which corresponds to $\sqrt{\Lambda M^2/3}$) characterizes the spacetime in the sense that it contains information about the relative positions of the horizons. This means that BH solutions with the same value of ΛM^2 can be scaled one into the other. Note that the case $\Lambda M^2 = 0$ describes both KM (which is KdS in the limit $\Lambda \to 0$, as we have seen), dS universe (which is KdS in the limit $M \to 0$) and Minkowski spacetime ($M = \Lambda = 0$).

In the following, we are interested in studying quasinormal mode frequencies of KdS spacetime for $M \neq 0$. Since all the quantities which are relevant for this problem scale with the BH mass, we can define an equivalence relation by saying that two BH solutions are equivalent if they can be scaled into each other. From this definition, it follows that all KM BHs are equivalent to each other, while KdS BHs can be subdivided into equivalence classes labeled by the value of ΛM^2 (KM BHs form the equivalence class with $\Lambda M^2 = 0$). Note that this definition only makes sense for problems which scale with the BH mass M and with the cosmological constant Λ, but not for other kinds of problems. For example, as mentioned also in [29], if we were studying the emission of determined massive particle species (characterized by a specific mass) by BHs due to Hawking radiation, the problem would not scale with M, because the mass of the particles is fixed for a particle species and does not scale with the black hole's mass. Therefore, in this case, it would not make sense to define this equivalence relation.

[5] $\lim_{\Lambda\to 0} \omega_\Lambda = \lim_{\Lambda\to 0} \omega r_C = \lim_{\Lambda\to 0} \omega\sqrt{3/\Lambda} = \infty$.

[6] $\lim_{M\to 0} a_M = \lim_{M\to 0} a/M = \infty$.

2.3.1 Astrophysical black holes

In our work, we want to study astrophysical BHs. For this purpose, we need to determine the equivalence class, as defined above, to which they belong. To do this, we estimate the value of ΛM^2 that characterizes them.

Astrophysical black holes have masses between 10^{-1} and 10^9 solar masses, which in geometrized units corresponds to

$$\begin{aligned}(10^{-1} - 10^9)M_\odot &= (10^{-1} - 10^9) \cdot 1.989 \cdot 10^{30}\, kg \cdot \frac{G}{c^2}\frac{m}{kg} \\ &\sim (10^2 - 10^{12})\, m,\end{aligned} \tag{2.55}$$

where we have used that $M_\odot = 1.989 \cdot 10^{30}$ is the mass of the sun, G is the gravitational constant and c is the speed of light. Observations suggest that the cosmological constant has a value of $\Lambda \sim 10^{-52}\, m^{-2}$ in geometrized units (cf. (2.16)). Therefore, for astrophysical black holes, we expect

$$\Lambda M^2 \sim 10^{-48} - 10^{-28}. \tag{2.56}$$

The values of ΛM^2 for some types of astrophysical BHs are reported in Table 1.

BH type	BH mass (in $M_\odot$ units)	Value of ΛM^2
sub-solar mass BH	10^{-1}	10^{-48}
stellar mass BH	10	10^{-44}
intermediate BH	10^4	10^{-38}
supermassive BH	10^9	10^{-28}

Table 1: Values of ΛM^2 for four types of astrophysical black holes.

3 Quasinormal modes of black holes in de Sitter spacetime

3.1 Introduction on quasinormal modes

When a black hole undergoes a gravitational, electromagnetic or scalar perturbation, the time evolution of the initial displacement from its equilibrium state is dominated at late times by 'quasinormal modes' (henceforth QNMs), damped oscillations with single complex frequencies whose real and imaginary parts represent the oscillation frequency and the damping rate, respectively. The 'normal' part in the name refers to the close analogy to normal modes (although there are some important differences), while the 'quasi' expresses the fact that they are not stationary in time, as normal modes are, but are strongly damped. These oscillations involve the spacetime metric between the black hole horizon and the cosmological horizon (or spatial infinity, if no CEH is present, i.e. if $\Lambda = 0$).

According to the no-hair theorem in standard general relativity, the QNM frequencies only depend on the parameters of the black hole (mass, angular momentum and charge), but they are independent of the initial perturbation that excited them, which only affects their amplitude. It was first shown by Otsuki and Futamase in [13] that they also depend on the value of the cosmological constant Λ.

In this section, which is taken from Nollert [30], Chandrasekhar [31] and from Yoshida, Uchikata and Futamase [19], we define QNMs and explain how to derive them in a general case. In particular, we focus on gravitational perturbations. Typically, one is interested in studying the gravitational QNMs emitted after the coalescence of two compact objects while settling down to a BH, in a stage called "ringdown" ([32]).

QNMs are a concept that arises from linearized perturbation calculations. Hence, the starting point to derive them is perturbation theory. For gravitational perturbations, the standard method to apply consists in regarding the metric as the sum of the unperturbed background metric $\bar{g}_{\mu\nu}$ and a perturbation $h_{\mu\nu}$ ($|h_{\mu\nu}| \ll 1$):

$$g_{\mu\nu} = \bar{g}_{\mu\nu} + h_{\mu\nu}, \tag{3.1}$$

inserting this ansatz into the Einstein field equations and keeping terms up to the first order in $h_{\mu\nu}$. However, this method is not convenient for the study of BH perturbations, since the calculations become too complicated. Instead, one prefers to make use of the Newman-Penrose tetrad formalism[7] to obtain

[7] We do not describe this formalism in detail, but we refer the reader to chapters 7 and

the master equations of linear perturbations. In this formalism, gravitational perturbations are described by the Newman-Penrose scalar quantities:

$$\Psi_0 := -C_{\mu\nu\lambda\sigma} l^\mu m^\nu l^\lambda m^\sigma, \tag{3.2}$$

$$\Psi_4 := -C_{\mu\nu\lambda\sigma} n^\mu \bar{m}^\nu n^\lambda \bar{m}^\sigma, \tag{3.3}$$

where $C_{\mu\nu\lambda\sigma}$ is the Weyl tensor. These quantities encode all information about the gauge invariant part of the ingoing and the outgoing radiation, respectively. In this work, we only focus on the outgoing part, described by Ψ_4.

The gravitational perturbation of a KM BH is described by a second-order partial differential equation. In general, the master equations for linear perturbations on a stationary and axially symmetric spacetime are not separable into ordinary differential equations for each variable. One surprising fact, which was first shown by Teukolsky [33], is that BHs are an exception. Because of the spacetime symmetries, the variables time t and azimuthal angle φ only contribute to the perturbation amplitude with a phase factor $e^{-i\omega t} e^{im\varphi}$, where ω is the complex QNM frequency. The remaining variables can then be separated by making the following ansatz:

$$\Psi = R(r) S(\theta) e^{-i\omega t + im\varphi}. \tag{3.4}$$

After inserting this ansatz in the master equations, one obtains two ordinary differential equations, which are named the Teukolsky equations. Thanks to these equations, together with appropriate boundary conditions, one can calculate the QNMs of a KM BH. The same applies to KdS BHs, as was shown in [19].

The handling of the QNM problem is to some extent similar to the study of normal modes. In normal-mode analysis, one usually has a system of ordinary differential equations and imposes boundary conditions such that the solutions must vanish outside a finite region of space. However, perturbations of black holes are different. In fact, the region which one considers is the metric between the BEH and the CEH (or spatial infinity), but the perturbations propagate throughout all space and cannot be zero outside a finite region. Instead, one requires the perturbation to be purely ingoing at the BEH and purely outgoing at the CEH (or at spatial infinity). These boundary conditions, applied to the radial Teukolsy equation, reflect the physical fact that nothing can escape from the BH horizon or come in through the CEH. If the CEH is not present, the condition simply means that one does not want gravitational radiation unrelated to the original perturbation to come from spatial infinity and disturb the system.

8 of [31] for a complete handling.

Another important difference between QNMs and normal modes is that quasinormal modes do not form a complete basis set for the space of solutions, in general, while normal modes do. Therefore, it is not possible to describe the time evolution of any initial perturbation as a superposition of such quasinormal modes. However, a signal may be analysed in terms of quasinormal modes, in the attempt to extract parameters such as frequency and damping factor.

The QNMs are labeled with quantum numbers (s, l, m), where s is the spin weight (which is related to the spin S by $S = |s|$), m is the azimuthal quantum number and l is an integer satisfying $l \geq \max(|s|, |m|)$, which is called angular quantum number. This is due to the fact that, mathematically, their angular part is represented by spin-weighted spheroidal harmonics (cf. Appendix A). As shown by Leaver [12], for each set of angular quantum numbers (s, l, m), a black hole possesses an infinite number of QNM frequencies $\{\omega_{nlm} : n = 0, 1, 2, ...\}$. These are labeled by an additional quantum number n, that be interpreted as the radial mode number, and the frequencies are labeled by the rule $|\mathrm{Im}(\omega_{(n+1)lm})| > |\mathrm{Im}(\omega_{nlm})|$ at the limit $a \to 0$. This means that the fundamental mode ($n = 0$) has the smallest damping factor and therefore predominates the QNM evolution at late times.

The QNM spectrum of KM, depicted in Figure 2, is very well known. Let us revise it and comment on its features.

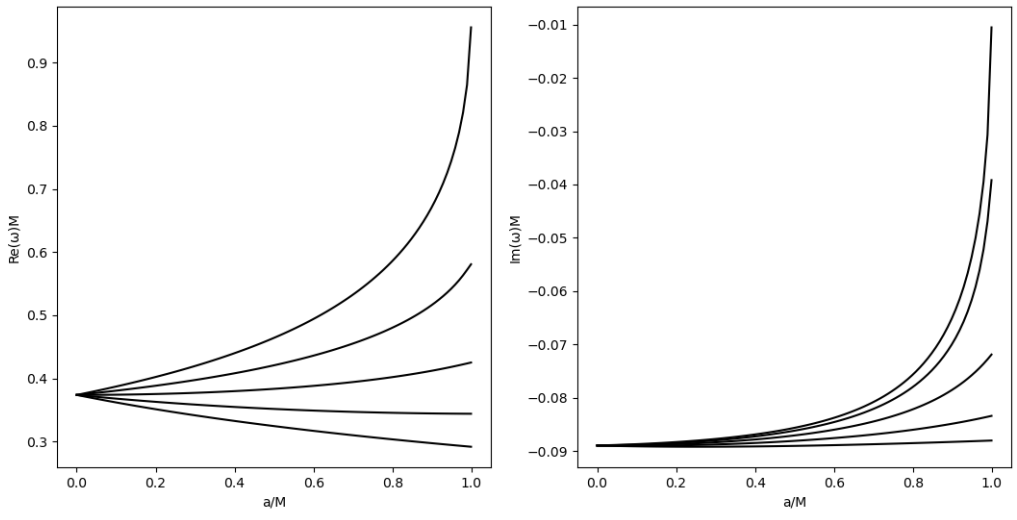

Figure 2: QNM spectrum representing the $(s, l) = (-2, 2)$ mode of a KM BH. This plot was generated using the 'qnm' package for Python [34] (cf. Appendix C).

As mentioned in [19], the effects of the BH rotation on the KM QNM spectrum can be summarized as follows:

- At $a = 0$ and for a given value of l, the frequencies do not depend on the value of the azimuthal quantum number m.

- When increasing a, the azimuthal degeneracy is resolved in a way that resembles the Zeeman splitting, and the dependency on m appears. The real part of the modes associated to positive values of m increases significantly, while the real part of those having $m < 0$ decreases slowly. The imaginary part of modes associated to $m > 0$ increases rapidly, making the modes less damped, while the imaginary part of modes with $m \leq 0$ increases less significantly.

Yoshida, Uchikata and Futamase define the modes with negative m as "retrograde", suggesting that the decrease in the real part of the frequency with increasing spin is due to frame dragging effect caused by the rotation of the system, similarly to what happens in presence of the Coriolis force in Newtonian mechanics. Inspired by this hint, we attempt to give a more precise explanation of the phenomenon.

We begin by briefly reminding the reader of the frame-dragging effect (cf. chapter 33.4 of [1] for a more detailed discussion). As it is well known, the KM metric is given in Boyer-Lindquist coordinates as in (2.45) with respect to an observer lying infinitely far away from the BH, who is at rest with respect to the "fixed stars". With respect to this reference system, the local inertial frame at radius r rotates with an angular velocity given by (cf. eq. (7) in [19]):

$$\Omega(r) = \frac{a}{r^2 + a^2}. \tag{3.5}$$

We note that, because of the way it is defined in (3.4), the frequency ω is directly related to the angular phase velocity of the wave pattern revolving the axis with respect to the observer at infinity (as it was already suggested in [19]). This can be seen by rewriting the phase factor in (3.4) as:

$$e^{im\varphi - i\omega t} = e^{-\mathrm{Im}(\omega)t} e^{i(m\varphi - \mathrm{Re}(\omega)t)}. \tag{3.6}$$

Here, m acts as a wavenumber and $\mathrm{Re}(\omega)$ as an angular frequency. Therefore, the angular phase velocity with respect to the observer at infinity Ω_∞ can be expressed as $\Omega_\infty = \mathrm{Re}(\omega)/m$. Note that, once a positive direction (clockwise or counterclockwise) is fixed, this also determines the sign of m and hence the direction of the wave pattern. Modes associated to positive (negative) values of m have positive (negative) angular velocity, and therefore the wave pattern associated to them moves in (positive) negative direction ("prograde" and "retrograde" motion, respectively). For $m = 0$, the dependence of the wave on φ disappears, and so the wave pattern becomes constant in space (for fixed r, θ and t). Note that, as we have seen above, reversing the direction of

positive rotation is a symmetry which leaves the phase velocity, as well as the damping factor, invariant[8].

If the BH is non-rotating, one sees that the real part of all modes is the same. If the BH has a non-zero spin, then, due to frame-dragging effect, all modes would have the same $\mathrm{Re}(\omega)$ only with respect to a local observer near the BH, which rotates with the same angular velocity as the BH[9], but not with respect to the global system defined by (2.45). For the latter observer, the velocity of the frame is summed to the one of the modes and, since the $\mathrm{Re}(\omega)$ correspond to the observed phase velocity divided by m, the frequencies of the various modes are not the same anymore. To see this, we can write the angular velocity of the m-mode in the local frame at radius r, $\bar{\Omega}(r)$, as

$$\bar{\Omega}(r) = \Omega_\infty - \Omega(r), \tag{3.7}$$

or

$$\omega = \bar{\omega}(r) + m\Omega(r) = \bar{\omega}(r) + m\frac{a}{r^2+a^2}, \tag{3.8}$$

where $\bar{\omega}(r) = m\bar{\Omega}(r)$ (also note that $\lim_{r\to\infty}\bar{\omega}(r) = \omega$). Equation (3.8) also appears in [19]. From this equation, the dependence of the real part of the QNM frequencies on m becomes clear. In fact, a local observer which lies at a small radius r will rotate with an angular velocity $\bar{\omega}(r)$ which is similar to the one of the BH. From his point of view, the BH will appear to be close to a Schwarzschild BH, and he would not see the splitting in the frequencies. So, $\bar{\omega}(r)$ would not depend on m. The splitting as observed in the system defined by (2.45) is then due to the $ma/(r^2+a^2)$ term, which causes the frequency of the modes associated to negative m's to decrease, while the frequency associated to positive m's to increase as a increases (at least from $a = 0$ to $a = r$).

The imaginary part of the spectrum, which represents the damping factor as a function of a, splits in a way similar to real part, but the values always remain negative. Unlike for the real part, we do not know a physical explanation for the splitting.

3.2 Motivation and goal

There are two main motivations to study QNMs of a BH: The first one is that they allow to determine whether the spacetime is stable under perturbations

[8]The QNMs of the KM BH ([12]) and the ones of the KdS BH ([19]) present the symmetry $(\omega, m) \to (-\omega^*, -m)$, which means that the two QNMs characterized by the same phase velocities of the wave pattern revolving the symmetry axis, $\mathrm{Re}(\omega)/m$ and $\mathrm{Re}(-\omega^*)/-m$, and the same damping time $\mathrm{Im}(\omega)$ and $\mathrm{Im}(-\omega^*)$, are identical. This is clear from a physical point of view, and will become clear also mathematically once we will write the Teukolsky equations explicitly. Because of this symmetry, one normally considers only the modes whose real part of the frequency is positive in the limit $a \to 0$.

[9]although we are not sure whether this is possible.

or not, the second is that they contain information about the fundamental parameters of the BH solution, such as M, a and Λ.

To study the stability, one assumes a harmonic time dependence $e^{-i\omega t}$ of the perturbations (this is possible since all spacetimes considered are stationary, as mentioned above), where ω is the complex QNM frequency. If $\mathrm{Im}(\omega)$ is negative, the amplitude decays in time and the spacetime is stable under the considered perturbation. If $\mathrm{Im}(\omega) = 0$, the oscillations are not damped and the spacetime is said to be neutrally stable. If $\mathrm{Im}(\omega)$ is positive, the amplitudes of the solutions grow exponentially in time and the spacetime is said to be unstable. The stability of the SM and KM BH has been studied ([35], [2], [36], [37]) and it has been shown that these types of BHs are stable under gravitational perturbations. For the KdS BH, the stability under gravitational and electromagnetic perturbations was studied in [19], and no unstable modes were found.

To extract information about the fundamental parameters of the BH from the complex QNM frequencies, one needs to know the QNM frequency spectrum of the considered spacetime model as a function of M and a, which can be determined numerically.

Currently, one assumes the spacetimes to be asymptotically Minkowski and uses the known KM spectrum, depicted in Figure 2, to infer the BH parameters from the detected QNM frequencies. As discussed in section 2.3, for a fixed value of ΛM^2 ($\Lambda M^2 = 0$ for KM BH), the frequency and the angular momentum scale with the BH mass. Therefore, if one knows one or more complex frequencies with sufficient accuracy, the mass and the angular momentum of the BH can be determined from the spectrum.

However, observational tests suggest that the spacetime is not asymptotically flat, and therefore one should consider the spectrum of KdS QNMs rather than the KM one as a model to recover the BH parameters. Such a spectrum was first determined in [19] for some values of ΛM^2, but not for the values corresponding to astrophysical BHs (see Table 1).

In this work, we aim to quantify the effects of assuming a KdS model instead of a KM one to determine mass and angular momentum of astrophysical BHs. To do this, we first need to compute the QNM frequency spectra of KdS BHs described in Table 1. Then, we need to study how these spectra differ from the KM QNM spectrum qualitatively and quantitatively, and whether these differences are measurable with the existing gravitational wave detectors. If it was the case, then the mass and the angular momentum of astrophysical BHs should be computed using the KdS QNM model instead of the KM one to obtain more accurate values.

To study qualitative differences, we have to plot the spectra corresponding

to the different cases in the same graph. Since we want to compare the case $\Lambda M^2 = 0$ to the cases of Table 1, it is convenient to make use of units of $M = 1$. We therefore plot $\omega_M = \omega M$ versus $a_M = a/M$ to obtain the spectra, like in Figure 2.

Once the QNM spectra as a function of M, a and Λ is determined, we quantify the differences between them. Concretely, we proceed in the following way: We first choose two modes with large amplitude[10], like e.g. $(l = 2, m = 2)$ and $(l = 3, m = 3)$ and, for fixed M and a, we compute:

$$\Delta_\Lambda := |\omega_{(2,2)}(\Lambda) - \omega_{(3,3)}(\Lambda)|, \tag{3.9}$$

where $\omega_{(l,m)}(\Lambda)$ indicates the complex QNM frequency of the (l, m) mode at a given value of Λ. We compute this for $\Lambda = 0$ and for $\Lambda = \Lambda_{obs} \sim 10^{-52} m^{-2}$ and for the BH masses of Table 1. Then, we determine whether the difference

$$\Delta := |\Delta_{\Lambda=0} - \Delta_{\Lambda=\Lambda_{obs}}| \tag{3.10}$$

is measurable or not[11].

In the next sections, we describe in detail how QNMs of BHs in a dS background can be derived and computed numerically, and we apply these numerical methods to solve the problems described above. We begin by discussing the SdS case and then move to the more general case of KdS QNMs. The reason why we start with SdS, which is a special case of KdS, is that it represents the easiest case. Moreover, the SdS QNM frequencies will be used as starting values for numerical algorithms that allow to compute the KdS QNM frequencies. After this, in section 3.5, we will discuss the measurability of the above mentioned frequency differences.

3.3 Schwarzschild-de Sitter spacetime

In this section, we investigate QNMs of SdS spacetime following Otsuki and Futamase [13], Ferrari and Mashhoon [11] and Zhidenko [38].

We begin by presenting how to obtain the master equations using Newman-Penrose formalism and then focus on their solutions.

[10] As explained in [32], the ringdown phase is dominated by the mode $(2, 2)$, also called dominant mode. Depending on the mass ratio of the compact objects that merged forming the BH, the $(3, 3)$ mode can become the subdominant mode with highest amplitude, and hence the easiest to detect with high accuracy.

[11] As mentioned above, if one assumes the black hole to be KM, to every measured difference $|\omega_{(2,2)} - \omega_{(3,3)}|$ one can associate a value of (M, a). However, if the difference Δ is resolvable, the cosmological constant cannot be neglected. In this case, the same values of (M, a) must be associated to a different Λ or, equivalently, to a measured value of $|\omega_{(2,2)} - \omega_{(3,3)}|$ one must associate different values of (M, a).

For applying perturbation theory, a convenient choice of the tetrad basis is represented by the principle Newman-Penrose null tetrad $(l^\mu, n^\mu, m^\mu, \bar{m}^\mu)$:

$$l^\mu = \left(\left(1 - \frac{2M}{r} - \frac{\Lambda r^2}{3} \right)^{-1}, 1, 0, 0 \right), \tag{3.11a}$$

$$n^\mu = \left(\frac{1}{2}, -\frac{1}{2} \left(1 - \frac{2M}{r} - \frac{\Lambda r^2}{3} \right), 0, 0 \right), \tag{3.11b}$$

$$m^\mu = \frac{1}{\sqrt{2}r} \left(0, 0, 1, \frac{i}{sin\theta} \right), \tag{3.11c}$$

$$\bar{m}^\mu = m^{*\mu}. \tag{3.11d}$$

where $m^{*\mu}$ indicates the complex conjugate of m^μ. As explained in section 3.1, Newman-Penrose formalism allows to obtain master equations for the gravitational perturbations, described by the scalars Ψ_0 and Ψ_4 defined in (3.2) and (3.3). These quantities are characterized by the spin weights $s = 2$ and $s = -2$, respectively. To underline this, one can define the so called Teukolsky wave-function ψ_s for $s = \pm 2$ as

$$\begin{aligned} \psi_2 &= \Psi_0, \\ \psi_{-2} &= \rho^{-4} \Psi_4, \end{aligned} \tag{3.12}$$

where $\rho = \sqrt{r^2 + a^2 \cos^2 \theta}$. For the moment, we keep the subscript s, but later we will focus only on the mode $s = -2$, representing outgoing gravitational radiation. As we have mentioned in section 3.1, the separation of variables is achieved with the following ansatz:

$$\psi_s = {}_sR_l^m(r) {}_sS_l^m(\theta) e^{-i\omega t + im\varphi}, \tag{3.13}$$

where ω is the complex QNM frequency and l and m are the angular and the azimuthal quantum numbers, respectively. Henceforth, the subscripts s and l and the superscript m are omitted. After separating the variables, one obtains the angular and radial Teukolsky equations for $R(r)$ and $S(\theta)$. A peculiarity of the SdS case is that, contrary to the KdS case which we will discuss later, the frequency ω is only contained in the radial equation, which can be cast in the simple form

$$\left(\frac{d^2}{dr^{*2}} + \omega^2 - V(r^*) \right) R(r^*) = 0, \tag{3.14}$$

where the effective potential takes the form

$$V(r^*) = f(r) \left(\frac{l(l+1)}{r^2} - \frac{6M}{r^3} \right), \tag{3.15}$$

where $f(r) = 1 - \frac{2M}{r} - \frac{\Lambda r^2}{3}$ and $r = r(r^*)$, where r^* is the tortoise coordinate, which maps $r = r_+$ to $r^* = -\infty$ and $r = r'_+$ to $r^* = +\infty$ and is defined by the transformation

$$dr^* = \frac{dr}{f(r)}. \tag{3.16}$$

The potential (3.15) vanishes at the locations of the two horizons, i.e. for $r^* \to \pm\infty$. The QNMs are defined to be the solutions of (3.14) that satisfy the boundary conditions of purely outgoing waves at infinity and purely ingoing waves at the horizon, and so the radial part must satisfy[12]

$$R(r^*) \propto e^{\pm i\omega r^*}, \text{ for } r^* \to \pm\infty. \tag{3.17}$$

The exact QNM frequencies are usually determined numerically using the so-called *continued fractions method* devised by Leaver [12] (see also Moss and Norman [14] and Yoshida and Futamase [16]). However, an implementation of this method presents some numerical difficulties, as we will discuss later for the more general case of KdS. Another possibility consists in making use of the *Heun's function method*, which we will discuss later for KdS as well. Here, we decide to follow Zhidenko [38] and Ferrari and Mashhoon [11] (see also Moss and Norman [14]), who use the Pöschl-Teller approximation to compute the QNM frequencies analytically. A further possibility, which we do not discuss, consists in applying the WKB approximation (cf. e.g. [13]).

3.3.1 Quasinormal mode frequencies via the Pöschl-Teller potential approximation

This method consists in approximating the potential $V(r^*)$ with a potential of similar shape, for which the solutions of equation (3.14) can be evaluated analytically. This requirement is satisfied by the Pöschl-Teller potential, which has the form

$$V_{PT}(r^*) = \frac{V_0}{\cosh^2\left(\frac{r^*}{b}\right)}, \tag{3.18}$$

where

$$b := \frac{1}{\sqrt{-\frac{1}{2V_0}\frac{d^2V(r_0^*)}{dr^{*2}}}}, \tag{3.19}$$

r_0^* is the position of the maximum of $V(r^*)$ and $V_0 := V(r_0^*)$.

We now follow [11] to show how to compute the QNM frequencies analytically for this approximate potential. The idea is to map equation (3.14) to a Schrödinger-like wave equation, such that the solutions of (3.14) satisfying the boundary condition (3.17) are mapped to bound states of the new equation. The bound states of the Schrödinger equation, as it is well known, can be computed analytically. After computing them, one considers the inverse map and obtains the QNMs.

[12]The reason why we impose exactly this boundary condition will be explained later in the more general case of KdS QNMs (see equation (3.87)).

To do this, one considers the following transformation

$$\begin{aligned} r^* &\to -ir^* \\ (V_0, b) &\to (V_0, -ib). \end{aligned} \tag{3.20}$$

For simplicity, let us denote $p = (V_0, b)$ and $p' = (V_0, -ib)$. It can be easily seen from (3.18) that the potential remains invariant under this transformation

$$V(-ir^*, p') = V(r^*, p). \tag{3.21}$$

One then defines the functions ϕ and Ω such that

$$\phi(r^*, p) = R(-ir^*, p') \tag{3.22}$$

$$\Omega(p) = \omega(p'). \tag{3.23}$$

Then, since

$$\begin{aligned} \frac{d^2}{dr^{*2}}\phi(r^*, p) &= -\frac{d^2}{dr^{*2}}R(-ir^*, p') = (\omega^2(p') - V)R(-ir^*, p') \\ &= (\Omega^2(p) - V)\phi(r^*, p), \end{aligned} \tag{3.24}$$

ϕ satisfies the equation:

$$\frac{d^2\phi}{dr^{*2}} + (-\Omega^2 + V)\phi = 0, \tag{3.25}$$

and the boundary conditions imposed in (3.17) are reduced to

$$\phi(r^*, p) = R(-ir^*, p') \propto e^{\pm i\omega(p')(-ir^*)} = e^{\pm i\Omega(-ir^*)} = e^{\pm \Omega r^*}, \text{ for } r^* \to \pm\infty. \tag{3.26}$$

If one compares equation (3.25) with the time-independent Schroedinger equation (TISE), one sees that, if $\Omega = \mathrm{Re}(\Omega) < 0$, solving equation (3.25) with the boundary conditions (3.26) corresponds to finding the bound states of the TISE, with the potential[13] $-V$, which correspond to the eigenvalues Ω^2.

The bound states of the potential $-V_{PT}$ can be computed analytically and are given by (cf. Appendix A of [11])[14]:

$$\Omega_n(V_0, b) = \frac{1}{b}\left[-\sqrt{\frac{1}{4} + V_0 b^2} + (n + \frac{1}{2})\right], \tag{3.27}$$

[13]Note that QNMs do not necessarily have to satisfy the condition $\Omega = \mathrm{Re}(\Omega) < 0$. However, the ones which do satisfy it can be mapped to bound states of the TISE. Therefore, this method only allows to compute those QNMs for which this condition is satisfied, but not all QNMs.

[14]Because of the fact that we define ω in (3.32) in a different way than in [11], the signs in equation (26) of [11] must be changed.

where $n \geq 0$ is an integer[15]. Since the inverse transformation to (3.20) is

$$\begin{aligned} r^* &\to i r^* \\ (V_0, b) &\to (V_0, ib), \end{aligned} \tag{3.28}$$

the QNMs are obtained from $\Omega_n(V_0, ib)$[16]

$$\omega_n(V_0, b) = \Omega_n(V_0, ib) = \frac{1}{b}\left[\pm\sqrt{V_0 b^2 - \frac{1}{4}} - (n + \frac{1}{2})i\right], \tag{3.29}$$

where we have used that $4V_0b^2 > 1$ (for $4V_0b^2 \leq 1$, $\mathrm{Re}(\omega_n) = 0$, and hence no propagating solution exists).

3.3.2 Implementation

We have implemented a code in *Mathematica* to compute the QNMs frequencies of the SdS BH using the formulae obtained in the previous section.

We consider the potential $V(r)$ of eq. (3.15). Using the fact that $r = r(r^*)$, $\frac{dr}{dr^*} = f(r)$ and the chain rule, we compute $\frac{d^2}{dr^{*2}}V(r)$ as follows:

$$\frac{d^2}{dr^{*2}}V(r) = f(r) \cdot \frac{d}{dr}f(r) \cdot \frac{d}{dr}V(r) + f(r)^2 \cdot \frac{d^2}{dr^2}V(r). \tag{3.30}$$

The location r_0 $(= r_0(r_0^*))$ of the maximum of $V(r)$ and the value of $V(r_0)$ are found numerically using the 'Maximize' function. Then, the parameter b is computed using eq. (3.19), and the quasinormal mode frequencies are computed using eq. (3.29).

In our computations, we use $M = 1$ units and keep 40 digits of precision in all intermediate values in order to reduce the errors due to numerical truncations, as suggested in [38]. The code is reported in Appendix D.1.

3.3.3 Results

For $n = 0$ and $l = 2$, we have computed the QNM frequency as a function of the cosmological constant. The results are plotted in Figure 3 and 4. We have checked our code by comparing our results to the ones reported in [38].

[15]Note that for $n = 0$ (which is the case we are interested in), the condition $\Omega = \mathrm{Re}(\Omega) < 0$ is satisfied.

[16]Here, the "$\pm$" is necessary because we have that $\Omega_n(V_0, ib) = \frac{1}{b}\left[-\sqrt{V_0 b^2 - \frac{1}{4}} - (n + \frac{1}{2})i\right]$, but only if we consider $\omega_n(V_0, b) = \frac{1}{b}\left[\sqrt{V_0 b^2 - \frac{1}{4}} - (n + \frac{1}{2})i\right]$ we can have the inverse transformation with $\omega(V_0, -ib) = \Omega_n(V_0, b)$. The "$\pm$", for what we have understood, reflects the fact that the problem is symmetric under the transformation $(\omega \to -\omega*, m \to -m)$, as we have seen in section 3.1. Therefore, we are free to choose the sign, and in the following we choose to use a "+".

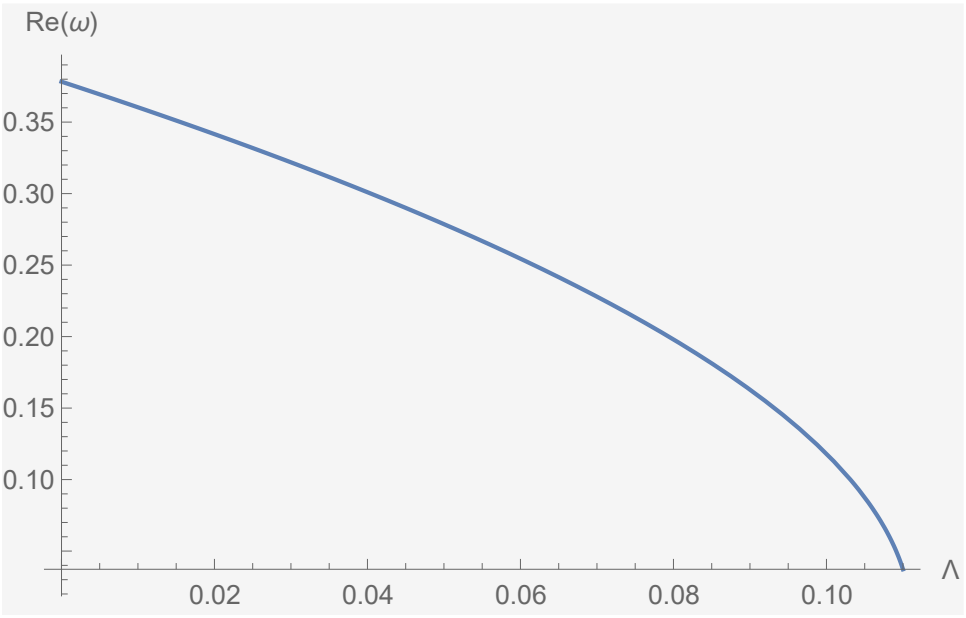

Figure 3: Real part of the QNM frequency of a SdS BH ($n = 0$, $l = 2$) as a function of the cosmological constant. The quantities are given in units of $M = 1$.

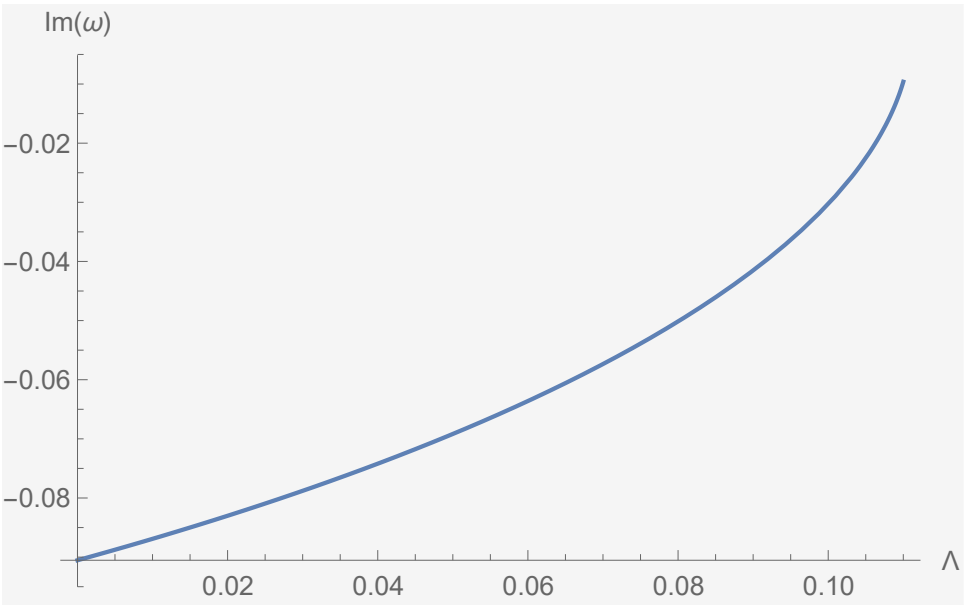

Figure 4: Imaginary part of the QNM frequency of a SdS BH ($n = 0$, $l = 2$) as a function of the cosmological constant. The quantities are given in units of $M = 1$.

We compare the limit $\Lambda \to 0$ with the value of the Schwarzschild QNM obtained with the continued fractions method using the 'qnm' package for Python ([34]). The results are reported in Table 2. The relative error is of $1,3\%$ for the real part and of $1,7\%$ for the imaginary part of the frequencies.

Pöschl-Teller approximation	'qnm' package
$0.3785 - 0.0905i$	$0.3737 - 0.0890i$

Table 2: Flat limit for the mode characterized by $n = 0$ and $l = 2$. The continued fractions method [34] and the Pöschl-Teller approximation were used, and the results are given in units of $M = 1$.

3.4 Kerr-de Sitter spacetime

In this section, we present two methods for computing the QNM frequencies of KdS BHs: the *Heun's function method* and the *continued fractions method*. In chronological order, we first studied and implemented in *Python* the continued fractions method described by Yoshida, Uchikata and Futamase in [19], but we noticed that this method does not work for BHs with small values of ΛM^2 and is therefore useless in the study of astrophysical BHs. So, we tried to improve it by translating the code into *Mathematica* language to increase the working precision[17], but this did not help. However, towards the end of the thesis period, a paper was published on arXiv[18] by Hatsuda ([20]), who suggested to make use of a new class of functions, implemented by *Mathematica* in its most recent version[19], to overcome the problem. These functions, called Heun's functions, represent an optimized version of what is implemented "by hand" with the continued fractions method, and therefore work much better. We therefore decided to make use of Hatsuda's method to achieve our goals.

We begin by introducing the theory behind the two methods, which is taken from [20] and [19]. Then, we discuss the numerical implementations and report the results. In order to do this as logically as possible, we decide not to respect the chronological order and to start with the Heun's function method.

First of all, we briefly present how to derive the master equations for the gravitational perturbations of the KdS BH. A convenient choice of the tetrad

[17] *Python* only allows to perform computations with machine precision, while *Mathematica* allows to work with arbitrary precision.

[18] `https://arxiv.org/`

[19] *Mathematica 12.1*, released in March 2020.

basis is represented by the principle Newman-Penrose null tetrad $(l^\mu, n^\mu, m^\mu, \bar{m}^\mu)$:

$$l^\mu = \left(\frac{(1+\alpha)(r^2+a^2)}{\Delta_r}, 1, 0, \frac{(1+\alpha)a}{\Delta_r} \right), \tag{3.31a}$$

$$n^\mu = \frac{1}{2\rho^2}((1+\alpha)(r^2+a^2), -\Delta_r, 0, a(1+\alpha)), \tag{3.31b}$$

$$m^\mu = \frac{1}{(r+ia\cos\theta)\sqrt{2\Delta_\theta}} \cdot \left(ia(1+\alpha)\sin\theta, 0, \Delta_\theta, \frac{i(1+\alpha)}{\sin\theta} \right) \tag{3.31c}$$

$$\bar{m}^\mu = m^{*\mu}, \tag{3.31d}$$

where $m^{*\mu}$ indicates the complex conjugate of m^μ. In a similar way as described in section 3.3, one obtains the master equations for the quantities ψ_s, where s is the spin weight. The separation of variables is again achieved by making the ansatz:

$$\psi_s =_s R_l^m(r)\,{}_sS_l^m(\theta)e^{-i\omega t+im\varphi}, \tag{3.32}$$

where ω is the complex oscillation frequency. Henceforth, the subscripts s and l and the superscript m are omitted. The angular and radial Teukolsky equations are then given by:

$$\begin{aligned} &\frac{d}{dx}\left[(1+\alpha x^2)(1-x^2)\frac{d}{dx}S(x)\right] + [\lambda - s(1-\alpha) + \frac{(1+\alpha)^2}{\alpha}a^2\omega^2 - 2\alpha x^2 + \\ &\frac{1+\alpha}{1+\alpha x^2}\cdot\left(2s(\alpha m - (1+\alpha)a\omega)x - \frac{(1+\alpha)^2}{\alpha}a^2\omega^2 + 2m(1+\alpha)a\omega + s^2\right) \\ &- \frac{(1+\alpha)^2m^2}{(1+\alpha x^2)(1-x^2)} - \frac{(1+\alpha)(s^2+2smx)}{1-x^2}]S(x) = 0, \end{aligned} \tag{3.33}$$

and

$$\begin{aligned} &\Delta_r^{-s}\frac{d}{dr}\left[\Delta_r^{s+1}\frac{d}{dr}R(r)\right] + \frac{1}{\Delta_r}\left[(1+\alpha)^2K^2 - is(1+\alpha)K\frac{d\Delta_r}{dr}\right]R(r) \\ &+ \left[4is(1+\alpha)\omega r - \frac{2\alpha}{a^2}(s+1)(2s+1)r^2 + 2s(1-\alpha) - \lambda\right]R(r) = 0, \end{aligned} \tag{3.34}$$

where $x = \cos\theta$, $K = \omega(r^2+a^2) - am$ and λ is the angular separation constant. In the following, we only consider $s = -2$, which represents the outgoing part of the gravitational perturbation.

An analytical expansion of the separation constant λ can be found in equation (4.18) of [17], where $\xi = a\omega$ and $\alpha = \frac{\Lambda a^2}{3}$. In the non-rotating limit $a \to 0$ (i.e., $\xi \to 0$ and $\alpha \to 0$), equation (3.33) becomes an eigenvalue equation for λ, and we have $\lambda \to l(l+1) - s(s-1)$. In particular, the non rotating limit of λ does not depend on the cosmological constant Λ. By inserting this value in equation (3.34), one then obtains the master equation (3.14) for a SdS BH.

In the flat limit $\Lambda \to 0$ (i.e. $\alpha \to 0$), the angular Teukolsky equation for KdS BH perturbations (3.33) reduces to the angular Teukolsky equation for KM BH perturbations, the so-called spin-weighted spheroidal equation[20] (equation (8) of [33]). The relation between the separation constant A in [33] and λ is $\lambda|_{\alpha=0} = A + 2s - 2cm + c^2$.

3.4.1 Quasinormal mode frequencies via the Heun's function method

In order to investigate quasinormal modes of KdS spacetime, one can employ the formalism developed by Suzuki, Takasugi and Umetsu ([17]), who showed that the angular and the radial Teukolsky equations are mapped to the so-called Heun's equation.

We begin by considering the angular equation. Equation (3.33) has five regular singularities at $x = \pm 1, \pm i/\sqrt{\alpha}$ and ∞. However, the singularity at ∞ is a removable (cf. [20], [17]). To see its relation to the Heun's differential equation (cf. Appendix B), one first applies the following Möbius transformation that matches the locations of the regular singular points of the two differential equations:

$$z = \frac{1 - \frac{i}{\sqrt{\alpha}}}{2} \frac{x+1}{x - \frac{i}{\sqrt{\alpha}}}. \tag{3.35}$$

This transformation maps the points $x = -1, 1, -i/\sqrt{\alpha}, i/\sqrt{\alpha}, \infty$ to the points $z = 0, 1, z_s, \infty, z_\infty$, given by

$$z_a := z\left(x = \frac{-i}{\sqrt{\alpha}}\right) = \frac{i(1 + i\sqrt{\alpha})^2}{4\sqrt{\alpha}}, \tag{3.36}$$

$$z_\infty := z(x \to \infty) = -\frac{i(1 + i\sqrt{\alpha})}{2\sqrt{\alpha}}. \tag{3.37}$$

To factor out the singularity at $z = z_\infty$, we consider the following transformation:

$$S(x) = \tilde{S}(z) = z^{A_1}(z-1)^{A_2}(z - z_a)^{A_3}(z - z_\infty)y(z), \tag{3.38}$$

where

$$A_1 = \frac{m-s}{2}, \;\; A_2 = -\frac{m+s}{2}, \;\; A_3 = \frac{i}{2}\left(\frac{1+\alpha}{\sqrt{\alpha}}a\omega - \sqrt{\alpha}m - is\right). \tag{3.39}$$

The new function $y(z)$ now satisfies the Heun's differential equation (see Appendix B):

$$y''(z) + \left(\frac{2A_1+1}{z} + \frac{2A_2+1}{z-1} + \frac{2A_3+1}{z-z_a}\right)y'(z) + \frac{\rho_+\rho_- z + u}{z(z-1)(z-z_a)}y(z) = 0, \tag{3.40}$$

[20] Solutions of this equation are represented by the so-called spin-weighted spherical harmonics (see Appendix A for an introduction). Therefore, in the limit $\alpha \to 0$, solutions of equation (3.33) are represented by these functions. For this reason, they are labeled by the same quantum numbers s, l, m as their $\alpha \to 0$ limit.

where

$$\begin{aligned}\rho_+ = 1, \quad \rho_- = 1 - s - im\sqrt{\alpha} + ic\left(\sqrt{\alpha} + \frac{1}{\sqrt{\alpha}}\right), \\ u = -\left[\frac{i\lambda}{4\sqrt{\alpha}} + \frac{1}{2} + A_1 + \left(m + \frac{1}{2}\right)(A_3 - A_3^*)\right],\end{aligned} \tag{3.41}$$

where A_3^* is obtained by replacing i in A_3 by $-i$. Note that the point z_∞ is not a singular point anymore, and that the following relation is satisfied:

$$(2A_1 + 1) + (2A_2 + 1) + (2A_3 + 1) = \rho_+ + \rho_- + 1. \tag{3.42}$$

The relationship between these constants and those in Appendix B is the following:

$$a = z_a, \quad q = -u, \quad \alpha = \rho_+, \quad \beta = \rho_-, \tag{3.43}$$

$$\gamma = 2A_1 + 1, \quad \delta = 2A_2 + 1, \quad \epsilon = 2A_3 + 1. \tag{3.44}$$

One then investigate the behaviour of the solutions of equation (3.33) near the regular singular points $x = -1$ ($z = 0$) and $x = 1$ ($z = 1$). Near $x = -1$ ($z = 0$), one denotes the two local solutions as:

$$S_0^1(x) := z^{A_1}(z-1)^{A_2}(z-z_a)^{A_3}(z-z_\infty)y_0^1(z), \tag{3.45}$$

$$S_0^2(x) := z^{A_1}(z-1)^{A_2}(z-z_a)^{A_3}(z-z_\infty)y_0^2(z). \tag{3.46}$$

For $z \to 0$, the solutions of the Heun equation behave as

$$y_0^1(z) \sim 1, \tag{3.47}$$

$$y_0^2(z) \sim z^{1-\gamma} = z^{-2A_1}. \tag{3.48}$$

Therefore, since $z = (x+1)\cdot(1 - \frac{i}{\sqrt{\alpha}})/2(x - \frac{i}{\sqrt{\alpha}})$, the solutions of the angular Teukolsky equation behave for $x \to -1$ as

$$S_0^1(x) \sim (1+x)^{A_1} = (1+x)^{\frac{m-s}{2}}, \tag{3.49}$$

$$S_0^2(x) \sim (1+x)^{-A_1} = (1+x)^{-\frac{m-s}{2}}. \tag{3.50}$$

In the case where $m - s > 0$, the solution that is regular at $x = -1$ is $S_0^1(x)$, while if $m - s < 0$, the regular solution at $x = -1$ is $S_0^2(x)$. If $m = s$, both solutions are equivalent. Near $x = 1$ ($z = 1$), one denotes the two solutions as:

$$S_1^1(x) := z^{A_1}(z-1)^{A_2}(z-z_a)^{A_3}(z-z_\infty)y_1^1(z), \tag{3.51}$$

$$S_1^2(x) := z^{A_1}(z-1)^{A_2}(z-z_a)^{A_3}(z-z_\infty)y_1^2(z). \tag{3.52}$$

For $z \to 1$, the solutions of the Heun equation behave as

$$y_1^1(z) \sim 1, \tag{3.53}$$

$$y_1^2(z) \sim (1-z)^{1-\delta} = (1-z)^{-2A_2}. \tag{3.54}$$

Therefore, since $(1-z) = (x-1)\cdot(1+\frac{i}{\sqrt{\alpha}})/(2(x-\frac{i}{\sqrt{\alpha}}))$, the solutions of the Teukolsky equation behave for $x \to 1$ as

$$S_1^1(x) \sim (x-1)^{A_2} = (x-1)^{-\frac{m+s}{2}}, \tag{3.55}$$

$$S_1^2(x) \sim (x-1)^{-A_2} = (x-1)^{\frac{m+s}{2}}. \tag{3.56}$$

In the case where $m+s>0$, the solution that is regular at $x=1$ is $S_1^2(x)$, while if $m+s<0$, the regular solution at $x=1$ is $S_1^1(x)$. If $m=-s$, both cases are equivalent.

We recall from above that one needs to find a solution that is regular at both $x=-1$ and $x=1$. With the aim to find a solution that satisfies this two-point boundary value problem, one considers the connection relations between the local solutions at $x=-1$ and $x=1$ in the intersection of the two convergence domains:

$$S_0^1(x) = C_{11}S_1^1(x) + C_{12}S_1^2(x), \tag{3.57}$$

$$S_0^2(x) = C_{21}S_1^1(x) + C_{22}S_1^2(x). \tag{3.58}$$

Note that, as explained in Appendix B, since the roots of the indicial equation at $x=1$, 0 and $1-\delta$, are both integers, the solutions $S_1^1(x)$ and $S_1^2(x)$ are not necessarily linear independent. However, as will become clear later, this does not cause a problem. From the above discussion on the regularity of the solutions, one sees that the behavior of the solutions depends on the values of m and s. We consider the case $(s,l)=(-2,2)$ for concreteness. Since $|m| \leq l$, we have in our specific case that $m-s \geq 0$ and $m+s \leq 0$. Therefore, the regular solution at $x=-1$ is $S_0^1(x)$ and at $x=1$ the regular solution is $S_1^1(x)$. For this reason, we want the coefficient C_{12} to vanish and the solutions $S_0^1(x)$ and $S_1^1(x)$ to be linearly dependent. This can be achieved by means of lemma B.1 in Appendix B.1, imposing the following condition on the Wronskian:

$$W(S_0^1(x), S_1^1(x); x) = 0 \tag{3.59}$$

for every z lying in the intersection of the two convergence domains. One can directly impose the condition

$$W(y_0^1(z), y_1^1(z); z) = 0, \tag{3.60}$$

which implies (3.59). Note that the value of the Wronskian does not depend on z.

We proceed now by presenting the radial Teukolsky equation in a similar way. One considers the following Möbius transformation:

$$z = \frac{(r'_+ - r_-)(r-r_+)}{(r'_+ - r_+)(r-r_-)}, \tag{3.61}$$

which maps the points $r'_-, r_-, r_+, r'_+, \infty$ to the points $z_r, \infty, 0, 1, z_\infty$, where

$$z_r := \frac{(r'_+ - r_-)(r'_- - r_+)}{(r'_+ - r_+)(r'_- - r_-)} \tag{3.62}$$

and

$$z_\infty := \frac{r'_+ - r_-}{r'_+ - r_+}. \tag{3.63}$$

Note that $z_r > 1$. One also considers the transformation:

$$R(r) = \tilde{R}(z) = z^{B_1}(z-1)^{B_2}(z-z_r)^{B_3}(z-z_\infty)^{2s+1}y_r(z), \tag{3.64}$$

where

$$B_1 = \frac{i(1+\alpha)K(r_+)}{\Delta'_r(r_+)}, \quad B_2 = \frac{i(1+\alpha)K(r'_+)}{\Delta'_r(r'_+)}, \quad B_3 = \frac{i(1+\alpha)K(r'_-)}{\Delta'_r(r'_-)}. \tag{3.65}$$

Note that, using $\Omega(r_i) = \frac{a}{r_i^2+a^2}$ and $\kappa(r_i) = \frac{\Delta'_r(r_i)}{2(1+\alpha)(r_i^2+a^2)}$ (the angular velocity and the surface gravity at the event horizon r_i), $K(r_i) = \omega(r_i^2+a^2) - am$ and $\bar{\omega}(r_i) = \omega - m\Omega(r_i) = \omega - \frac{a}{r_i^2+a^2}$, one can rewrite B_1, B_2 and B_3 as:

$$B_1 = \frac{i\bar{\omega}(r_+)}{2\kappa(r_+)}, \quad B_2 = \frac{i\bar{\omega}(r'_+)}{2\kappa(r'_+)}, \quad B_3 = \frac{i\bar{\omega}(r'_-)}{2\kappa(r'_-)}. \tag{3.66}$$

The new function $y_r(z)$ now satisfies the Heun's differential equation

$$\begin{aligned} y''_r(z) + &\left(\frac{2B_1+s+1}{z} + \frac{2B_2+s+1}{z-1} + \frac{2B_3+s+1}{z-z_r}\right) y'_r(z) \\ &+ \frac{\sigma_+\sigma_- z + v}{z(z-1)(z-z_r)} y_r(z) = 0, \end{aligned} \tag{3.67}$$

where

$$\begin{aligned} \sigma_+ = 2s+1, \quad \sigma_- = s+1 - \frac{2i(1+\alpha)K(r_-)}{\Delta'_r(r_-)}, \\ v = \frac{(1+s)(1+2s)r'_-}{r_- - r'_-} + \frac{3\lambda - 2s(3-a^2\Lambda) + \Lambda(1+s)(1+2s)r_+(r_+ + r'_+)}{\Lambda(r_- - r'_-)(r_+ - r'_+)} - \\ \frac{2i(1+2s)(3+a^2\Lambda)(r_+ r_-\omega + a^2\omega - am)}{\Lambda(r_- r'_-)(r_- - r_+)(r_+ - r'_+)}. \end{aligned} \tag{3.68}$$

Note that, again, the point z_∞ is not a singular point anymore. The following identities have been used for the derivation

$$r_+ + r'_+ + r_- + r'_- = 0 \tag{3.69}$$

and

$$\frac{K(r_+)}{\Delta'_r(r_+)} + \frac{K(r_-)}{\Delta'_r(r_-)} + \frac{K(r'_+)}{\Delta'_r(r'_+)} + \frac{K(r'_-)}{\Delta'_r(r'_-)} = 0 \tag{3.70}$$

The relationship between these constants and the ones in Appendix B is the following:

$$a = z_r, \quad q = -v, \quad \alpha = \sigma+, \quad \beta = \sigma_-, \tag{3.71}$$

$$\gamma = 2B_1 + s + 1, \quad \delta = 2B_2 + s + 1, \quad \epsilon = 2B_3 + s + 1. \tag{3.72}$$

One then proceeds by investigating the behavior of the solutions of equation (3.34) near its regular singular points $r = r_+$ ($z = 0$) and $r = r'_+$ ($z = 1$). Near $r = r_+$ ($z = 0$), one denotes the two local solutions as:

$$R_0^1(r) := z^{B_1}(z-1)^{B_2}(z-z_r)^{B_3}(z-z_\infty)^{2s+1}y_{r0}^1(z), \tag{3.73}$$

$$R_0^2(r) := z^{B_1}(z-1)^{B_2}(z-z_r)^{B_3}(z-z_\infty)^{2s+1}y_{r0}^2(z). \tag{3.74}$$

For $z \to 0$, the solutions of the Heun's differential equation behave as

$$y_{r0}^1(z) \sim 1, \tag{3.75}$$

$$y_{r0}^2(z) \sim z^{1-\gamma} = z^{-2B_1-s}. \tag{3.76}$$

Therefore, since $z = (r - r_+)\frac{(r'_+ - r_-)}{(r'_+ - r_+)(r - r_-)}$, the solutions of the angular Teukolsky equation behave for $r \to r_+$ as

$$R_0^1(r) \sim (r-r_+)^{B_1} = (r-r_+)^{\frac{i(1+\alpha)K(r_+)}{\Delta'_r(r_+)}} = (r-r_+)^{\frac{i\tilde{\omega}(r_+)}{2\kappa(r_+)}}, \tag{3.77}$$

$$R_0^2(r) \sim (r-r_+)^{-s-B_1} = (r-r_+)^{-s-\frac{i(1+\alpha)K(r_+)}{\Delta'_r(r_+)}} = (r-r_+)^{-s-\frac{i\tilde{\omega}(r_+)}{2\kappa(r_+)}}, \tag{3.78}$$

where one uses (3.65) and (3.66). Similarly, near $x = 1$ ($z = 1$), one denotes the two local solutions as:

$$R_1^1(r) := z^{B_1}(z-1)^{B_2}(z-z_r)^{B_3}(z-z_\infty)^{2s+1}y_{r1}^1(z), \tag{3.79}$$

$$R_1^2(r) := z^{B_1}(z-1)^{B_2}(z-z_r)^{B_3}(z-z_\infty)^{2s+1}y_{r1}^2(z). \tag{3.80}$$

For $z \to 1$, the solutions of the Heun equation behave as

$$y_1^1(z) \sim 1, \tag{3.81}$$

$$y_1^2(z) \sim (1-z)^{1-\delta} = (1-z)^{-s-2B_2}. \tag{3.82}$$

Therefore, since $(1 - z) = (r - r'_+)\frac{(r_- - r_+)}{(r'_+ - r_+)(r - r_-)}$, the solutions of the Teukolsky equation behave for $r \to r'_+$ as

$$R_1^1(r) \sim (r-r'_+)^{B_2} = (r-r'_+)^{\frac{i(1+\alpha)K(r'_+)}{\Delta'_r(r'_+)}} = (r-r'_+)^{\frac{i\tilde{\omega}(r'_+)}{2\kappa(r'_+)}}, \tag{3.83}$$

$$R_1^2(r) \sim (r-r'_+)^{-s-B_2} = (r-r'_+)^{-s-\frac{i(1+\alpha)K(r'_+)}{\Delta'_r(r'_+)}} = (r-r'_+)^{-s-\frac{i\tilde{\omega}(r'_+)}{2\kappa(r'_+)}}. \tag{3.84}$$

The idea is now to construct a solution that is purely ingoing at $r = r_+$ and purely outgoing at $r = r'_+$. In order to identify which of the two local

solutions one has to choose at each regular singular point, one first introduces the tortoise coordinate r_*, defined by:

$$r_* = \frac{\ln|r-r_+|}{2\kappa(r_+)} + \frac{\ln|r-r_-|}{2\kappa(r_-)} + \frac{\ln|r-r'_+|}{2\kappa(r'_+)} + \frac{\ln|r-r'_-|}{2\kappa(r'_-)}, \tag{3.85}$$

or

$$\frac{dr_*}{dr} = (1+\alpha)\frac{r^2+a^2}{\Delta_r}. \tag{3.86}$$

Using this definition, one can write

$$(r-r_i)^{\frac{i\bar{\omega}(r_i)}{2\kappa(r_i)}} = e^{\ln|r-r_i|\frac{i\bar{\omega}(r_i)}{2\kappa(r_i)}} \sim e^{i\bar{\omega}(r_i)r_*}. \tag{3.87}$$

Therefore, the solutions of the radial Teukolsky equation behave near r_+ and r'_+ as

$$R_0^1(r) \sim e^{i\bar{\omega}(r_+)r_*}, \tag{3.88}$$

$$R_0^2(r) \sim (r-r_+)^{-s}e^{-i\bar{\omega}(r_+)r_*}, \tag{3.89}$$

and

$$R_1^1(r) \sim e^{i\bar{\omega}(r'_+)r_*}, \tag{3.90}$$

$$R_1^2(r) \sim (r-r'_+)^{-s}e^{-i\bar{\omega}(r'_+)r_*}, \tag{3.91}$$

respectively. Since one has assumed the time dependence of the perturbation to be $e^{-i\omega t}$, outgoing waves have the form $e^{-i(\omega t - kr_*)}$, while ingoing waves have the form $e^{-i(\omega t + kr_*)}$, where k is the wave number, which corresponds to $\bar{\omega}(r_i)$ in this case. Therefore, $R_0^1(r)$ and $R_1^1(r)$ represent purely outgoing waves, while $R_0^2(r)$ and $R_1^2(r)$ represent purely ingoing waves. One considers the connection relations between the local solutions at $r = r_+$ and at $r = r'_+$ in the intersection of the two convergence domains:

$$R_0^1(r) = C_{11}R_1^1(r) + C_{12}R_1^2(r), \tag{3.92}$$

$$R_0^2(r) = C_{21}R_1^1(r) + C_{22}R_1^2(r). \tag{3.93}$$

To impose the boundary conditions described above, one requires the coefficient C_{22} to vanish and the solutions $R_0^2(r)$ and $R_1^1(r)$ to be linearly dependent. Since the roots of the indicial equation at $r = r'_+$, 0 and $1-\delta$ are not both integers, the local solutions at $r = r'_+$ are linearly independent. As explained in Appendix B.1, the coefficient C_{22} can then be expressed as

$$C_{22} = \frac{W(R_1^1(r), R_0^2(r); r)}{W(R_1^1(r), R_1^2(r); r)}, \tag{3.94}$$

which reduces to

$$C_{22} = \frac{W(y_{r1}^1(z), y_{r0}^2(z); z)}{W(y_{r1}^1(z), y_{r1}^2(z); z)}, \tag{3.95}$$

as can be seen using the properties of the determinant. Note that the ratio of the Wronskians does not depend on z. Thus, the condition which has to be imposed is the following[21]

$$\frac{W(y^1_{r1}(z), y^2_{r0}(z); z)}{W(y^1_{r1}(z), y^2_{r1}(z); z)} = 0. \tag{3.97}$$

For a given value of a and Λ, since the left-hand sides of both equations (3.60) and (3.97) only depend on the frequency ω and the separation constant λ but are independent of z, one can evaluate them at a point z which lies in both convergence circles of the local solutions at $z = 0$ and $z = 1$. For this purpose, we choose $z = 1/2$, as suggested in [20]. Equations (3.60) and (3.97) then form a system of nonlinear algebraic equations for ω and λ. In the next section, we show how to solve this system numerically. Note that for $a = 0$ (SdS case) the angular Teukolsky equation (3.33) does not contain ω anymore. Therefore, the angular problem trivializes and the angular eigenvalue λ takes the form $\lambda|_{a=0} = l(l+1) - s(s-1)$. In this case, one only needs to solve equation (3.97) for ω using this value of λ.

3.4.2 Implementation

Equations (3.60) and (3.97) are implemented by making use of the *Mathematica* 'HeunG' function (cf. [39] and Appendix B) and are solved simultaneously by a numerical algorithm. Here, we use the *Mathematica* function 'FindRoot', which makes use of the Newton's method. The code for this task is taken directly from the *Mathematica* notebook from [20] and is reported in Appendix D.2.2. Here, we briefly explain how it is structured.

In order to determine the solutions of the system using the Newton's algorithm, one needs to feed the function 'FindRoot' with appropriate starting values. One can proceed in two ways. The first possibility consists in using the continuity of the frequency ω and the separation constant λ as a function of ΛM^2 for a given value of a. One therefore fixes a value of the spin parameter a and use the known values of the frequency ω and the separation constant λ of the KM BH ($\Lambda M^2 = 0$) as starting values for determining $\omega(\Lambda M^2)$ and $\lambda(\Lambda M^2)$ at a small values[22] of ΛM^2 . The new values are then used as new

[21] We have followed the reasoning of Hatsuda in [20], but in our opinion it would have been enough to impose the condition of linear dependence on the solutions $R^2_0(r)$ and $R^1_1(r)$ as was done for the angular Teukolsky equations,

$$W(y^1_{r1}(z), y^2_{r0}(z); z) = 0, \tag{3.96}$$

without the need to use Cramer's Rule.

[22] Note that this is possible because the $\Lambda \to 0$ limit of the KdS Teukolsky equations

starting values and ΛM^2 is increased of a small amount. The second possibility consists in fixing a value of ΛM^2 and using the continuity of ω and λ as a function of the spin parameter a. As a starting value at $a = 0$, one can use the known values of ω and λ of the SdS BH[23], computed as described in section 3.3. Note that the choice of the starting values completely specifies the quantum numbers n and l, which are otherwise not contained in the Teukolsky equations (unlike m and s).

Since our purpose is to study astrophysical black holes, which are characterized by a small value of ΛM^2, and in exploring the flat limit for a given value of a, we prefer the first method. Moreover, since we want to fix the BH mass and vary the value of Λ, we will work in units of $M = 1$. From now on, instead of ΛM^2, we will then just write Λ. We summarize the steps of the algorithm in a schematic way:

1. Choose quantum numbers s, l and m and fix a value of a/M (we can just write a in the units which we have chosen).

2. Compute the value of ω and λ for the Kerr-Minkowski case using the 'qnm' package for Python ([34]).

3. Increase Λ of the amount 1/10000.

4. Estimate new starting values by varying the previous values of a small amount[24]

$$\omega_{0,\text{new}} = \omega_{\text{old}} - \frac{1-i}{20000}, \tag{3.98}$$

$$\lambda_{0,\text{new}} = \lambda_{\text{old}} + \frac{1+i}{20000}, \tag{3.99}$$

   and solve the system of equations (3.60) and (3.97) using the Newton's algorithm ('FindRoot').

5. Return to point 3. and repeat an arbitrary number of times (a maximum number of steps is given by $\Lambda_{\text{max}} \cdot 10000$, where $\Lambda_{\text{max}} = \Lambda_{\text{max}}(a, M = 1)$ is given by equation (2.53), but for studying astrophysical BHs 20 iterations are enough).

6. Return to point 1. and vary the value of m, which can take $2l + 1$ values $m = -l, ..., l$.

corresponds to the KM Teukolsky equations. Therefore, the limit $\Lambda \to 0$ of the solutions of the KdS master equation should correspond to the solution of the KM master equation

[23]This is possible because the $a \to 0$ limit of the KdS Teukolsky equations corresponds to the SdS Teukolsky equtions. Therefore, the limit $a \to 0$ of the solutions of the KdS master equation should correspond to the solution of the SdS master equation

[24]This estimation is based on the results of other numerical codes (like e.g. the one of [19]), where it is shown that $\text{Re}(\omega)$ decreases and $\text{Im}(\omega)$ increases as Λ increases.

This procedure can be repeated for different values of a. We choose to consider ten equally distant values of a, from $a = 0$ to 0.9 as well as $a = 0.999999999$. For all the computations, we use at least 50 digits precision. The data are then saved in a .csv file.

Next, we perform a fit of the values of the real and imaginary parts of the frequency for each value of a using the *Mathematica* 'Fit' function and the function $\sum_{n=0}^{N} f_n \Lambda^n$ as a model. We choose[25] $N = 18$. We then check that the limit for $\Lambda \to 0$ corresponds to the values for the KM case, by comparing it with the values obtained with the 'qnm' package.

After this, we evaluate this fit at four different values of Λ, which, in units of $M = 1$, correspond to the four types of astrophysical BHs of Table 1, where we take the cosmological constant to be $\Lambda \sim 10^{-52} m^{-2}$. For these BH types, we also check our results by comparing the limit $a \to 0$ of the frequencies with the SdS frequencies obtained with the Pöschl-Teller approximation.

Finally, for each BH, we compute the differencies (3.10).

3.4.3 Results

Here, we report the results obtained with the Heun's function method. We first discuss the numerical code and check that it works by studying the limits of the modes $l = 2$ and $m = -2, -1, 0, 1, 2$ and for the $(l, m) = (3, 3)$ mode, but we only report the data for the $(2, 2)$ mode as an example (the results for the other modes are similar). Then, we compute and report the relevant quantities.

The code works quite well in the portion of the parameter space that we are considering, although it is a bit slow, especially for $a > 0.8$ and for negative values of m. For all the tested modes, at $a = 0.9$, it is not possible to consider more than 6 iterations of the algorithm, because the code does not allow to go further. The code does not seem to work for 0.999999999.

In Figures 5 and 6, we report the plots, in $M = 1$ units, of $\mathrm{Re}(\omega)$ and $\mathrm{Im}(\omega)$ as a function of Λ for the $(2, 2)$ mode and $a = 0.6$ as an example. The plots at different values of a are very similar to these ones. In particular, all the plots are almost linear in the range that we are considering.

For each value of a and for each value of m, we extrapolate the value of ω in the limit $\Lambda \to 0$, which corresponds to the f_0 in the fitted model from above. We then compare this value with the KM QNM frequency obtained using the 'qnm' package. However, since the 'qnm' package is written in *Python* and not

[25] To choose the value of N, we refer to the *Mathematica* notebook of [20]. Here, the Taylor polynomial at $\Lambda = 0$, $\sum_{n=0}^{N} f_n \Lambda^n$, is used as a model and N is varied dynamically until the first 40 digits of $\mathrm{Re}(f_0)$ and $\mathrm{Im}(f_0)$ are stable, which happens at $N = 18$.

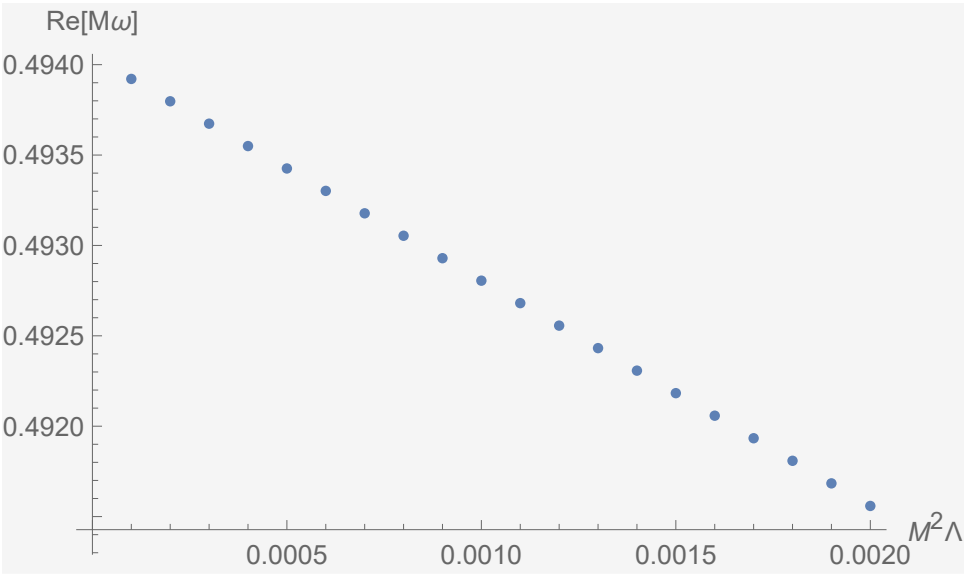

Figure 5: $\mathrm{Re}(\omega)$ as a function of ΛM^2 for $(l, m) = (2, 2)$ and $a = 0.6$

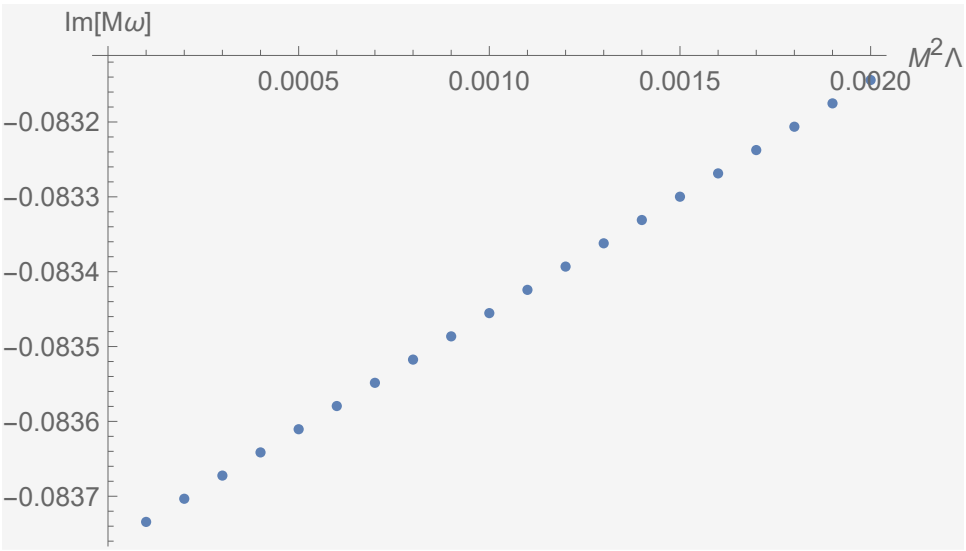

Figure 6: $\mathrm{Im}(\omega)$ as a function of ΛM^2 for $(l, m) = (2, 2)$ and $a = 0.6$

in *Mathematica*, it only allows to compute the values using machine precision. Therefore, we can only check if the values correspond up to the first 16 decimal digits. Some machine precision results are reported in Tables 3 and 4 as an example. The values seem to agree at least in the first 10 to 15 digits.

source / a	present code	'qnm' package
0	0.3736716844180418	0.3736716844180417
0.1	0.3870175383664503	0.3870175383664508
0.2	0.4021453242476555	0.4021453242476556
0.3	0.4195266817638514	0.4195266817638519
0.4	0.4398419217353871	0.4398419217353868
0.5	0.4641230259759383	0.4641230259759386
0.6	0.4940447817813842	0.4940447817813843
0.7	0.5326002435597860	0.532600243551018
0.8	0.5860169749088703	0.5860169749088701
0.9	0.6711237414772702	0.671614272132163
0.999999999	?	0.9999541560971394

Table 3: Values of $\mathrm{Re}(\omega)$ for $\Lambda = 0$ and $(l, m) = (2, 2)$ ($M = 1$ units).

source / a	present code	'qnm' package
0	- 0.08896231568893569	-0.08896231568893546
0.1	-0.0887056990276413	-0.08870569902764017
0.2	-0.08831116620760301	-0.08831116620760186
0.3	-0.08772927189431198	-0.08772927189431111
0.4	-0.08688196202939836	-0.08688196202939791
0.5	-0.08563883498806401	-0.0856388349880652
0.6	-0.08376520216104089	-0.08376520216104325
0.7	- 0.08079287317663332	-0.08079287315500867
0.8	-0.07562955235606014	-0.07562955235606074
0.9	- 0.06482177058675801	-0.06486923587579639
0.999999999	?	$-1.114065293254156 \cdot 10^{-5}$

Table 4: Values of $\mathrm{Im}(\omega)$ for $\Lambda = 0$ and $(l, m) = (2, 2)$ ($M = 1$ units).

Furthermore, we check whether the values obtained with this code for $a = 0$ correspond to the values of the SdS QNM frequencies computed as described in section 3.3. The results are reported in Tables 5 and 6. Here, the relative error is of 1,2% for the real part and 1,7% for the imaginary part of the frequencies, but this is due to the fact that the Pöschl-Teller method only allows to compute the frequencies in an approximate way. We have therefore checked that the code is in agreement with previously computed results.

Source / Λ	Present code	Pöschl-Teller approximation
10^{-48}	0.37367	0.37827
10^{-44}	0.37367	0.37827
10^{-38}	0.37367	0.37827
10^{-28}	0.37367	0.37827

Table 5: Values of $\mathrm{Re}(\omega)$ for the mode $(l, m) = (2, 2)$ at $a = 0$ for different values of Λ, corresponding to different astrophysical BH types ($M = 1$ units).

Source / Λ	Present code	Pöschl-Teller approximation
10^{-48}	-0.088962	-0.090531
10^{-44}	-0.088962	-0.090531
10^{-38}	-0.088962	-0.090531
10^{-28}	-0.088962	-0.090531

Table 6: Values of $\mathrm{Im}(\omega)$ for the mode $(l, m) = (2, 2)$ at $a = 0$ for different values of Λ, corresponding to different astrophysical BH types ($M = 1$ units).

We now compute the frequency differences defined in (3.10). Since the values of Λ (in $M = 1$ units) for astrophysical BHs are smaller than the size of the step (10^{-4}) chosen in the procedure described above, we obtain the frequencies that we are looking for by means of an extrapolation, using the fitted model from above. For computing Δ, we need to work at high precision and therefore we do not use the values of the KM QNM of the 'qnm' package. Instead, we use the flat limit that we have extrapolated above (corresponding to the values of f_0). The values of Δ are reported in Table 7 in SI units[26].

[26]The conversion in from $M = 1$ to SI units is done as follows:

$$\Delta_{SI} = \Delta_M \cdot \frac{c}{M_i} \tag{3.100}$$

Since the order of magnitude seems not to depend on a, we simply report the order of magnitude of the results for each BH type.

BH type	Re(Δ) [s^{-1}]	Im(Δ) [s^{-1}]
sub-solar mass BH	10^{-40}	10^{-40}
stellar mass BH	10^{-41}	10^{-41}
intermediate BH	10^{-38}	10^{-38}
supermassive BH	10^{-33}	10^{-33}

Table 7: Values of Δ in SI units for four types of astrophysical BHs.

3.4.4 Quasinormal mode frequencies via the continued fractions method

The first method which we have introduced makes use of the *Mathematica* function 'HeunG' to compute Heun's functions. However, one could also find an explicit form for these functions and implement them "by hand". Following [19], we describe here, to the best of our understanding, how to obtain such an explicit form, and then implement the numerical method to compute it.

Following [19], one may express the solution $y(z)$ of the Heun's differential equation (3.40) which is regular at $z = 0$ as a series expansion:

$$y(z) = \sum_{n=0}^{\infty} a_n z^n. \tag{3.101}$$

One then considers physical boundary conditions and constructs a solution of (3.33) that is finite both at $x = -1$ and at $x = 1$. A solution that satisfies these conditions is the following:

$$S(x) = \tilde{S}(z) = z^{|A_1|}(z-1)^{|A_2|}(z-z_a)^{|A_3|}(z-z_\infty)\sum_{n=0}^{\infty} a_n z^n, \tag{3.102}$$

provided that the series converges at $z = 1$ (at $z = 0$, the series obviously converges). In fact, one has:

$$S(x) \to \begin{cases} (x+1)^{|m-s|/2} & \text{as } x \to -1 \\ (x-1)^{|m+s|/2} & \text{as } x \to 1. \end{cases} \tag{3.103}$$

By inserting this ansatz into equation (3.33), one obtains the following three-term recurrence relation for the coefficients a_n's:

$$\alpha_n^\theta a_{n+1} + \beta_n^\theta a_n + \gamma_n^\theta a_{n-1} = 0, \tag{3.104}$$

where M_i is the mass of the BH type i in geometrized units and c is the speed of light.

with the initial values $a_0 = 1$ and $\alpha_0^\theta a_1 + \beta_0^\theta a_0 = 0$. The coefficients in equation (3.104), in $\Lambda = 3$ units[27], are

$$\alpha_n^\theta = z_a(1+n)(1+n+2A_1), \tag{3.105}$$

$$\beta_n^\theta = u_0 - (1+z_a)n^2 - [1+2A_3+z_a+2A_2z_a+2A_1(1+z_a)]n, \tag{3.106}$$

$$\gamma_n^\theta = -1-2A_3+2A_1(n-1)+2A_2(n-1)+2A_3n+n^2+u_1, \tag{3.107}$$

where

$$\begin{aligned} u_1 =& \frac{1}{2}[2+4A_3+4A_2(1+A_3)+4A_1(1+A_2+A_3) \\ &+ m^2 - 2iams + s^2 + 2is\omega + 2ia^2s\omega], \end{aligned} \tag{3.108}$$

$$\begin{aligned} u_0 =& -\frac{i}{8a}[-2A_2-2A_1(1+2A_2)-m^2-2s+s^2 \\ &+ a^2\{2A_2+A_1(2+4A_2)-3m^2+2s-4ms-s^2\} \\ &+ 4a^3(m+s)\omega - 2ia\{2+2A_2+4A_3 \\ &+ A_1(6+4A_2+8A_3)+m^2-2ms+s^2 \\ &+ 2im\omega + 2is\omega\} + 2\lambda]. \end{aligned} \tag{3.109}$$

It remains to determine under which condition the series converges at $x = 1$. As it is written in [19], the large n behavior of a_n can take one of the two expressions:

$$\lim_{n\to\infty}\frac{a_{n+1}}{a_n} = \frac{1}{z_a} - \frac{1-2A_3}{z_a}\frac{1}{n} + ... \tag{3.110}$$

or

$$\lim_{n\to\infty}\frac{a_{n+1}}{a_n} = 1 - (1-2A_2)\frac{1}{n} + ... \tag{3.111}$$

Since $z_a > 1$ and $1-2A_2 \leq 1$, expression (3.110) ensures that $\lim_{n\to\infty}\frac{a_{n+1}}{a_n} < 1$, which ensures the convergence of the series by the ratio test. Expression (3.110) is obtained if one requires the solution of the recurrence relation (3.104) to be minimal. By Theorem 1.1 of [40], this is equivalent to the condition in terms of continued fractions given by:

$$0 = \beta_0^\theta - \frac{\alpha_0^\theta\gamma_1^\theta}{\beta_1^\theta - \frac{\alpha_1^\theta\gamma_2^\theta}{\beta_2^\theta - (\alpha_2^\theta\gamma_3^\theta/\beta_3^\theta - ...)}}, \tag{3.112}$$

which can be also expressed with the easier notation

$$0 = \beta_0^\theta - \frac{\alpha_0^\theta\gamma_1^\theta}{\beta_1^\theta -}\frac{\alpha_1^\theta\gamma_2^\theta}{\beta_2^\theta -}\frac{\alpha_2^\theta\gamma_3^\theta}{\beta_3^\theta -}... \tag{3.113}$$

[27]For simplicity, we report the expressions in units of $\Lambda = 3$, which are the units used in [19].

The right-hand side of equation (3.112) is a function of λ and ω. One can abbreviate it as $A(\omega, \lambda)$ and rewrite (3.112) as

$$A(\omega, \lambda) = 0. \tag{3.114}$$

One calls equation (3.114) the angular eigenvalue equation for the present problem.

One applies the same reasoning to the radial Teukolsky equation (3.34). One focuses on the case where $\Delta_r = 0$ has four real roots $r'_- < r_- < r_+ < r'_+$. Equation (3.34) has then five regular singularities at $r = r_\pm, r'_\pm, \infty$, but, as before, the singularity at $r = \infty$ is apparent and removable. Again, following [19] and [18], one considers a Möbius transformation that matches the singular points of the radial Teukolsky equation to the ones of the Heun's differential equation (B.1). However, in order to follow closely the work of Yoshida, Uchikata and Futamase ([19]), on which our numerical code is based, we do not consider the same Möbius transformation as above, but the following one[28]:

$$z = \frac{(r_- - r'_-)(r - r_+)}{(r_- - r_+)(r - r'_-)}. \tag{3.115}$$

This transformation maps the points $r = r'_-, r_-, r_+, r'_+, \infty$ to the points $z = \infty, 1, 0, z_r, z_\infty$, where

$$z_r := \frac{(r_- - r'_-)(r'_+ - r_+)}{(r_- - r_+)(r'_+ - r'_-)}, \tag{3.116}$$

$$z_\infty := \frac{r_- - r'_-}{r_- - r_+}. \tag{3.117}$$

As for the angular case, one may express the solution $y_r(z)$ that is regular at $z = 0$ as a series expansion:

$$y_r(z) = \sum_{n=0}^{\infty} d_n \left(\frac{z}{z_r}\right)^n. \tag{3.118}$$

To factor out the singularity at $z = z_\infty$, one considers the following transformation:

$$R(r) = \tilde{R}(z) = (-z)^{B_1}(1-z)^{B_2}\left(\frac{z - z_r}{1 - z_r}\right)^{B_3}\left(\frac{z - z_\infty}{1 - z_\infty}\right)^{2s+1} y_r(z), \tag{3.119}$$

where B_1, B_2 and B_3 are defined as

$$B_1 = \frac{i\bar{\omega}(r_+)}{2\kappa(r_+)}, \quad B_2 = \frac{i\bar{\omega}(r_-)}{2\kappa(r_-)}, \quad B_3 = \frac{i\bar{\omega}(r'_+)}{2\kappa(r'_+)}. \tag{3.120}$$

[28]There are 4! possibilities to map the four regular singular points of the Teukolsky radial equation (recall that the singularity at $r = \infty$ is apparent and removable) to the four regular singular points of the Heun's equation. In the previous chapter, we have chosen one trasformation that maps the positions of the BH and of the cosmological horizons, $r = r_+$ and $r = r'_+$, to the points $z = 0$ and $z = 1$. Here, we consider a Möbius transformation so that $r = r_+$ and $r = r'_+$ are mapped to $z = 0$ and $z = z_r$.

The function $y_r(z)$ then satisfies a Heun's differential equation similar to (3.67).

One then considers physical boundary conditions and constructs a solution which is purely ingoing at $r = r_+$ and purely outgoing at $r = r'_+$. Following a similar reasoning as the one of the previous section, one sees that a solution that satisfies the physical boundary conditions is the following:

$$R(r) = \tilde{R}(z) = (-z)^{B'_1}(1-z)^{B'_2}\left(\frac{z-z_r}{1-z_r}\right)^{B'_3}\left(\frac{z-z_\infty}{1-z_\infty}\right)^{2s+1}\sum_{n=0}^{\infty} d_n\left(\frac{z}{z_r}\right)^n, \tag{3.121}$$

where

$$B'_1 = -s - \frac{i\bar{\omega}(r_+)}{2\kappa(r_+)}, \quad B'_2 = \frac{i\bar{\omega}(r_-)}{2\kappa(r_-)}, \quad B'_3 = \frac{i\bar{\omega}(r'_+)}{2\kappa(r'_+)}, \tag{3.122}$$

provided that the series converges at $z = z_r$ (at $z = 0$ it clearly converges). In fact, one can then check that

$$R \to \begin{cases} (r-r_+)^{-s-i\bar{\omega}(r_+)/2\kappa(r_+)} & \text{as } r \to r_+ \\ (r-r'_+)^{i(\bar{\omega}(r'_+)/2\kappa(r'_+))} & \text{as } r \to r'_+. \end{cases} \tag{3.123}$$

By inserting this ansatz into the radial Teukolsky equation, one obtains the following three-term recurrence relation for the coefficients:

$$\alpha^r_n d_{n+1} + \beta^r_n d_n + \gamma^r_n d_{n-1} = 0, \tag{3.124}$$

with initial values $d_0 = 1$ and $\alpha^r_1 d_1 + \beta^r_1 d_0 = 0$. The coefficients in equation (3.124) are given, in units of $\Lambda = 3$, by:

$$\alpha^r_n = (1+n)(1+2B_1+n+s), \tag{3.125}$$

$$\beta^r_n = v_0 - (1-x_r)n^2 - \{1+2B_3+2s+x_r+2B_2x_r+2sx_r+2B_1(1+x_r)\}n, \tag{3.126}$$

$$\gamma^r_n = \{-1+2(B_1+B_2+B_3)(n-1)+n^2-3s+3ns+v_1\}x_r, \tag{3.127}$$

where

$$v_1 = (B_1+B_2+B_3-b_4+s+1)(B_1+B_2+B_3+b_4+2s+1), \tag{3.128}$$

$$
\begin{aligned}
v_0 =& \frac{-1}{(r_+ - r_-)(r'_+ - r'_-)}[\lambda + 2s(a^2-1) + \{B_2 - b_2 s + B_2 s - b_1(2b_2 + s) \\
&+ B_1(1 + 2B_2 + s)\} r'_+ r'_- - \{-1 + 2b_1^2 + (-3 + b_2 + b_3 + b_4)s - 2s^2 \\
&+ b_1(2b_2 + 2b_3 + 2b_4 + 5s)\} r_+^2 - \{B_2 + B_3 - b_2 s - b_3 s + B_2 s + B_3 s \\
&- 2b_1(b_2 + b_3 + s) + 2B_1(1 + B_2 + B_3 + s)\} r_+ r'_- + \{1 + 2b_1^2 + B_3 \\
&+ 3s + b_2 s + b_4 s + B_3 s + 2s^2 + B1(1 + 2B_3 + s) + 2b_1(b_2 + b_4 \\
&+ 2s)\} r_+ r'_+ + \{1 + 2b_1^2 + B_2 + 3s + b_3 s + b_4 s + B_2 s + 2s^2 + B_1(1 \\
&+ 2B_2 + s) + 2b_1(b_3 + b_4 + 2s)\} r_+ r_- + \{B_3 - b_3 s + B_3 s - b_1(2b_3 \\
&+ s) + B_1(1 + 2B_3 + s)\} r_- r'_- - \{1 + 2b_1^2 + B_2 + B_3 + 3s + b_4 s \\
&+ B_2 s + B_3 s + 2s^2 + 2B_1(1 + B_2 + B_3 + s) + b_1(2b_4 + 3s)\} r_- r'_+ \\
&- 4is\omega(1 + a^2) r_+],
\end{aligned}
\tag{3.129}
$$

$$
B_1 = B'_1, \qquad B_2 = B'_2, \qquad B_3 = B'_3, \tag{3.130}
$$

(not to be confused with the B_1, B_2 and B_3 defined in (3.120)) and

$$
b_1 = i\frac{\bar{\omega}(r_+)}{2\kappa(r_+)}, \quad b_2 = i\frac{\bar{\omega}(r_-)}{2\kappa(r_-)}, \quad b_3 = i\frac{\bar{\omega}(r'_+)}{2\kappa(r'_+)}, \quad b_4 = i\frac{\bar{\omega}(r'_-)}{2\kappa(r'_-)}. \tag{3.131}
$$

It remains to determine under which conditions the series converges at $z = z_r$. As explained in [19], the large n behavior of d_n shows that

$$
\lim_{n\to\infty} \frac{d_{n+1}}{d_n} = x_r + x_r(s - 1 + 2B_2)\frac{1}{n} + ..., \tag{3.132}
$$

or

$$
\lim_{n\to\infty} \frac{d_{n+1}}{d_n} = 1 - (s - 1 + 2B_3)\frac{1}{n} + ... \tag{3.133}
$$

Because $z_r > 1$ and $\mathrm{Re}(s - 1 + 2B_3) < 0$, expression (3.133) ensures that $\lim_{n\to\infty} \frac{d_{n+1}}{d_n} < 1$, which ensures the convergence of the series by the ratio test. Expression (3.133) is equivalent to the condition for the recurrence relation (3.124) to be minimal, which can be written in terms of continued fractions as:

$$
0 = \beta_0^r - \frac{\alpha_0^r \gamma_1^r}{\beta_1^r -} \frac{\alpha_1^r \gamma_2^r}{\beta_2^r -} \frac{\alpha_2^r \gamma_3^r}{\beta_3^r -} .... \tag{3.134}
$$

The right-hand side of equation (3.134) is a function of ω and λ. One can abbreviate it as $B(\omega, \lambda)$ and rewrite (3.134) as

$$
B(\omega, \lambda) = 0. \tag{3.135}
$$

This equation is known as the radial eigenvalue equation for this problem.

For a given value of a and M, equations (3.114) and (3.135) represent a system of nonlinear equations for the parameters ω and λ, in a similar way as in the previous chapter. In the next section, we show how to solve this system numerically.

3.4.5 Implementation

The two equations (3.114) and (3.135) can be solved simultaneously by a numerical algorithm. To do this, we have implemented the method described in [19] in *Python*, first, and then in *Mathematica*, to take advantage of its ability to perform computations with arbitrary precision. The code is reported in Appendix D.2.1. Here, we explain how it is structured.

Following [19], and contrary to the previous method, we use $\Lambda = 3$ units[29] and begin by fixing a value of M/r_C (or M, in $\Lambda = 3$ units). We determine $\omega(a)$ and $\lambda(a)$, using continuity of the QNM frequency and of the separation constant as a function of a and the values of SdS QNMs as starting values. As before, the starting values completely specify the value of the quantum numbers n and l.

The crucial part in this algorithm is the evaluation of the functions $A(\omega, \lambda)$ and $B(\omega, \lambda)$, since they are represented by infinite continued fractions. To do this, we make use of the *modified Lentz's algorithm*, which we describe in Appendix C.1. To evaluate $A(\omega, \lambda)$, we set

$$a_n = -\gamma_n^\theta \alpha_{n-1}^\theta, \qquad b_n = \beta_n^\theta. \tag{3.136}$$

Similarly, to evaluate $B(\omega, \lambda)$, we set

$$a_n = -\gamma_n^r \alpha_{n-1}^r, \qquad b_n = \beta_n^r. \tag{3.137}$$

In both of the cases, we use a tolerance of eps $= 10^{-10}$ and set the parameter 'tiny' to 10^{-30}.

In the *Python* code, we use the 'scipy.optimize.root' function and Newton's method to determine the solutions of the system. In *Mathematica*, as before, we use the function 'FindRoot' instead.

We summarize the steps of the algorithm in a schematic way below.

1. Choose s, l and m and fix a value of $M/r_C = \sqrt{\Lambda M^2/3}$ (we can simply write M in the chosen units). The corresponding maximum value for the spin parameter, $a_{\max}$, can then be computed as explained in section 2.2.2.

2. Set a to $a = 10^{-3} \cdot a_{\max}$.

3. Compute the value of ω for the SdS BH for the given value of M, using the Pöschl-Teller approximation[30], and use this as a starting value. The

[29] To make use of the expressions that we found in [19] directly, we use the same units ($\Lambda = 3$) used in their paper during the computations. We then convert the frequencies into $M = 1$ units at the end by multiplying them by the conversion factor r_C/M.

[30] The code of Appendix D.1 gives the values of ω in units of $M = 1$. To convert these values into units of $\Lambda = 3$, it suffices to multiply them by the conversion factor M/r_C.

starting value for λ is given by $\lambda|_{a=0} = l(l+1) - s(s-1)$. Note that in this case the starting value for λ does not depend on s, m and ω, as contrary to above.

4. Use the Newton's algorithm to find a solution of the system given by (3.114) and (3.135). $A(\omega, \lambda)$ and $B(\omega, \lambda)$ are evaluated every time using the modified Lentz's algorithm. The Jacobian is estimated numerically by the 'scipy.optimize.root' function (*Python*) or the 'FindRoot' function (*Mathematica*).

5. Increase a of the amount $10^{-3} \cdot a_{\max}$ ($a_{\text{new}} = a_{\text{old}} + 10^{-3} \cdot a_{\max}$).

6. Estimate new starting values by extrapolating the value of $\omega(a_{\text{new}})$ and $\omega(\lambda_{\text{new}})$ from the three previous values of $\omega(a)$ and $\lambda(a)$, if possible, using a polynomial interpolation (this method was suggested in [41]). If this is not possible, then use the values of $\omega(a_{\text{old}})$ and $\lambda(a_{\text{old}})$ as starting values.

7. Return to point 4 and repeat until a reaches the value of $a_{\max}$, then stop.

8. Return to point 1 and vary the value of m, which can take $2l+1$ integer values $m = -l, ..., l$.

This procedure can be repeted for different values of M. For all the *Mathematica* computations, we use 60 digits of precision, while in *Python* we use machine precision. The data are saved in a .npy file (Python) or in a .csv file (Mathematica). One can then fit the data and obtain the plot of Re(ω) and Im(ω) as a function of the spin parameter. The results are discussed below.

3.4.6 Results

By means of the code described in the previous section, we tried to analyze the fundamental ($n = 0$) quasinormal mode frequencies of KdS BH with $l = 2$ and $m = -2, -1, 0, 1, 2$. We tested the code with the same BH types which were studied in [19], i.e. for $M = 0.01290$, 0.1205, 0.1582, 0.1789, 0.1893, 0.1924, 0.1982.

For $0.1582 \leq M \leq 0.1924$, we managed to obtain the same results as in [19] for $a \leq 0.75 \cdot a_{\max}$. In the region where $a > 0.75 \cdot a_{\max}$, our code outputs values that do not correspond to the ones reported in [19]. The reason for this is probably that the graphs of the functions after $a > 0.75 \cdot a_{\max}$ are very steep for high values of M (cf. plots in [19]). To solve this problem, the length of the step should be decreased in order to obtain a better estimation of the next starting value. However, by doing this, the computations slow down a lot. Furthermore, the code seems to work better for higher values of m.

For $M = 0.01290$, 0.1205 and lower values, our code outputs wrong values already after the first step (and even when considering smaller steps). This prevents us from using it for studying astrophysical BH (for which $M \leq 10^{-14}$). We do not know why we cannot obtain the same results as in [19], but we suspect that this is due to the fact that our starting values, generated by an approximation, are not close enough to the roots of the system of equations (3.114) and (3.135), and Newton's algorithm jumps and converges towards the wrong root. It is not a problem of precision, since the *Mathematica* code presents the same issues as the *Python* code. Yoshida, Uchikata and Futamase obtained their starting values with the code described in [16], which probably allows to obtain more accurate starting values. However, it is said in [16] that this code only works well for nearly extremal BH. Therefore, we deduce that black holes with M much smaller than 0.01290 were not studied in [19], even if it has not been explicitely stated.

The problem described above could lie in the fact that, as explained in [30], the boundary condition that one imposes,

$$\psi(\omega, r_*) \sim e^{i\omega r_*} \ \ as\ r_* \to \infty, \quad \psi(\omega, r_*) \sim e^{-i\omega r_*} \ \ as\ r_* \to -\infty, \tag{3.138}$$

means that for $\mathrm{Im}(\omega) < 0$ (like in our case) QNMs diverge exponentially towards the CEH and towards the BEH. Therefore, the convergence of the continued fractions depends on the imaginary part of the frequencies. This is a problem when trying to determine the frequencies numerically, especially for modes whose imaginary part has a large absolute value. This happens in particular for BHs characterized by small vales of M, as can be seen in the plots of [19] and in Figure 7. A further problem could lie in the choice of the units ($\Lambda = 3$), which causes the frequencies to assume very large values for small values of M/r_C, generating numerical problems.

Some results are reported in Figure 7 in units of $M = 1$. If converted in units of $\Lambda = 3$, they correspond to the plots displayed in [19].

3.5 Detectability of quasinormal modes

3.5.1 Theory

In this section, we discuss how to determine whether the quantitative differences (Δ) between the KM and KdS QNM spectra are measurable or not.

If one considers that a detector measures the frequency f of a signal as

$$f = \frac{\text{number of samples}}{\Delta t}, \tag{3.139}$$

then a condition for the detectability of such a frequency is that one has to be able to measure long enough to collect at least one sample. The minimum

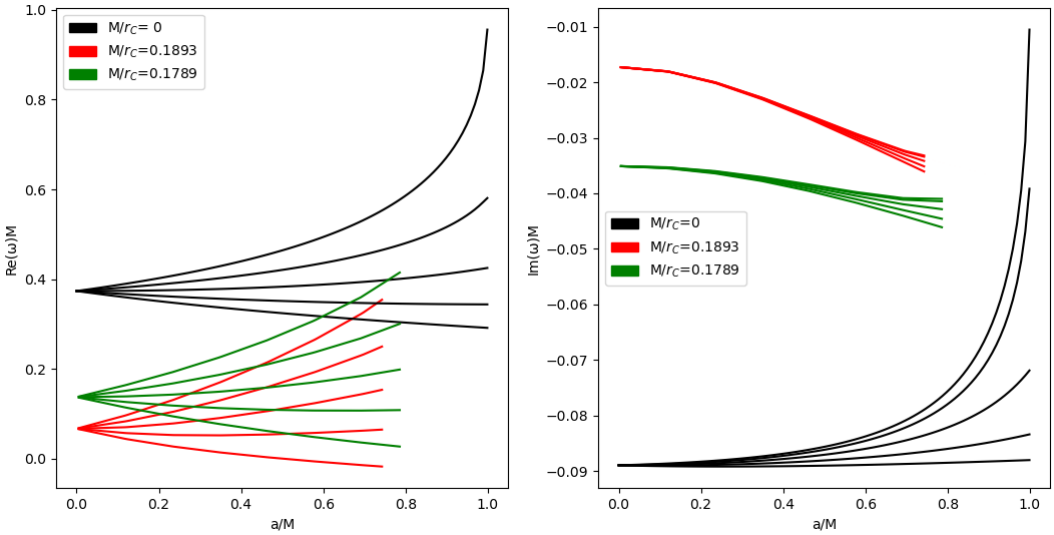

Figure 7: QNM frequencies as a function of a for some values of M/r_C (geometrized units are used). The modes considered are the ones with $l = 2$ and $m = -2, -1, 0, 1, 2$. The black spectrum was generated with the 'qnm' package, while the remaining spectra were generated with our *Python* code.

sampling period needed to resolve an angular frequency difference of Δ can then be expressed as[31]

$$\Delta t = 2\pi\Delta^{-1}. \tag{3.140}$$

3.5.2 Results

We first check whether the minimum sampling time (3.140) represents a plausible period of time for sampling our data. Using the data of Table 7, we deduce that the minimum sampling time needed to resolve the frequency difference is

$$\Delta t \sim 10^{33}\,\mathrm{s}, \tag{3.141}$$

which is of course too long. We deduce that such a frequency difference is too tiny to be measurable.

3.6 Results

We now summarize and discuss the results which we have obtained.

Between the two methods which we have considered, the Heun's function method is the one that works better, because it makes use of the *Mathematica* 'HeunG' function, which enables to compute the solutions of the Heun's differential equation in a very optimized way. It works well for small values

[31] The relation between angular frequency ω and frequency f is given by $f = \omega/2\pi$.

of ΛM^2 and it is therefore the most useful for our purpose. However, because of its high working precision, it is very slow. The continued fractions method, instead, only works for nearly extremal BHs, but it is slightly faster.

By comparing our results with the known limits, we have verified numerically that the QNM frequencies of KdS spacetime tend to the ones of SdS spacetime for $a \to 0$ and to the ones of KM spacetime for $\Lambda \to 0$.

We now analyse the qualitative effects of the cosmological constant on the QNM spectrum, which are visible from Figure 7. The features of the KM spectrum ($\Lambda M^2 = 0$, in black in the figure) were discussed in section 3.1. We now see how these features change as ΛM^2 varies.

By increasing the value of the cosmological constant, at a fixed mass, the BEH and the CEH come closer, reducing the size of the spacetime between the two. As one can see from Figure 7, this has the effect of lowering the real part of the QNM frequency of a non rotating BH. We do not know how to explain this, but this reminds us to what happens with normal modes of a guitar string, for example, where the frequency of the modes also depends on the size of the medium (length of the string). Because of the considerations made in section 3.1, this also means that the velocity of the wave pattern of a non-rotating BH becomes lower in absolute value for all the modes. As a result, for a rotating BH, the whole spectrum is approximately shifted[32] to lower frequencies.

When a non-rotating BH becomes almost extremal, the absolute value of the phase velocity of the wave pattern around the axis is very low. If the BH is rotating, for negative modes, summing this small negative value to the velocity of the local frame near the horizon gives a positive angular velocity with respect to the system defined by (2.41). In this global frame, one then observes that the retrograde modes become prograde. Multiplying this positive velocity with a negative m gives a negative $\mathrm{Re}(\omega)$. This explains the negative frequencies appearing in Figure 7 for nearly extremal BHs at high spins.

An interesting question is whether the negative frequencies are measurable or not. If they were, this fact would constitute a clear observational evidence of a positive cosmological constant. However, even if it were possible to distinguish between positive and negative frequencies, negative frequencies will never be observed for two reasons. First of all, this phenomenon only appears for nearly extremal BHs, which are not astrophysical. Secondly, the frequencies plotted in Figure 7 are measured in the global frame, and correspond to what an observer lying infinitely far away from the BH sees. However, when the

[32]Note that an increase in the spin parameter a also has an effect on the position of the horizons and increases the distance between the BEH and the CEH, as discussed in section 2.2.2. This could have an effect on the QNM spectrum too, and it could explain why the spectrum is not exactly shifted.

cosmological constant is increased, a CEH appears. The local observer must then lie between the two horizons to measure the QNM frequencies, and not at infinity. This means that the observer is subject to frame-dragging effect and must accelerate in order to be at rest with respect to the global system. For nearly extremal BHs, however, this is not possible anymore, because the two horizons are so close that the CEH lies in the ergosphere of the BH. Hence, the observer cannot avoid rotating with respect to the global frame. Therefore, from his point of view, the BH would have a lower spin, and he may not see any negative frequency.

So far, we have discussed the qualitative features of how the real part of the frequency spectrum changes with ΛM^2. We now briefly discuss the imaginary part.

For what we can deduce from Figure 7, as ΛM^2 increases, the absolute value of the damping factor decreases for all modes, but the values always remain negative, which means that no unstable mode is found for $l = 2$ and $m = -2, -1, 0, 1, 2$, at least in the region between the outer and the cosmological horizon. This is in agreement with what was found in [19]. However, the spectrum is not only shifted, but it is also distorted.

To sum up, it seems that qualitative differences between KM and KdS BHs only become important for almost extremal BHs, but are not observable for astrophysical BHs. Moreover, from the results of Section 3.5, it seems that no quantitative differences in the frequencies can be measured. We therefore conclude that the parameters of astrophysical BHs can be recovered using a KM model without producing a measurable error.

4 Summary and outlook

We devoted the first part of the thesis to the study of the features of the Kerr-de Sitter metric. We verified that in the flat limit the Kerr-de Sitter metric reduces to the Kerr-Minkowski metric, while in the non-rotating limit it tends to the Schwarzschild-de Sitter metric. We summarized the results about the space of black hole parameters for which a Kerr-de Sitter solution exists and we discussed the extremal cases, corresponding to situations where two or more horizons overlap. We identified two possible length scales for the Kerr-de Sitter spacetime: the mass, M, and the position of the cosmological horizon of empty de Sitter spacetime, r_C. We understood how to classify Kerr-de Sitter black holes based on the ratio between these two length scales and defined an equivalence relation by saying that two black holes are equivalent if they are characterized by the same value of M/r_C, because this means that they can be scaled into each other. To the best of our knowledge, this fact was not explained in a clear manner before. We also summarized sensible choices of units to describe Kerr-de Sitter spacetime, which reflect the choice of the scale. We then introduced quasinormal modes of Kerr-Minkowski black holes, focusing on gravitational perturbations, and provided a physical interpretation of the degeneracy splitting of the spectrum, based on some hints which were given in [19].
The second part of the thesis was devoted to implement a code to compute the quasinormal mode frequencies of the Kerr-de Sitter black holes numerically. We first implemented the solutions of the Teukolsky equations using the continued fractions method, following [19], but we found out that this code does not work for astrophysical black holes, which are characterized by a small value of the ratio M/r_C. We then used the code already implemented by Hatsuda in [20], which works very well in this region of the parameter space. We computed the difference between the frequencies of the $(2, 2)$ and $(3, 3)$ modes for four astrophysical black hole types and for fixed mass and spin parameter. For each of them, we compared this difference with the same quantity computed for the Kerr-Minkowski black hole and found out that the difference is not measurable. We also commented on the qualitative behaviour of the quasinormal mode spectrum as a function of M/r_C and, based again on some suggestions of [19], we provided a plausible explanation for the appearance of negative quasinormal mode frequencies in nearly extremal Kerr-de Sitter black holes.

This thesis lays the foundations for further studies. First of all, the quantitative differences between quasinormal mode frequencies of Kerr-Minkowski black holes and astrophysical Kerr-de Sitter black holes for other overtone

modes need to be investigated. Furthermore, it remains to understand to what extent the frequency differencies are affected by the propagation of the radiation in de Sitter spacetime, along the path between the black hole horizon and the observer. Finally, it would be interesting to investigate the production of quasinormal modes by black holes in the vicinity of other masses instead of in the vacuum.

Appendices

A Spin-weighted spheroidal harmonics

As shown by Teukolsky in [33], the solutions of the master equations of black holes' linear perturbations can be separated in an angular and a radial part. To describe the angular part, in the case of a Schwarzschild-Minkowski black hole, *spin weighted spherical harmonics* ${}_sY_{lm}$ ([42], [43]) are often employed. However, these functions are not suitable for studying perturbations of Kerr-Minkowski black holes. In these cases, as first realized by Teukolsky ([44], [45]), it is more convenient to use the so-called *spin weighted spheroidal harmonics* ${}_sS_{lm}$. In fact, each quasinormal mode of a Kerr-Minkowski black hole can be associated to one of these functions: ${}_sS_{lmn} = {}_sS_{lm}(a\omega_{lmn})$.
In the following, we define the spin weighted spheroidal harmonics and list their properties. We follow [41], [46], [47] and [34].

Spin-weighted spheroidal harmonics are defined as

$$ {}_sS_{lm}(\theta,\varphi;c) := \frac{1}{2\pi}\,{}_sS_{lm}(\cos\theta;c)e^{im\varphi}, \tag{A.1} $$

where ${}_sS_{lm}(\cos\theta;c)$ is the *spin weighted spheroidal function*, which satisfies the angular Teukolsky equation:

$$ \begin{aligned} &\frac{d}{dx}\left[(1-x^2)\frac{d}{dx}[{}_sS_{lm}(x;c)]\right] \\ &\quad + \left[c^2x^2 - 2csx + s + {}_s\,A_{lm}(c) - \frac{(m+sx)^2}{1-x^2}\right]_s S_{lm}(x;c) = 0, \end{aligned} \tag{A.2} $$

where $x = \cos\theta$, $c = a\omega$ is the oblateness parameter, θ is the Boyer-Lindquist polar angle, ω is the quasinormal mode frequency and ${}_sA_{lm}$ is the angular separation constant. The *spin-weight* s takes the values $s = 0, \pm1, \pm2$ for massless scalar, vector and tensor perturbations, respectively. The relation between the spin weight s and the spin S is the following: $S = |s|$. l is an integer satisfying the inequality $l \geq \max(|m|,|s|)$ and m can take $2l+1$ integer values between $-l$ and l.

The spin-weighted spheroidal harmonics are generalizations of the spin-weighted spherical harmonics, which represent the non-rotating limit $a \to 0$: ${}_sY_{lm} =_s S_{lm}(\theta,\phi;0)$, for which

$$ {}_sA_{lm} = l(l+1) - s(s+1). \tag{A.3} $$

Spin-weighted spheroidal harmonics with angular indices (l,m) are a superposition of spherical harmonics with the same value of m but different values

of l:

$$ {}_sS_{lm}(\theta,\phi;c) = \sum_{l'=l_{min}}^{\infty} C_{l'lm}(c)\,{}_sY_{l'm}(\theta,\phi). \tag{A.4} $$

The ${}_sY_{lm}$ form a complete orthogonal basis set for the space of solutions of (A.2), while the ${}_sS_{lm}(\theta,\phi;c)$ do not, in general.

The basic symmetries of the spin-weighted spheroidal functions follow from equation (A.2) using the transformations $\{s \to -s, x \to -x\}$, $\{m \to -m, x \to -x, c \to -c\}$ and complex conjugation. It follows that the spin-weighted spheroidal functions and the separation constants satisfy the following conditions (cf. [41]):

$$ {}_{-s}S_{lm}(x;c) = (-1)^{l+m}\,{}_sS_{lm}(-x;c), \tag{A.5} $$

$$ {}_sS_{l(-m)}(x;c) = (-1)^{l+s}{}_sS_{lm}(-x;-c), \tag{A.6} $$

$$ {}_sS^*_{lm}(x;c) =_s S_{lm}(x;c^*), \tag{A.7} $$

and

$$ -s A_{lm}(c) =_s A_{lm}(c) + 2s, \tag{A.8} $$

$$ {}_sA_{l(-m)}(c) =_s A_{lm}(-c), \tag{A.9} $$

$$ {}_sA^*_{lm}(c) =_s A_{lm}(c^*). \tag{A.10} $$

B Heun's differential equation

Here, report the theory about Heun's differential equation that is necessary to understand this work. This part is taken from [48] and [20].

Heun's differential equation is a second-order linear ordinary differential equation of the form

$$y''(z) + \left[\frac{\gamma}{z} + \frac{\delta}{z-1} + \frac{\epsilon}{z-a}\right] y'(z) + \frac{\alpha\beta(z-q)}{z(z-1)(z-a)} y(z) = 0 \tag{B.1}$$

with an extra condition on the coefficients:

$$\alpha + \beta + 1 = \gamma + \delta + \epsilon. \tag{B.2}$$

The coefficient q is called the *accessory parameter*. This equation has four regular singular points at $z = 0$, $z = 1$, $z = a$ and $z = \infty$ in $\mathbb{C} \cup \{\infty\}$.

For the purpose of this work, we are interested in studying the behavior of the solutions of this equation near the singular points $z = 0$, $z = 1$ and $z = z_a$. As explained in chapters 2.4 and 8 of [48] and in [20], near a regular singular point $c \in \mathbb{C}$, it is possible to construct a Frobenius solution of the Heun's function, i.e., a solution of the form

$$y_c^i(z) = (z-c)^{\alpha_{c,i}} \sum_{n=1}^{\infty} a_n^{c,i} (z-c)^n, \tag{B.3}$$

where $i = 1, 2$ and $\alpha_{c,i}$ is a constant that only depends on the parameters $\alpha, \beta.\gamma, \delta, \epsilon$ of equation (B.1). In particular, $\alpha_{c,i}$ with $i = 1, 2$ are solutions of a quadratic equation, called *indicial equation*, that only depends on these parameters. The two solutions $y_c^1(z)$ and $y_c^2(z)$ constructed in this way are linearly independent if $\alpha_{c,1} - \alpha_{c,2}$ is not an integer. In the case where $\alpha_{c,1} - \alpha_{c,2} \in \mathbb{Z}$, the linear independence of the solutions is not guaranteed. These Frobenius solutions are convergent inside a circle, whose radius is determined in general by the distance from the nearest singularity.

One denotes with

$$Hl(a, q; \alpha, \beta, \gamma, \delta, \epsilon; z) = \sum_{n=1}^{\infty} a_n^{0,1} z^n, \tag{B.4}$$

the local solution of the Heun's function which is regular at the singular point[33] $z = 0$ and use the normalization

$$Hl(a, q; \alpha, \beta, \gamma, \delta, \epsilon; 0) = 1. \tag{B.5}$$

[33] In *Mathematica*, this solution is called *Heun function*. However, in the literature, the term "Heun function" seems to denote a solution which is analytic at two singular points [20].

Using this notation and the fact that the two roots of the indicial equation $\alpha_{c,i}$ are 0 and $1-\gamma$ for $c=0$, 0 and $1-\delta$ at $c=1$, and 0 and $1-\epsilon$ at $c=a$, one can express the solutions near $z=0$ as given in [49]:

$$y_0^1(z) = Hl(a,q;\alpha,\beta,\gamma,\delta,\epsilon;z), \tag{B.6}$$

$$y_0^2(z) = z^{1-\gamma}Hl(a,(a\delta+\epsilon)(1-\gamma)+q;\alpha+1-\gamma,\beta+1-\gamma,2-\gamma,\delta;z). \tag{B.7}$$

the solutions near $z=1$ as:

$$y_1^1(z) = Hl(1-a,\alpha\beta-q;\alpha,\beta,\delta,\gamma;1-z), \tag{B.8}$$

$$y_1^2(z) = (1-z)^{1-\delta}Hl(1-a,((1-a)\gamma+\epsilon)(1-\delta)+\alpha\beta-q;\alpha+1-\delta, \beta+1-\delta,2-\delta,\gamma;1-z), \tag{B.9}$$

and the solutions near $z=a$ as:

$$y_a^1(z) = Hl\left(\frac{a}{a-1},\frac{\alpha\beta a-q}{a-1};\alpha,\beta,\epsilon,\delta;\frac{a-z}{a-1}\right), \tag{B.10}$$

$$y_a^2(z) = \left(\frac{a-z}{a-1}\right)Hl(\frac{a}{a-1},\frac{(a(\delta+\gamma)-\gamma)(1-\epsilon)}{a-1}+\frac{\alpha\beta a-q}{a-1}; \tag{B.11}$$

$$\alpha+1-\epsilon,\beta+1-\epsilon,2-\epsilon,\delta;\frac{a-z}{a-1}). \tag{B.12}$$

In *Mathematica*, the Heun function [39] is implemented as

$$\text{HeunG[a, q, }\alpha,\beta,\gamma,\delta,\text{ z]}. \tag{B.13}$$

Note that the parameter $\epsilon=\alpha+\beta+1-\gamma-\delta$ does not appear because it is not linear independent. 'HeunG' concides locally with Hl, while globally it represents the analytic continuation of Hl.

B.1 Wronskian method

For dealing with two-point boundary value problems between $z=0$ and $z=1$, like the ones presented in this work, it is useful to consider connection relations between the local solutions in different domains. In the intersection of the convergence circles at $z=0$ and $z=1$, we express the local solutions at $z=0$ as a linear combination of the two local solutions at $z=1$:

$$y_0^1(z) = C_{11}y_1^1 + C_{12}y_1^2, \tag{B.14}$$

$$y_0^2(z) = C_{21}y_1^1 + C_{22}y_1^2. \tag{B.15}$$

The connection coefficients $C_{ij}=C_{ij}(\omega,\lambda)$ are functions of the quasinormal mode frequency ω and of the separation constant λ, but do not depend on z. For our purposes, it is useful to express such coefficients as a function of the local solutions, since this allows to find useful relations to determine ω and λ. This can be done by means of the Wronskian method described below. We follow Hatsuda [20] and try to complete his reasoning by adding some explanations and calculations.

We begin with a useful definition, corresponding to Definition 2.2 of [48]:

Definition B.1 (Wronskian)**.** Let $y_1(z)$ and $y_2(z)$ be two meromorphic functions in a domain S. The Wronskian[34] of the functions $y_1(z)$ and $y_2(z)$ is then defined as

$$W(y_1, y_2; z) = y_1(z)y_2'(z) - y_1'(z)y_2(z), \quad z \in S.$$

$W(y_1, y_2; z)$ can be seen as the determinant of the matrix

$$\begin{pmatrix} y_1(z) & y_2(z) \\ \frac{dy_1(z)}{dz} & \frac{dy_2(z)}{dz} \end{pmatrix}.$$

The following lemma from [48], which relates the Wronskian with the angular dependence of two meromorphic functions, is also useful:

Lemma B.1. *Let $y_1(z)$ and $y_2(z)$ be two meromorphic functions in a domain S. A necessary and sufficient condition that $y_1(z)$ and $y_2(z)$ are linearly dependent is*

$$W(y_1, y_2; z) = 0, \quad z \in S.$$

In the case that the solutions y_1^1 and,y_1^2 are linearly independent, the following theorem, known as *Cramer's Rule*[35] (see Theorem 2.9 of [50]), will be useful:

Theorem B.1 (Cramer's Rule)**.** *Let A be an invertible $n \times n$ matrix and b an $n \times 1$ column vector. Denote by B_i the matrix obtained from A by replating the ith column of A by b. Then the linear system $Ax = b$ has unique solution $x = (x_1, x_2, ..., x_n)$, where*

$$x_i = \frac{\det B_i}{\det A}, \quad i = 1, 2, ..., n.$$

As an example, we apply this theorem to express the coefficient C_{12} as a function of the Wronskians of the local solutions of the Heun's equation at $z = 0$ and $z = 1$. We assume linear independence of y_1^1 and y_1^2 and consider equation (B.14) and its first derivative:

$$y_0^1(z) = C_{11}y_1^1 + C_{12}y_1^2, \tag{B.16}$$

$$\frac{dy_0^1(z)}{dz} = C_{11}\frac{dy_1^1}{dz} + C_{12}\frac{dy_1^2}{dz}. \tag{B.17}$$

This system of equations can be rewritten as

$$\begin{pmatrix} y_0^1(z) \\ \frac{dy_0^1(z)}{dz} \end{pmatrix} = \begin{pmatrix} y_1^1(z) & y_1^2(z) \\ \frac{dy_1^1(z)}{dz} & \frac{dy_1^2(z)}{dz} \end{pmatrix} \cdot \begin{pmatrix} C_{11} \\ C_{12} \end{pmatrix}. \tag{B.18}$$

[34] Józef Maria Hoëne-Wrónski (1778-1853), Polish mathematician.

[35] Gabriel Cramer (1704-1752), Swiss mathematician.

By means of Cramer's Rule, we can now express C_{12} as

$$C_{12} = \frac{\det \begin{pmatrix} y_1^1(z) & y_0^1(z) \\ \frac{dy_1^1(z)}{dz} & \frac{dy_0^1(z)}{dz} \end{pmatrix}}{\det \begin{pmatrix} y_1^1(z) & y_1^2(z) \\ \frac{dy_1^1(z)}{dz} & \frac{dy_1^2(z)}{dz} \end{pmatrix}} = \frac{W(y_1^1, y_0^1; z)}{W(y_1^1, y_1^2; z)}. \tag{B.19}$$

The same can be done with the remaining coefficients. Therefore, knowing the local solutions, it is possible to evaluate the connection coefficients.
Note that in the case where the local solutions at $z = 1$ are not linear independent, the Cramer's Rule cannot be applied, because $W(y_1^1, y_1^2; z) = 0$, and hence the matrix

$$\begin{pmatrix} y_1^1(z) & y_1^2(z) \\ \frac{dy_1^1(z)}{dz} & \frac{dy_1^2(z)}{dz} \end{pmatrix}$$

is not invertible.

C The 'qnm' package for python

The 'qnm' package ([34]) is an open-source *Python* package for computing the Kerr-Minkowski quasinormal mode frequencies, separation constants and spherical-spheroidal mixing coefficients (the $C_{l'lm}$ in equation (A.4)). It makes use of Leaver's continued fractions technique ([12]) to compute the radial eigenvalues and uses the Cook-Zalutskiy spectral approach ([41]) for determining the angular eigenvalues. The latter approach consists in transforming the angular Teukolsky equation in a simple matrix eigenvalue equation, which can be solved fast in *Python*.

We report here the Leaver's solver for computing continued fractions implemented in the 'qnm' package, as well as an introduction on the used algorithm.

C.1 Modified Lentz's algorithm

In the following, we present the *modified Lentz's algorithm*, which allows to evaluate infinite continued fractions expressions of the form

$$f(x) = b_0 + \cfrac{a_1}{b_1 + \cfrac{a_2}{b_2 + \cfrac{a_3}{b_3 + \cfrac{a_4}{b_4 + \dots}}}}. \tag{C.1}$$

This part is taken from [51].

Continued fractions often converge more rapidly than power series expansions, but unlike series, one cannot simply evaluate expression (C.1) from left to right and stop when the change is small. In order to proceed in this way, one needs to rewrite expression (C.1) in a more convenient way. One defines:

$$f_n = b_0 + \cfrac{a_1}{b_1 + \cfrac{a_2}{b_2 + \cfrac{a_3}{b_3 + \cfrac{\dots}{\dots + b_n}}}}, \tag{C.2}$$

and claims that this expression can be rewritten as

$$f_n = \frac{A_n}{B_n}, \tag{C.3}$$

where A_n and B_n are given by the following recurrence:

$$\begin{gathered} A_{-1} := 1, \quad B_{-1} := 0, \\ A_0 := b_0, \quad B_0 := 1, \\ A_j = b_j A_{j-1} + a_j A_{j-2}, \quad B_j = b_j B_{j-1} + a_j B_{j-2}, \quad j = 1, 2, ..., n. \end{gathered} \tag{C.4}$$

This can be easily proved by induction. This recurrence relation often generates very small or very large values for A_j and B_j. To solve this problem, one introduces the following ratios that allow to rescale intermediate results:

$$C_j := A_j / A_{j-1}, \quad D_j := B_{j-1} / B_j. \tag{C.5}$$

Using the relations (C.4), one can show that C_j and D_j satisfy the following recurrence relations:

$$C_j = b_j + a_j/C_{j-1}, \quad D_j = 1/(b_j + a_j D_{j-1}). \tag{C.6}$$

Step j of the algorithm consists in computing C_j and D_j using the relations (C.6), together with step $j-1$. f_j can then be expressed as

$$f_j = f_{j-1} C_j D_j. \tag{C.7}$$

It could happen that C_j or the denominator of D_j become 0. However, as shown by Thompson and Barnett in [52], one can fix this problem by shifting the term that is 0 by a small amount ('tiny'), e.g., 10^{-30}.

One proceeds in this way until $|f_j - f_{j-1}|/f_{j-1}$ is smaller than a given tolerance 'eps' (e.g. 10^{-10}). If one denotes:

$$C_j D_j =: \Delta_j, \tag{C.8}$$

then f_j can be rewritten as

$$f_j = f_{j-1} \Delta_j \tag{C.9}$$

and the stopping criterion as:

$$|\Delta_j - 1| < \text{eps}, \tag{C.10}$$

because $|f_j - f_{j-1}|/f_{j-1} = |\Delta_j - 1|$.

We report the scheme of the algorithm's step from [51], which is also used in the 'qnm' package:

- Set $f_0 = b_0$; if $b_0 = 0$, set $f_0 = \text{tiny}$.
- Set $C_0 = f_0$.
- Set $D_0 = 0$.
- For $j = 1, 2, ...$
  Set $D_j = b_j + a_j D_{j-1}$.
  If $D_j = 0$, set $D_j = \text{tiny}$.
  Set $C_j = b_j + a_j/C_{j-1}$.
  If $C_j = 0$, set $C_j = \text{tiny}$.
  Set $D_j = 1/D_j$.
  Set $\Delta_j = C_j D_j$.
  Set $f_j = f_{j-1}\Delta_j$.
  If $|\Delta_j - 1| < \text{eps}$, then exit.

Below, we report an implementation of the modified Lentz's algorithm which is contained in the 'qnm.contfrac' file of the 'qnm' package.

Listing 1: *Python* code for the modified Lentz's algorithm, taken from [34]

```
import numpy as np

def lentz(a, b, tol=1.e-10, N_min=0, N_max=np.Inf, tiny=1.e-30):
    """ Compute a continued fraction via modified Lentz's method.

    Parameters
    ----------
    a: callable returning numeric.
    b: callable returning numeric.

    tol: float [default: 1.e-10]
      Tolerance for termination of evaluation.

    N_min: int [default: 0]
      Minimum number of iterations to evaluate.

    N_max: int or comparable [default: np.Inf]
      Maximum number of iterations to evaluate.

    tiny: float [default: 1.e-30]
      Very small number to control convergence of Lentz's method when
      there is cancellation in a denominator.

    Returns
    -------
    (float, float, int)
      The first element of the tuple is the value of the continued
      fraction. The second element is the estimated error. The third
      element is the number of iterations.

    """

    f_old = b(0)

    if (f_old == 0):
        f_old = tiny

    C_old = f_old
    D_old = 0.
```

```
conv = False

j = 1

while ((not conv) and (j < N_max)):

    aj, bj = a(j), b(j)

    D_new = bj + aj * D_old

    if (D_new == 0):
        D_new = tiny

    C_new = bj + aj / C_old

    if (C_new == 0):
        C_new = tiny

    D_new = 1./D_new
    Delta = C_new * D_new
    f_new = f_old * Delta

    if ((j > N_min) and (np.abs(Delta - 1.) < tol)): # converged
        conv = True

    # Set up for next iter
    j = j + 1
    D_old = D_new
    C_old = C_new
    f_old = f_new

# Success or failure can be assessed by the user
return f_new, np.abs(Delta - 1.), j-1
```

D The numerical codes

D.1 Schwarzschild-de Sitter

The complex quasinormal mode frequencies of a Schwarzschild-de Sitter black hole can be computed with the *Mathematica* code reported in listing 2 via the Pöschl-Teller approximation when the ratio $M/r_C = \sqrt{\Lambda M^2/3}$ and the quantum numbers n and l are given (here are $M/r_C = 0.1893$, $n = 0$ and $l = 2$ as an example).

Listing 2: Mathematica code for computing QNM frequencies of a SdS BH.

```
(*Input ratio M/r_C*)
ratio = 1893/10000

(*Setting the units*)
Lam = 3*ratio^2 (*This is Λ in units of M=1*)
M = 1

(*Setting the quantum numbers*)
l = 2
n = 0

(*Computing SdS QNM using the Poeschl-Teller approximate potential*)
f[r_] := 1-(2*M/r)-Lam*r^2/3
roots = r /. Solve[-Lam/3*r^3+r-2*M==0,r, WorkingPrecision->40]
pot[r_]:= f[r]*(l*(l+1)/r^2-6*M/r^3)
secondder[r_]:= pot''[r]*f[r]^2+pot'[r]*f'[r]*f[r]
max = Maximize[{ pot[r], Part[roots,2]<= r <= Part[roots,3]}, r]
V0 = Part[max,1]
r0 = r /. Last[max]
b = Sqrt[1/(-1/(2*V0)*secondder[r0])]
omega = 1/b*(Sqrt[V0*b^2-1/4]-(n+1/2)*I)
```

D.2 Kerr-de Sitter

D.2.1 Quasinormal mode frequencies via the continued fractions method

The code reported in listing 3 is the direct implementation, written in *Python*[36], of the continued fractions method described in [19] for the computation of

[36] We have also implemented a *Mathematica* version, which does exactly the same computations. However, since it leads to the same results, we do not report it here.

Kerr-de Sitter quasinormal mode frequencies. Here, the fundamental ($n = 0$) frequencies are computed in units of $\Lambda = 3$ when the ratio M/r_C and the quantum numbers s, l and m are given (here are $M/r_C = 0.1893$, $s = -2$, $l = 2$ and $m = 2$ as an example). Note that a starting value, corresponding to the value of the Schwarzschild-de Sitter quasinormal mode frequency (in $\Lambda = 3$ units) associated with the given value of M/r_C, must be provided.

Listing 3: Python code for computing quasinormal mode frequencies of a Kerr-de Sitter black hole via the continued fractions method.

```
import cmath
import numpy as np
from scipy.optimize import root
from qnm.contfrac_modified import lentz # This is the function reported
    in listing 1 and slightly modified to make the continued fractions
    depend on omega and lambda.

### Angular eigenvalue equation ###

def A3(om,a,alph):
    return 1j/2*((1+alph)/np.sqrt(alph)*a*om-np.sqrt(alph)*m-s*1j)

def zs(alph):
    return 1j*(1+1j*np.sqrt(alph))**2/(4*np.sqrt(alph))

def u1(om,a,alph):
    return 0.5*(2+4*A3(om,a,alph)+4*A2*(1+A3(om,a,alph))+4*A1*(1+
        A2+A3(om,a,alph))+m**2-2j*a*m*s+s**2+2j*s*om+2j*a**2*s*
        om)

def u0(om,lam,a,alph):
    return -1j/(8*a)*(-2*A2-2*A1*(1+2*A2)-m**2-2*s+s**2+a
        **2*(2*A2+A1*(2+4*A2)-3*m**2+2*s-4*m*s-s**2)+4*a**3*(m
        +s)*om-2j*a*(2+2*A2+4*A3(om,a,alph)+A1*(6+4*A2+8*A3(om,
        a,alph))+m**2-2*m*s+s**2+2j*m*om+2j*s*om)+2*lam)

def alpha_theta_n(n,alph):
    return zs(alph)*(1+n)*(1+n+2*A1)

def beta_theta_n(n,om,lam,a,alph):
    return u0(om,lam,a,alph)-(1+zs(alph))*n**2-(1+2*A3(om,a,alph)+zs
        (alph)+2*A2*zs(alph)+2*A1*(1+zs(alph)))*n
```

```
def gamma_theta_n(n,om,a,alph):
    return -1-2*A3(om,a,alph)+2*A1*(n-1)+2*A2*(n-1)+2*A3(om,a,
        alph)*n+n**2+u1(om,a,alph)

### modified Lentz algorithm ###

def aa(n,om,a,alph,M):
    return -gamma_theta_n(n,om,a,alph)*alpha_theta_n(n-1,alph)

def b(n,om,lam,a,alph,M):
    return beta_theta_n(n,om,lam,a,alph)

def A(om,lam,a,alph,M):
    return lentz(aa,b,om,lam,a,alph,M, tol = 1e-15)[0]

### Radial eigenvalue equation ###

def horizons(M,a,alph):
    p = np.array([-alph/a**2,0,1-alph,-2*M,a**2])
    r = np.roots(p)
    for i in range(len(r)):
        if r.imag[i]!=0:
            return "No KdS Black hole possible!"
    return np.sort(r)

def deriv_ri(M,a,alph,ri):
    return -4*alph/a**2*ri**3+2*(1-alph)*ri-2*M

def kappa(M,a,alph,ri):
    return 1./(2*(1+alph)*(ri**2+a**2))*deriv_ri(M,a,alph,ri)

def Om(ri,a):
    return a/(ri**2+a**2)

def om_bar(om,ri,a):
    return om-m*Om(ri,a)

def B1(M,a,alph,om):
    rplus = horizons(M,a,alph)[2]
```

```
    kplus = kappa(M,a,alph,rplus)
    return -s-(om_bar(om,rplus,a)/(2*kplus))*1j

def B2(M,a,alph,om):
    rminus = horizons(M,a,alph)[1]
    kminus = kappa(M,a,alph,rminus)
    return (om_bar(om,rminus,a)/(2*kminus))*1j

def B3(M,a,alph,om):
    rplusplus = horizons(M,a,alph)[3]
    kplusplus = kappa(M,a,alph,rplusplus)
    return (om_bar(om,rplusplus,a)/(2*kplusplus))*1j

def b1(M,a,alph,om):
    rplus = horizons(M,a,alph)[2]
    kplus = kappa(M,a,alph,rplus)
    return (om_bar(om,rplus,a)/(2*kplus))*1j

def b2(M,a,alph,om):
    return B2(M,a,alph,om)

def b3(M,a,alph,om):
    return B3(M,a,alph,om)

def b4(M,a,alph,om):
    rminmin = horizons(M,a,alph)[0]
    kminmin = kappa(M,a,alph,rminmin)
    return (om_bar(om,rminmin,a)/(2*kminmin))*1j

def v1(M,a,alph,om):
    B11 = B1(M,a,alph,om)
    B22 = B2(M,a,alph,om)
    B33 = B3(M,a,alph,om)
    b44 = b4(M,a,alph,om)
    return (B11+B22+B33-b44+s+1)*(B11+B22+B33+b44+2*s+1)

def v0(M,a,alph,om,lam):
    rmm = horizons(M,a,alph)[0]
    rm = horizons(M,a,alph)[1]
    rp = horizons(M,a,alph)[2]
```

```
    rpp = horizons(M,a,alph)[3]
    b11 = b1(M,a,alph,om)
    b22 = b2(M,a,alph,om)
    b33 = b3(M,a,alph,om)
    b44 = b4(M,a,alph,om)
    B11 = B1(M,a,alph,om)
    B22 = B2(M,a,alph,om)
    B33 = B3(M,a,alph,om)
    return -1/((rp-rm)*(rpp-rmm))*(lam+2*s*(a**2-1)+(B22-b22*s+
        B22*s-b11*(2*b22+s)+B11*(1+2*B22+s))*rpp*rmm-(-1+2*b11
        **2+(-3+b22+b33+b44)*s-2*s**2+b11*(2*b22+2*b33+2*b44+5*
        s))*rp**2-(B22+B33-b22*s-b33*s+B22*s+B33*s-2*b11*(b22+
        b33+s)+2*B11*(1+B22+B33+s))*rp*rmm+(1+2*b11**2+B33+3*s
        +b22*s+b44*s+B33*s+2*s**2+B11*(1+2*B33+s)+2*b11*(b22+
        b44+2*s))*rp*rpp+(1+2*b11**2+B22+3*s+b33*s+b44*s+B22*s
        +2*s**2+B11*(1+2*B22+s)+2*b11*(b33+b44+2*s))*rp*rm+(B33
        -b33*s+B33*s-b11*(2*b33+s)+B11*(1+2*B33+s))*rm*rmm
        -(1+2*b11**2+B22+B33+3*s+b44*s+B22*s+B33*s+2*s**2+2*
        B11*(1+B22+B33+s)+b11*(2*b44+3*s))*rm*rpp-4*1j*s*om*(1+a
        **2)*rp)

def xr(M,a,alph):
    rmm = horizons(M,a,alph)[0]
    rm = horizons(M,a,alph)[1]
    rp = horizons(M,a,alph)[2]
    rpp = horizons(M,a,alph)[3]
    return (rm-rmm)*(rpp-rp)/((rm-rp)*(rpp-rmm))

def alpha_r_n(n,M,a,alph,om):
    return (1+n)*(1+2*B1(M,a,alph,om)+n+s)

def beta_r_n(n,M,a,alph,om,lam):
    xrr = xr(M,a,alph)
    B11 = B1(M,a,alph,om)
    B22 = B2(M,a,alph,om)
    B33 = B3(M,a,alph,om)
    v00 = v0(M,a,alph,om,lam)
    return v00-(1+xrr)*n**2-(1+2*B33+2*s+xrr+2*B22*xrr+2*s*xrr
        +2*B11*(1+xrr))*n
```

```
def gamma_r_n(n,M,a,alph,om):
    xrr = xr(M,a,alph)
    B11 = B1(M,a,alph,om)
    B22 = B2(M,a,alph,om)
    B33 = B3(M,a,alph,om)
    v11 = v1(M,a,alph,om)
    return (-1+2*(B11+B22+B33)*(n-1)+n**2-3*s+3*n*s+v11)*xrr

### Modified Lentz algorithm ###

def ar(n,om,a,alph,M):
    return -gamma_r_n(n,M,a,alph,om)*alpha_r_n(n-1,M,a,alph,om)

def br(n,om,lam,a,alph,M):
    return beta_r_n(n,M,a,alph,om,lam)

def B(M,a,alph,om,lam):
    return lentz(ar,br,om,lam,a,alph,M,tol = 1e-15)[0]

### Initial guess ###

#lambda
def lam0(l,s):
    return l*(l+1)-s*(s-1)

#omega (take the value of the Schwarzschild-de Sitter QNM frequency)
def om0(M):
    return 0.3522-0.09070j

def x0(l,s,M):
    x0=np.array([om0(M),lam0(l,s)],dtype=complex)
    return np.array([x0.real[0], x0.imag[0],x0.real[1], x0.imag[1]])


### Solving the system of continued fractions equations using scipy.
    optimize.root ###

''' Since scipy.optimize.root only works with real numbers, we pack
    complex numbers into vectors of real numbers'''
```

```
def func(x,a,alph,M): # This is a vector function func(om,lam) = (A(om,
    lam), B(om,lam)), where x is an array (Re(om),Im(om),Re(lam),Im(lam
    ))
    xx = np.array([x[0]+x[1]*1j,x[2]+x[3]*1j])
    func = np.array([A(xx[0],xx[1],a,alph,M), B(M,a,alph,xx[0],xx[1])],
        dtype = complex)
    return np.array([func[0].real,func[0].imag,func[1].real,func[1].imag])

def solve(a,alph,M,x0):
    sol = root(func,x0,args=(a,alph,M), method = 'hybr',options={'xtol': 1
        e-9,'eps': 1e-15})
    return np.array([sol[0]+sol[1]*1j,sol[2]+sol[3]*1j])

### Defining the physical parameters ###

M = 0.1893 # M/r_C
a_max = 0.1978 # maximum value of the spin parameter
Lam = 3 # cosmological constant

s = -2 # spin weight
l = 2 # angular quantum number
m = 2 # azimuthal quantum number

A1 = abs(m-s)/2
A2 = abs(m+s)/2

x00 = x0(l,s,M) # initial guess

ang_mom = [0.001*a_max]
omega_real = []
omega_imag = []
lam_real = []
lam_imag = []

### The algorithm ###

i = 0
while ang_mom[-1] <= a_max:
    print("a =", ang_mom[i])
    a = ang_mom[i]
```

```
alph = Lam*a**2/3
sol  = solve(a,alph,M,x00)
omega_real.append(sol.real[0])
omega_imag.append(sol.imag[0])
lam_real.append(sol.real[1])
lam_imag.append(sol.imag[1])
if  i<2:
    x00 = np.array([sol.real[0], sol.imag[0], sol.real[1], sol.imag[1]])
    np.save('omega_real_M={0},m={1}'.format(M,m),omega_real)
    np.save('omega_imag_M={0},m={1}'.format(M,m),omega_imag)
    np.save('ang_mom_M={0},m={1}'.format(M,m),ang_mom)
    ang_mom.append(ang_mom[i]+1e-1*a_max)
    i+=1
else:
    x1om = omega_real[i-2:]
    x2om = omega_imag[i-2:]
    x1lam = lam_real[i-2:]
    x2lam = lam_imag[i-2:]
    c1om = np.polyfit(ang_mom[i-2:], x1om,2)
    c2om = np.polyfit(ang_mom[i-2:], x2om,2)
    c1lam = np.polyfit(ang_mom[i-2:], x1lam,2)
    c2lam = np.polyfit(ang_mom[i-2:], x2lam,2)
    np.save('ang_mom_M={0},m={1}'.format(M,m),ang_mom)
    ang_mom.append(ang_mom[i]+1e-1*a_max)
    x00 = np.array([np.polyval(c1om,ang_mom[i+1]),np.polyval(c2om,
        ang_mom[i+1]),np.polyval(c1lam,ang_mom[i+1]),np.polyval(
        c2lam,ang_mom[i+1])])
    np.save('omega_real_M={0},m={1}'.format(M,m),omega_real)
    np.save('omega_imag_M={0},m={1}'.format(M,m),omega_imag)
    i+=1
```

D.2.2 Quasinormal mode frequencies via the Heun's function method

The code reported in listing 4 is taken directly from the *Mathematica* notebook of [20]. Here, the Kerr-de Sitter quasinormal mode frequencies are computed in units of $M = 1$ when the values of s, l, m and a are given (here is $s = -2$, $l = 2$, $m = 2$ and $a = 0.6$ as an example). Note that a starting value, corresponding to the values of the Kerr-Minkowski quasinormal mode frequency (in $M = 1$ units) and separation constant at the given value of a must be provided. This can be done using the 'qnm' package for *Python*.

Listing 4: Mathematica code for computing quasinormal mode frequencies of a Kerr-de Sitter black hole via the Heun's function method.

```
(*This part computes Wronskians of angular solutions*)

angular[{s_,l_,m_},{M_,Λ_,a_},{ω_,λ_}]:=Block[{α 0,aH,A1,A2,A3,
    A3c,c,α,β,γ,δ,ϵ,q,y01,y02,y11,y12},α0=(Λ a^2)/3;
aH=-((1-I/Sqrt[α0])^2/(4I/Sqrt[α0]));c=a ω;
A1=(m-s)/2; A2=-((m+s)/2); A3=I/2 ((1+α0)/Sqrt[α0] c-m Sqrt[α0]-
    I s); A3c=-I/2 ((1+α0)/Sqrt[α0] c-m Sqrt[α0]+I s);
α=1; β=1-s-I m Sqrt[α0]+I c(Sqrt[α0]+1/Sqrt[α0]); γ=2A1+1; δ=2A2
    +1;ϵ=2A3+1;
q=(I λ)/(4Sqrt[α0])+1/2+A1+(m+1/2)(A3-A3c);
y01[z_]:=HeunG[aH,q,α,β,γ,δ,z];
y02[z_]:=z^(1-γ) HeunG[aH,(aH δ+ϵ)(1-γ)+q,α+1-γ,β+1-γ,2-γ,δ,z] ;
y11[z_]:=HeunG[1-aH,αβ-q,α,β,δ,γ,1-z];
y12[z_]:=(1-z)^(1-δ) HeunG[1-aH,((1-aH)γ+ϵ)(1-δ)+α β-q,α+1-δ,β
    +1-δ,2-δ,γ,1-z];

Which[(m-s>=0)&&(-m-s>=0),Det[{{y01[z],y11[z]},{y01'[z],y11'[z]}}]/.
    z->1/2,
(m-s>=0)&&(-m-s<0),Det[{{y01[z],y12[z]},{y01'[z],y12'[z]}}]/.z->1/2,
(m-s<0)&&(-m-s>=0),Det[{{y02[z],y11[z]},{y02'[z],y11'[z]}}]/.z->1/2,
(m-s<0)&&(-m-s<0),Det[{{y02[z],y12[z]},{y02'[z],y12'[z]}}]/.z->1/2]]

(*This part computes Wronskians of radial solutions*)

radial[{s_,l_,m_},{M_,Λ_,a_},{ω_,λ_},prec_]:=Block[{
    MinPrecision = prec,MaxExtraPrecision=2prec,Δr,Kr,α0,rp,rm,rpp,
    rmp,B1,B2,B3,aH,α,β,γ,δ,ϵ,q,y01,y02,y11,y12,con},
Δr[r_]:=(r^2+a^2)(1-Λ/3 r^2)-2M r;
Kr[r_]:=ω(r^2+a^2)-a m;
α0=(Λ a^2)/3;
{rmp,rm,rp,rpp}=Sort[r/.NSolve[Δr[r]==0,r,WorkingPrecision->prec]];
aH=((rpp-rm)(rmp-rp))/((rpp-rp)(rmp-rm));
B1=(I(1+α0)Kr[rp])/Δr'[rp];B2=(I(1+α0)Kr[rpp])/Δr'[rpp];B3=(I(1+α0)
    Kr[rmp])/Δr'[rmp];
α=2s+1;β=s+1-(2I(1+α0)Kr[rm])/Δr'[rm];
γ=2B1+s+1;δ=2B2+s+1;ϵ=2B3+s+1;
q=-(((1+s) (1+2 s)rmp )/(rm-rmp)+(3 λ-2 s (3-a^2 Λ)+Λ(1+s) (1+2 s)
```

```
    rp (rp+rpp))/(Λ(rm−rmp) (rp−rpp) )−(2 I (1+2 s) (3+a^2 Λ) (rp rm ω
    +a^2 ω−a m))/(Λ(rm−rmp) (rm−rp) (rp−rpp) ));
y01[z_]:=HeunG[aH,q,α,β,γ,δ,z];
y02[z_]:=z^(1−γ) HeunG[aH,(aH δ+ϵ)(1−γ)+q,α+1−γ,β+1−γ,2−γ,δ,z] ;
y11[z_]:=HeunG[1−aH,α β−q,α,β,δ,γ,1−z];
y12[z_]:=(1−z)^(1−δ) HeunG[1−aH,((1−aH)γ+ϵ)(1−δ)+α β−q,α+1−δ,β
    +1−δ,2−δ,γ,1−z];
Det[{{y02[z],y11[z]},{y02'[z],y11'[z]}}]/Det[{{y12[z],y11[z]},{y12'[z],y11
    '[z]}}]/.z−>1/2]

(*This part computes QNM eigenvalues for given parameters*)

Clear[QNMdS]
QNMdS[{s_,l_,m_},{M_,Λ_,a_},{ωini_,λini_},prec_]:=QNMdS[{s,l,m
    },{M,Λ,a},{ωini,λini},prec]=If[a==0,N[FindRoot[radial[{s,l,m},{M,Λ,a
    },{ω,l(l+1)−s(s−1)},prec+10],{ω,ωini},WorkingPrecision−>prec+10],
    prec],N[FindRoot[{angular[{s,l,m},{M,Λ,a},{ω,λ}],radial[{s,l,m},{M,Λ,
    a},{ω,λ},prec+10]},{{ω,ωini},{λ,λini}},WorkingPrecision−>prec+10],
    prec]]

(*Kerr in the flat limit*)

s0=−2;l0=2;m0=2;
a0=0.6;
ωflat= 0.4940447817813843−0.08376520216104325*I; (* This value was
    computed using the qnm package for Python*)
Aflat= 3.1453865994337304+0.15669038538845884*I;(* This value was
    computed using the qnm package for Python*)
λflat=Aflat+2s−2m c+c^2/.{s−>s0,m−>m0,c−>a0*ωflat}

(*The following computations take much time*)

Clear[Kerr]
step=1/10000;
Kerr[step]={ω,λ}/.QNMdS[{s0,l0,m0},{1,step,a0},{ωflat,λflat},50]
Kerr[Λ_]:=Kerr[Λ]={ω,λ}/.QNMdS[{s0,l0,m0},{1,Λ,a0},Kerr[Λ−step
    ]−1/20000 {1−I,−1−I},50]

stepnumber = 20
```

```
ls=Monitor[Table[{p*step,Kerr[p*step]},{p,1,stepnumber}],p];
lsreω=Table[{ls[[i,1]],ls [[ i ,2,1]]// Re},{i,Length[ls]}]
lsimω=Table[{ls[[i,1]],ls [[ i ,2,1]]// Im},{i,Length[ls]}]
ListPlot[lsreω,AxesLabel->{"\!\(\*SuperscriptBox[\(M\), \(2\)]\)Λ","
    Re[Mω]"}]
ListPlot[lsimω,AxesLabel->{"\!\(\*SuperscriptBox[\(M\), \(2\)]\)Λ","
    Im[Mω]"}]
Export[StringReplace["lsreω,a=0,m=1,l=2.csv",{"0" -> ToString[N[a0
    ]],"1" -> ToString[m0],"2" -> ToString[N[l0]]}],lsreω]
Export[StringReplace["lsimω,a=0,m=1,l=2.csv",{"0" -> ToString[N[a0
    ]],"1" -> ToString[m0],"2" -> ToString[N[l0]]}],lsimω]

Table[{o,Coefficient[Fit[lsreω,Table[Λ^i,{i,0,o}],Λ],Λ,0]},{o,5,19}]//
    TableForm
Table[{o,Coefficient[Fit[lsimω,Table[Λ^i,{i,0,o}],Λ],Λ,0]},{o,5,19}]//
    TableForm

lsreω+ I lsimω
Fit[ lsreω+I lsimω,Table[Λ^i,{i,0,18}],Λ]
N[Coefficient[%,Λ,0],20]
%-ωflat
```

E Tunneling formalism in the study of particle emission rates from black holes due to Hawking radiation

This Appendix is intended to explain why the first topic proposed for this master's thesis, which concerned the application of tunneling formalism to the computation of particle emission rates from a black hole due to Hawking radiation, was problematic. First, we would like to briefly introduce the formulae for the emission rates and the application of tunneling in the study of Hawking radiation. Then, we will mention the problems that this method presents. For simplicity, we restrict ourselves to the emission of massless particles from Schwarzschild-Minkowski black holes.

E.1 Theory

E.1.1 Emission rates

Hawking radiation is a phenomenon, first described by Hawking in [53] (see also [54] and [55]), that arises when considering quantum field theory in a curved spacetime, treating the metric classically and the matter fields quantum mechanically. This theory, developed for Schwarzschild-Minkowski and Kerr-Minkowski black holes, relies on the fact that the notion of particle can only be defined unambiguously in flat but not in curved spacetime. The quantum states are therefore defined at infinity, and their interaction with the spacetime curvature is described by operators that map these initial states to final states, again defined at infinity, in a way that resembles scattering theory.

By means of this theory, Hawking derived the formula

$$\langle N_{j\omega lmp} \rangle = \frac{\Gamma_{j\omega lmp}}{\exp[2\pi\kappa^{-1}(\omega - m\Omega)] \pm 1}, \tag{E.1}$$

for the *expected emission rate*, as observed infinitely far from the black hole, of particles of species j in a wave mode labeled by energy ω, the spheroidal harmonic quantum number l, the axial quantum number m and the polarization p. $\Gamma_{j\omega lmp}$ is called in [56] the *absorption probability* (or *greybody factor*)[37] for an incoming wave of that mode. The quantities κ and Ω are the surface gravity and the angular velocity, and are related to the black hole's mass M, area A and angular momentum J by the first law of black hole's thermodynamics: $dM = \kappa/8\pi dA + \Omega dJ$. The plus (minus) is for fermions (bosons).

[37] The coefficient $\Gamma_{j\omega lmp}$ represents the probability for a particle emitted by the black hole to reach infinity and not to fall back into the hole.

As first noted by Hawking in [53], equation (E.1) corresponds to the rate of thermal emission of a perfect blackbody at a temperature given, in Planck units, by

$$T_H = \kappa/2\pi. \tag{E.2}$$

The rates at which the mass and angular momentum of a Kerr-Minkowski black hole decrease are given by the formula (cf. [56] and [29]):

$$-\frac{d}{dt}\begin{pmatrix} M \\ J \end{pmatrix} = \sum_{j,l,m,p} \int_0^\infty d\omega \, \langle N_{j\omega lmp} \rangle \begin{pmatrix} \omega \\ m \end{pmatrix}. \tag{E.3}$$

To use this formula (E.3), one should first know the value of $\Gamma_{j\omega lmp}$, whose computation is nontrivial and is normally achieved using perturbation theory (cf. [8]). The question we asked ourselves is whether this calculation can be simplified using a formalism other than perturbation theory, like the tunneling formalism. In the following, we will see why this is not possible with the current understanding of the tunneling formalism applied to black holes.

E.1.2 Hawking radiation as tunneling

Hawking provided a heuristic interpretation of the phenomenon of particle emission from black holes, which relies on the fact that the Killing vector field is time-like ouside the black hole horizon, space-like inside and light-like on the horizon. Therefore, only particle states with positive energy are allowed outside the horizon, but both positive and negative energy particle states can occur inside. One can imagine Hawking radiation as being the result of one of the following two scenarios. First, a pair of particles[38], one with positive and the other with negative energy, can be produced from vacuum just beneath the event horizon, and the positive energy particle can escape the black hole via quantum tunneling through the horizon (note that this would not be allowed classically). The second scenario imagines a pair of particles[38], one with positive and the other with negative energy, as being producted just outside the horizon. The negative energy particle state tunnels, or falls, into the black hole through the horizon, while the positive energy particle escapes to infinity. In both scenarios, this process causes loss of mass by the black hole.

Parikh and Wilczek [57] (see also [58] and [59] for a review) proposed a derivation of Hawking radiation which corresponds directly to this heuristic picture, using tunneling formalism to compute the expected emission rate by black holes, although, as written by Hawking in [53], the tunneling interpretation is "heuristic only and should not be taken too literally". In the following,

[38] One could also consider a particle-antiparticle pair. However, Hawking's derivation in [53] predicts the production of particle pairs.

we present the method that they used in their derivations, also called the *null geodesic method*. Another method, the so-called *Hamilton-Jacobi method*, is described in [59], but we did not review it.

E.1.3 Choice of the coordinates

The first thing to do, in order to apply the tunneling formalism, is to define the notion of a particle. As said above, a particle can be uniquely defined only in flat spacetime, but not, for example, in the vicinity of a black hole event horizon. To solve this problem, as explained in [59], one can choose a particular coordinate system and define an observer dependent vacuum relative to which it is possible to define the notion of particle uniquely. Since the purpose of the calculations is to compute a probability, this approach is justified in [59] by saying that, if the probability is coordinate invariant, it will not depend on the coordinate system that one chooses.

Following [57] and [58], one chooses a coordinate system which is not singular across the horizon, like the Gullstrand-Painlevé coordinate system. The metric in these coordinates is given by

$$ds^2 = -\left(1 - \frac{2M}{r}\right) dt^2 + 2\sqrt{\frac{2M}{r}} dt dr + dr^2 + r^2(d\theta^2 + sin^2\theta d\phi). \tag{E.4}$$

Here, r, θ and ϕ are the Schwarzschild coordinates, and $t = t_S + f(r)$, where t_S is the Schwarzschild time and $f(r)$ satisfies $f'(r)\left(1 - \frac{2M}{r}\right) = \frac{2M}{r}$ (see [58]).

One then looks for curves that are both radial (to study outgoing and ingoing geodesics) and null (associated to massless particles):

$$0 = \left(\frac{ds}{dt}\right)^2, \tag{E.5}$$

$$0 = -\left(1 - \frac{2M}{r}\right) + 2\sqrt{\frac{2M}{r}}\dot{r} + \dot{r}^2, \tag{E.6}$$

$$\dot{r} = \pm 1 - \sqrt{\frac{2M}{r}}, \tag{E.7}$$

where "+" is used for the outgoing and "−" is used for the ingoing geodesics when ouside the event horizon. When inside the horizon, both geodesics are ingoing.

E.1.4 WKB approximation

Normally, for the calculation of the trasmission coefficient for tunneling through a potential barrier, one makes use of the WKB approximation[39]. This method

[39] In the WKB method, the particle is treated quantum mechanically (first quantisation) and the wavefunction is cast as an exponential, $e^{T(x)+iS(x)}$, where amplitude and phase are

is used to find solutions before, in and after the classically forbidden region. Then, one matches the coefficients for continuity and the resulting *emission rate*[40] is given in Planck units by

$$\Gamma_{\text{em}} \propto e^{-2\,\text{Im}(S)}, \tag{E.8}$$

where S is the reduced action for the tunneling process, i.e.

$$S = \int_{r_1}^{r_2} dr\, p_r, \tag{E.9}$$

where r_1 and r_2 are the beginning and ending points of the potential barrier.

To study the tunneling process through the event horizon, the idea is to apply these results directly to the black hole case[41]. In this case, S is the action for the tunneling process across the event horizon, and r_1 and r_2 are the positions of the event horizon before and after the particle of energy ω has tunneled out[42]. The imaginary part of the action is then computed as follows:

$$\begin{aligned}
\text{Im}S &= \text{Im}\int_{r_1}^{r_2} dr\, p_r && \text{(E.10)}\\
&= \text{Im}\int_{r_1}^{r_2} dr \int_0^{p_r} dp_r' && \text{(E.11)}\\
&\overset{(1)}{=} \text{Im}\int_{r_1}^{r_2} dr \int_M^{M-\omega} \frac{dH}{\dot{r}} && \text{(E.12)}\\
&= \text{Im}\int_{r_1}^{r_2} dr \int_0^{\omega} \frac{-d\omega'}{\dot{r}} && \text{(E.13)}\\
&\overset{(2)}{=} \text{Im}\int_0^{\omega} (-d\omega') \int_{r_1}^{r_2} \frac{dr}{1-\sqrt{\frac{2(m-\omega')}{r}}} && \text{(E.14)}\\
&\overset{(3)}{=} \text{Im}\int_0^{\omega} (-d\omega') \int_{r_1}^{r_2} dr \frac{\sqrt{r}}{\sqrt{r}-\sqrt{2(M-\omega')}+i\epsilon} && \text{(E.15)}\\
&= -\text{Im}\, i\pi \int_0^{\omega} (-d\omega') 4(M-\omega') && \text{(E.16)}\\
&= 4\pi\omega\left(M-\frac{\omega}{2}\right). && \text{(E.17)}
\end{aligned}$$

explicitly separated. The (semiclassical) WKB approximation is then made by expanding T and S as a power series of $\hbar$ and keeping the leading order term in the classical limit $\hbar \to 0$.

[40]The emission rate corresponds to the probability per unit time for one particle to tunnel through the potential barrier.

[41]One justifies the applicability of the WKB approximation in the vicinity of the black hole horizon by saying that a distant observer detects a wave with frequency ω_{obs}, which has been emitted with frequency $\omega_{\text{em}} \propto (1-2M/r)^{-1/2}\omega_{\text{obs}}$, and therefore the wavelength vanishes for an observer near the horizon, making the semiclassical approximation reliable.

[42]One takes into account the back reaction on the metric by saying that, if a particle of energy ω has tunneled out, the mass M of the black hole reduces to $M-\omega$, and consequently its horizon recedes to $2(M-\omega)$. So, one has $r_1 = 2M$ and $r_2 = 2(M-\omega)$, with $r_1 > r_2$. In fact, "it is the particle itself that secretely defines the tunneling barrier" [60].

In (1), one changes the integration from momentum to energy using that, in the Hamilton formalism, $\dot{r} = dH/dp_r$, where $H = M - \omega'$ with $0 \leq \omega' \leq \omega$ and M constant. In (2), one switches the order of the integration and uses equation (E.7) for the outgoing geodesics[43]. In (3) one regularises the integral, which is otherwise divergent, by shifting the energy to complex values, i.e. $\omega' \to \omega' + i\epsilon$.

Equation (E.8) can then be rewritten as

$$\Gamma_{\text{em}} \propto e^{-8\pi M\omega(1-\omega/2M)}. \tag{E.18}$$

If one uses the definition of the Hawking temperature, equation (E.2), and the fact that the surface gravity of a Schwarzschild black hole of mass M equals to $\kappa = 1/4M$, one can rewrite equation (E.18) as

$$\Gamma_{\text{em}} \propto e^{-\frac{\omega}{T_H}(1-\omega/2M)}. \tag{E.19}$$

E.1.5 Detailed balance condition

The next step in the computations of the expected emission rate consists in considering black hole thermodynamics and in making use of the detailed balance condition[44]. If one considers the system constituted by the black hole and the emitted particles, and one denotes by p_N the probability of the system of being in the state "black hole with N emitted particles", then the detailed balance condition requires that, at equilibrium,

$$p_{N-1}\Gamma_{\text{em}} = p_N\Gamma_{\text{abs}}, \tag{E.20}$$

where Γ_{abs} is the *absorption rate*, which represents the probability per unit time of emitting one particle. If one neglects the back reaction of the metric, the internal degrees of freedom of the black hole do not change, and the problem can be compared to the thermodynamic problem of a system in thermal equilibrium with a heat bath, where the heat bath here is represented by the black hole. Making use of the known results for this problem, and using again Planck units, one can write

$$p_N = \frac{e^{-N\omega/T}}{\sum_i e^{-E_i/T}} = \frac{e^{-(N-1)\omega/T}}{\sum_i e^{-E_i/T}} e^{-\omega/T} = p_{N-1}e^{-\omega/T}, \tag{E.21}$$

where the sum runs over all possible states i, with energy E_i, of the subsystem consisting of the emitted particles. Here, T denotes the temperature of the

[43] We are considering here only the case of a particle tunneling out of the horizon. As explained in [58] and [59], the process describing a particle falling into the horizon is mathematically the same, and the results are identical. That both processes contribute to the particle emission is something that only affects the amplitude of the process, and hence the proportionality factor of equation (E.8).

[44] For a detailed explanation, we refer the reader to the footnote at page 11 of [59].

bath. By combining equations (E.20) and (E.21), one obtains

$$\frac{\Gamma_{\text{em}}}{\Gamma_{\text{abs}}} = \frac{p_N}{p_{N-1}} = e^{-\omega/T}, \tag{E.22}$$

that is,

$$\Gamma_{\text{em}} = \Gamma_{\text{abs}}\, e^{-\omega/T}. \tag{E.23}$$

By comparing equation (E.23) with equation (E.19), and by assuming[45] $\omega \ll M$, one can identify the Hawking temperature T_H with the bath temperature T, and write

$$\Gamma_{\text{em}} = \Gamma_{\text{abs}}\, e^{-\omega/T_H}. \tag{E.24}$$

Finally, one makes use of the classical constraint

$$\Gamma_{\text{ab}} \pm \Gamma_{\text{em}} = |T_{j\omega lmp}|^2, \tag{E.25}$$

where the plus (minus) is for fermions (bosons) and where $T_{j\omega lmp}$ is called in [59] the *transmission coefficient of the black hole barrier*. By combining equations (E.24) with equation (E.25), one obtains

$$\Gamma_{\text{em}} = \frac{|T_{j\omega lmp}|^2}{e^{-\omega/T_H} \pm 1}. \tag{E.26}$$

E.1.6 Results

If one compares equation (E.26) with the formula (E.1) of the expected emission rate for Schwarzschild black holes ($\Omega = 0$), one sees that Γ_{em} corresponds to $\langle N_{j\omega lmp} \rangle$ and $|T_{j\omega lmp}|^2$ corresponds to $\Gamma_{j\omega lmp}$. However, the tunneling method does not provide a way to compute the $|T_{j\omega lmp}|^2$ explicitly, and therefore does not constitute an alternative to perturbation theory for computing the greybody factor $\Gamma_{j\omega lmp}$. Moreover, the tunneling method presents a number of issues and points to be clarified which we will briefly discuss in the next section.

E.2 Problems

During the review of the tunneling method, we came across a general lack of precision in the definition of terms, which often do not indicate the same quantity in different papers, leading to confusion. Furthermore, we have noticed that, to develop this formalism, one needs to make a series of assumptions which are not fully justifiable. We give here an overview of the problems that

[45] By assuming the energy of the particle being much smaller than the black hole mass, one can neglect the term $\omega/2M$ in equation (E.19). If the energy of the particle is not negligible, then equation (E.19) provides higher order corrections, but note that in this case the back reaction cannot be neglected.

we encountered, but a more detailed discussion of some of the issues can be found in a recent paper, [61], to which we also refer.

First of all, we are confused by the fact that the term *transmission coefficient* is used to indicate the emission rate in [58], while in [59] it indicates the greybody factor. Moreover, we wonder how these two "transmission coefficients" are related to the actual transmission coefficient for a tunneling process, given by

$$T = \frac{|\text{amplitude of the transmitted wave}|^2}{|\text{amplitude of the incoming wave}|^2}. \tag{E.27}$$

To understand this, it would be perhaps necessary to understand in detail how equation (E.8) is obtained in the case of tunneling through a potential barrier.

Secondly, as discussed also in [61], we are not sure if it makes sense to apply the results of the the WKB approximation, which are derived using quantum mechanics (first quantisation) in a Minkowski spacetime, to a phenomenon which, in Hawking's derivation, arises when considering quantum field theory in curved spacetime.

Moreover, the crucial ingredient in the computation of the imaginary part of the action (equations (E.10) to (E.17)) is played by energy conservation. Without considering the back reaction, the result of the computations would have been zero. However, in Hawking's derivation, the formula (E.1) can be obtained without considering the back reaction (cf. [53], [54], [55]).

Furthermore, the above derivation is observer dependent. In fact, even if it is assumed that the probability is a coordinate scalar, this is not formally proved. However, this and the previous problem may be solved using the Hamilton-Jacobi method instead of the null geodesic method. In fact, it is said that this method ignores the back reaction on the metric and applies to any well-behaved coordinate system across the horizon.

Finally, to cite directly [61], what one computes with this method "is a sort of rescaled Unruh temperature associated with world-lines tracing Killing trajectories near the horizon. This temperature is numerically equal to the Hawking temperature, but at this point no argument is known which identifies it with the Hawking effect". However, we did not go into the details of this point, which needs further investigation.

E.3 Summary

We investigated the tunneling formalism and its application in the derivation of Hawking radiation in the attempt of finding an easy way to compute the absorption probability, or greybody factor, contained in the formula of the expected particle emission rate from a black hole. We reviewed in particular the null geodesic method, and also made use of some notions of thermodynamics.

We found out that the tunneling formalism allows to recover the same formula for the emission rate as derived by Hawking, but does not allow to compute the greybody factor explicitly. Therefore, it does not seem to be useful for our purpose. Moreover, we noticed a general confusion in the use of the terms and a lack of justification of the assumptions used. This latter point is rather interesting and needs further investigation.

References

[1] C. W. Misner, K. S. Thorne, and J. A. Wheeler, *Gravitation*. W. H. Freeman and Company, 1973.

[2] C. Vishveshwara, "Stability of the schwarzschild metric," *Physical Review D*, vol. 1, no. 10, p. 2870, 1970.

[3] T. Regge and J. A. Wheeler, "Stability of a schwarzschild singularity," *Physical Review*, vol. 108, no. 4, p. 1063, 1957.

[4] S. Chandrasekhar and S. Detweiler, "The quasi-normal modes of the schwarzschild black hole," *Proceedings of the Royal Society of London. A. Mathematical and Physical Sciences*, vol. 344, no. 1639, pp. 441–452, 1975.

[5] S. Chandrasekhar, "On the equations governing the perturbations of the schwarzschild black hole," *Proceedings of the Royal Society of London. A. Mathematical and Physical Sciences*, vol. 343, no. 1634, pp. 289–298, 1975.

[6] S. A. Teukolsky, "Perturbations of a rotating black hole. i. fundamental equations for gravitational, electromagnetic, and neutrino-field perturbations," *The Astrophysical Journal*, vol. 185, pp. 635–648, 1973.

[7] W. H. Press and S. A. Teukolsky, "Perturbations of a rotating black hole. ii. dynamical stability of the kerr metric," *The Astrophysical Journal*, vol. 185, pp. 649–674, 1973.

[8] S. A. Teukolsky and W. Press, "Perturbations of a rotating black hole. iii-interaction of the hole with gravitational and electromagnetic radiation," *The Astrophysical Journal*, vol. 193, pp. 443–461, 1974.

[9] S. Chandrasekhar and S. Detweiler, "On the equations governing the gravitational perturbations of the kerr black hole," *Proceedings of the Royal Society of London. A. Mathematical and Physical Sciences*, vol. 350, no. 1661, pp. 165–174, 1976.

[10] S. Detweiler, "Black holes and gravitational waves. iii-the resonant frequencies of rotating holes," *The Astrophysical Journal*, vol. 239, pp. 292–295, 1980.

[11] V. Ferrari and B. Mashhoon, "New approach to the quasinormal modes of a black hole," *Physical Review D*, vol. 30, no. 2, p. 295, 1984.

[12] E. W. Leaver, "An analytic representation for the quasi-normal modes of kerr black holes," *Proceedings of the Royal Society of London. A. Mathematical and Physical Sciences*, vol. 402, no. 1823, pp. 285–298, 1985.

[13] H. Otsuki and T. Futamase, "Gravitational Perturbation of Schwarzschild-De Sitter Spacetime and Its Quasi-Normal Modes," *Progress of Theoretical Physics*, vol. 85, pp. 771–778, 04 1991.

[14] I. G. Moss and J. P. Norman, "Gravitational quasinormal modes for anti-de sitter black holes," *Classical and Quantum Gravity*, vol. 19, pp. 2323–2332, apr 2002.

[15] V. Cardoso and J. P. Lemos, "Quasinormal modes of the near extremal schwarzschild–de sitter black hole," *Physical Review D*, vol. 67, no. 8, p. 084020, 2003.

[16] S. Yoshida and T. Futamase, "Numerical analysis of quasinormal modes in nearly extremal Schwarzschild de Sitter spacetimes," *Physical Review D*, vol. 69, p. 064025, Mar. 2004.

[17] H. Suzuki, E. Takasugi, and H. Umetsu, "Perturbations of Kerr-de Sitter Black Holes and Heun's Equations," *Progress of Theoretical Physics*, vol. 100, pp. 491–505, Sept. 1998.

[18] H. Suzuki, E. Takasugi, and H. Umetsu, "Analytic solutions of the teukolsky equation in kerr-de sitter and kerr-newman-de sitter geometries," *Progress of theoretical physics*, vol. 102, no. 2, pp. 253–272, 1999.

[19] S. Yoshida, N. Uchikata, and T. Futamase, "Quasinormal modes of kerr–de sitter black holes," *Physical Review D*, vol. 81, p. 044005, Feb 2010.

[20] Y. Hatsuda, "Quasinormal modes of Kerr-de Sitter black holes via the Heun function," *arXiv e-prints*, p. arXiv:2006.08957, June 2020.

[21] M. Giammatteo and I. G. Moss, "Gravitational quasinormal modes for kerr anti-de sitter black holes," *Classical and Quantum Gravity*, vol. 22, no. 9, p. 1803, 2005.

[22] Planck Collaboration, "Planck 2018 results. vi. cosmological parameters," *A&A*, 2020.

[23] G. W. Gibbons and S. W. Hawking, "Cosmological event horizons, thermodynamics, and particle creation," *Physical Review D*, vol. 15, no. 10, p. 2738, 1977.

[24] L. Heisenberg, "A systematic approach to generalisations of General Relativity and their cosmological implications," *Physics Reports*, vol. 796, pp. 1–113, Mar. 2019.

[25] S. Akcay and R. A. Matzner, "The Kerr-de Sitter universe," *Classical and Quantum Gravity*, vol. 28, p. 085012, Apr. 2011.

[26] S. Bhattacharya, "Kerr-de Sitter spacetime, Penrose process, and the generalized area theorem," *Physical Review D*, vol. 97, p. 084049, Apr. 2018.

[27] A. G. Lemaître, "A Homogeneous Universe of Constant Mass and Increasing Radius accounting for the Radial Velocity of Extra-galactic Nebulae," *Monthly Notices of the Royal Astronomical Society*, vol. 91, pp. 483–490, 03 1931.

[28] C. M. Hirata, "Kerr black holes: Metric structure and regularity of particle orbits." http://www.tapir.caltech.edu/ chirata/ph236/2011-12/lec26.pdfpage=5, February 2012. Caltech M/C 350-17.

[29] D. N. Page, "Particle emission rates from a black hole. ii. massless particles from a rotating hole," *Physical Review D*, vol. 14, no. 12, p. 3260, 1976.

[30] H.-P. Nollert, "Quasinormal modes: the characteristic sound of black holes and neutron stars," *Classical and Quantum Gravity*, vol. 16, pp. R159–R216, nov 1999.

[31] S. Chandrasekhar, *The Mathematical Theory of Black Holes*. Oxford University Press, 1983.

[32] M. Cabero, J. Westerweck, C. D. Capano, S. Kumar, A. B. Nielsen, and B. Krishnan, "Black hole spectroscopy in the next decade," *Physical Review D*, vol. 101, p. 064044, Mar 2020.

[33] S. A. Teukolsky, "Rotating black holes: Separable wave equations for gravitational and electromagnetic perturbations," *Physical Review Letters*, vol. 29, pp. 1114–1118, Oct 1972.

[34] L. C. Stein, "qnm: A Python package for calculating Kerr quasinormal modes, separation constants, and spherical-spheroidal mixing coefficients," *Journal of Open Source Software*, vol. 4, no. 42, p. 1683, 2019.

[35] R. M. Wald, "Note on the stability of the schwarzschild metric," *Journal of Mathematical Physics*, vol. 20, no. 6, pp. 1056–1058, 1979.

[36] B. S. Kay and R. M. Wald, "Linear stability of schwarzschild under perturbations which are non-vanishing on the bifurcation 2-sphere," *Classical and Quantum Gravity*, vol. 4, no. 4, p. 893, 1987.

[37] B. F. Whiting, "Mode stability of the kerr black hole," *Journal of Mathematical Physics*, vol. 30, no. 6, pp. 1301–1305, 1989.

[38] A. Zhidenko, "Quasi-normal modes of Schwarzschild de Sitter black holes," *Classical and Quantum Gravity*, vol. 21, pp. 273–280, Jan. 2004.

[39] https://reference.wolfram.com/language/ref/HeunG.html, Accessed: 25.07.2020.

[40] W. Gautschi, "Computational aspects of three-term recurrence relations," *SIAM review*, vol. 9, no. 1, pp. 24–82, 1967.

[41] G. B. Cook and M. Zalutskiy, "Gravitational perturbations of the Kerr geometry: High-accuracy study," *Physical Review D*, vol. 90, p. 124021, Dec. 2014.

[42] E. T. Newman and R. Penrose, "Note on the bondi-metzner-sachs group," *Journal of Mathematical Physics*, vol. 7, no. 5, pp. 863–870, 1966.

[43] J. N. Goldberg, A. J. Macfarlane, E. T. Newman, F. Rohrlich, and E. C. G. Sudarshan, "Spinâs spherical harmonics and Ã°," *Journal of Mathematical Physics*, vol. 8, no. 11, pp. 2155–2161, 1967.

[44] S. A. Teukolsky, "Perturbations of a Rotating Black Hole. I. Fundamental Equations for Gravitational, Electromagnetic, and Neutrino-Field Perturbations," *Astrophysical Journal*, vol. 185, pp. 635–648, Oct. 1973.

[45] W. H. Press and S. A. Teukolsky, "Perturbations of a Rotating Black Hole. II. Dynamical Stability of the Kerr Metric," *Astrophysical Journal*, vol. 185, pp. 649–674, Oct. 1973.

[46] E. Berti and A. Klein, "Mixing of spherical and spheroidal modes in perturbed kerr black holes," *Physical Review D*, vol. 90, p. 064012, Sep 2014.

[47] E. Berti, V. Cardoso, and M. Casals, "Eigenvalues and eigenfunctions of spin-weighted spheroidal harmonics in four and higher dimensions," *Physical Review D*, vol. 73, p. 024013, Jan 2006.

[48] G. Kristensson, *Second Order Differential Equations*. Springer-Verlag New York, 2010. https://doi.org/10.1007/978-1-4419-7020-6.

[49] B. D. Sleeman and V. B. Kuznetsov, "Dlmf: 31 heun functions." https://dlmf.nist.gov/31, Accessed: 21.07.2020. Department of Applied Mathematics, University of Leeds, Leeds, United Kingdom.

[50] T. S. Shores, *Applied Linear Algebra and Matrix Analysis*. Springer, Cham, second edition ed., 2018. https://doi.org/10.1007/978-3-319-74748-4.

[51] W. H. Press, S. A. Teukolsky, W. T. Vetterling, and B. P. Flannery, *Numerical Recipes, The Art of Scientific Computing*. Cambridge University Press, third edition ed., 2007.

[52] I. Thompson and A. Barnett, "Coulomb and bessel functions of complex arguments and order," *Journal of Computational Physics*, vol. 64, no. 2, pp. 490–509, 1986.

[53] S. W. Hawking, "Particle creation by black holes," *Communications in mathematical physics*, vol. 43, no. 3, pp. 199–220, 1975.

[54] S. Hawking, "Particle creation by black holes," *Communications in Mathematical Physics*, vol. 46, no. 2, pp. 206–206, 1976.

[55] R. M. Wald, "On particle creation by black holes," *Communications in Mathematical Physics*, vol. 45, no. 1, pp. 9–34, 1975.

[56] D. N. Page, "Particle emission rates from a black hole: Massless particles from an uncharged, nonrotating hole," *Physical Review D*, vol. 13, pp. 198–206, Jan 1976.

[57] M. K. Parikh and F. Wilczek, "Hawking radiation as tunneling," *Physical Review Letters*, vol. 85, no. 24, p. 5042, 2000.

[58] C. Fleming, "Hawking radiation as tunneling," *University of Maryland. Department of Physics., Tech. Rep*, 2005.

[59] L. Vanzo, G. Acquaviva, and R. Di Criscienzo, "Tunnelling methods and hawking's radiation: achievements and prospects," *Classical and Quantum Gravity*, vol. 28, no. 18, p. 183001, 2011.

[60] M. Parikh, "a Secret Tunnel Through the Horizon," *International Journal of Modern Physics D*, vol. 13, pp. 2351–2354, Jan. 2004.

[61] A. D. Helfer, "Hawking radiation, quantum fields, and tunneling," *Physical Review D*, vol. 100, p. 025005, July 2019.